An Age-Calibrated Middle – Late Tonian Carbon Isotopic Record from northwestern Namibia

Ajani Bissick

Department of Earth and Planetary Sciences

McGill University

Downtown Campus

Supervisors: Professor Galen Halverson

Assistant Professor Joshua H.F.L. Davies

ABSTRACT

The ca. 760 Ma Devede Formation is a mixed clastic/carbonate unit in the Kaokoveld region of northwestern Namibia. Deposited prior to the relatively well studied Cryogenian "Snowball" glaciations, this unit preserves the oldest carbonates in the Otavi Group, thereby making it an important archive of information on Tonian Earth system evolution and the breakup of the Rodinia supercontinent. Despite its importance in understanding changes in the Earth's climate and surface processes preceding the Cryogenian glaciations, as well as the presence of a key dated (760 Ma) tuff bed, this unit remains largely understudied compared to other Tonian successions worldwide. Here, I present an integrated lithological, chemostratigraphic, and facies analysis of the Devede Formation based on a synthesis of new and previously published stratigraphic and sedimentological observations as well as stable isotope data (carbonate $\delta^{13}C$, $\delta^{18}O$).

Sequence stratigraphic interpretations and correlation across the Kaokoveld region provide a chronological and depositional framework for the Devede Formation. This framework highlights ten fourth-order depositional sequences and captures the gradual upsection shift from a distally steepened ramp to a rimmed carbonate platform. The basin-wide facies changes are manifested in the lower part of the Devede Formation by a northward transition from meter-scale shallowing upward cycles of shallow marine carbonates, with reddened exposure surfaces and a northward waning lower siliciclastic tongue, to less distinct decameter-scale cycles of cement-rich carbonates. The depositional environments represented by these facies are interpreted to range from supratidal sabkhas to relatively deep subtidal (below storm wave base) settings. Facies relationships and sequence stratigraphic surfaces are used to develop a basin-wide sequence stratigraphic framework. Within this framework, facies exert a moderate control on the carbon

isotope composition of carbonates, with negative $\delta^{13}C$ shifts linked to increased continental input in the south, while relative enrichments of up to 3‰ occur in tandem with the development of a restricted lagoon. A composite carbon isotope profile through the Devede Formation incorporates age constraints from a dated tuff in the upper Devede Formation. This new age calibrated profile will potentially facilitate correlations with other middle to late Tonian successions globally.

RÉSUMÉ

La formation de Devede, datant d'environ 760 Ma, présentant des sédiments siliciclastiques et carbonatés situés dans la région du Kaokoveld, dans le nord-ouest de la Namibie. Déposée avant les relativement bien étudiés épisodes de glaciation 'Snowball Earth', cette unité comprend les carbonates les plus anciens du groupe d'Otavi – une archive importante de l'évolution du système terrestre au Néoprotérozoïque et de la dislocation du supercontinent Rodinia. Malgré son importance pour la compréhension des changements climatiques et des processus de surface précédant ces glaciations, ainsi que la présence d'un lit de tuf daté (760 Ma), cette unité reste largement sous-étudiée par rapport à d'autres successions toniennes dans le monde entier. Je présente ici une analyse lithologique, chimiostratigraphique et des faciès de la formation de Devede, basée sur une synthèse d'observations stratigraphiques et sédimentologiques nouvelles et déjà publiées, ainsi que sur des données d'isotopes stables (carbonate $\delta^{13}C$, $\delta^{18}O$).

Les interprétations stratigraphiques séquentielles et la corrélation dans la région du Kaokoveld fournissent un cadre chronologique et sédimentaire pour la formation de Devede. Ce cadre met en évidence dix séquences de dépôt de quatrième ordre et enregistre le passage progressif, en amont de la section, d'une rampe distale à une plate-forme carbonatée. La transition, vers le nord, de cycles ascendants peu profonds à l'échelle métrique de carbonates peu profonds, avec des surfaces d'exposition et une langue siliciclastique allant vers le nord, vers des cycles moins distincts à l'échelle décamétrique de carbonates riches en ciment, nous permet d'interpréter des environnements de dépôt allant de sabkhas supratidaux à des environnements subtidaux relativement profonds (au-dessous de la limite des vagues de tempête). Dans ce cadre, il semble y avoir un certain degré de contrôle de faciès sur la composition isotopique des carbonates, avec des excursions négatives du $\delta^{13}C$ reliées à une augmentation de l'apport continental dans le sud,

tandis que la mise en place d'environnement de lagune restreinte favorise des excursions positives du δ^{13}C, allant jusqu'à 3‰. Le modèle de séquence est utilisé pour générer un profil isotopique composite intégré du δ^{13}C à travers la formation de Devede, en incorporant pour la première fois les contraintes d'âge des tufs synsédimentaires. Ce nouveau profil calibré en fonction de l'âge facilitera les corrélations potentielles avec d'autres successions du Tonien moyen à tardif à l'échelle globale.

ACKNOWLEDGMENTS

CONTRIBUTION OF AUTHORS

This thesis was written by A. Bissick and edited by G. Halverson and J. Davies. Fieldwork in 2015 and 2021 (measuring stratigraphic sections and sampling carbonates) was carried out by A. Bissick, K. Lamothe, P. Hoffman, and G. Halverson. Data from past seasons was provided by P. Hoffman and G. Halverson, much of it previously published in Hoffman *et al.* (2021). New carbon and oxygen isotope data were acquired by A. Bissick, under the direction of T.H. Bui, at McGill University.

This thesis is dedicated to my grandparents, who through their bravery, love, and sacrifices, taught me how to soar.

TABLE OF CONTENTS

Title	Page Number

LIST OF FIGURES

LIST OF TABLES

Title	Page Number

CHAPTER 1

1.1 Introduction

The tectonic history of the Neoproterozoic Era (1000 –541 Ma) is characterized by periods of crustal extension, rifting, and drifting, which ultimately led to the breakup of the supercontinent Rodinia (ca. 830–720 Ma) and the subsequent assembly of Gondwana (Hoffman, 1991; Pisarevsky *et al.*, 2003; Li *et al.*, 2008). The opening of new ocean basins and their subsequent closure resulted in extensive late Neoproterozoic sedimentary successions preserved in fold and thrust belts on multiple continents globally. These successions provide key archives for reconstructing paleoenvironmental evolution at a time when Earth's climate experienced extreme changes (Kirschvink, 1992; Hoffman *et al.*, 1998b) and when the earliest animals appeared and diversified (Canfield *et al.*, 2007; Gaucher and Sprechmann, 2009). Superimposed on the tectonic, climatic, and biospheric upheavals of the Neoproterozoic were dramatic fluctuations in the carbon isotopic composition ($\delta^{13}C$) of marine carbonates and a long-term increase in atmospheric and marine oxygen levels (Halverson *et al.*, 2009; Och and Shields, 2012).

It is widely argued that these various events and trends were inextricably linked through feedbacks between the solid Earth, atmospheric, oceanic, biospheric and climactic systems. Documenting these changes and evaluating their causal relationships fundamentally requires a coherent, age-calibrated geological record (Halverson *et al.*, 2018). Consequently, this thesis focuses on expanding the current pre-Cryogenian carbon isotope record in the Otavi Group of northwestern Namibia through a detailed study of the late Tonian Ombombo Subgroup, with a focus on the carbonate dominated Devede Formation. Another objective of this thesis is to provide a more precise U-Pb age-calibrated facies and carbon isotope ($\delta^{13}C$) record for the Middle to Late Tonian Devede Formation. Likewise, though seemingly significant fluctuations

in the carbon isotopic record (sustained high δ^{13}C up to 9‰) of the Devede carbonates have been observed, the mechanism controlling the expression of these unique geochemical signatures is still unknown. Geyman and Maloof (2021) have suggested that local processes associated with different settings on shallow carbonate platforms may obscure the record of changes in global seawater carbon isotope compositions, while Prave *et al.* (2022) recently demonstrated the important role that facies plays in contributing to the apparently highly enriched compositions that characterize the Paleoproterozoic Lomagundi event. Motivated by the hypothesis that facies plays a role in the high δ^{13}C values in Tonian carbonates (Figure 1.1; Halverson *et al.*, 2005), this project also examines the potential influence of facies on the Devede carbon isotope record.
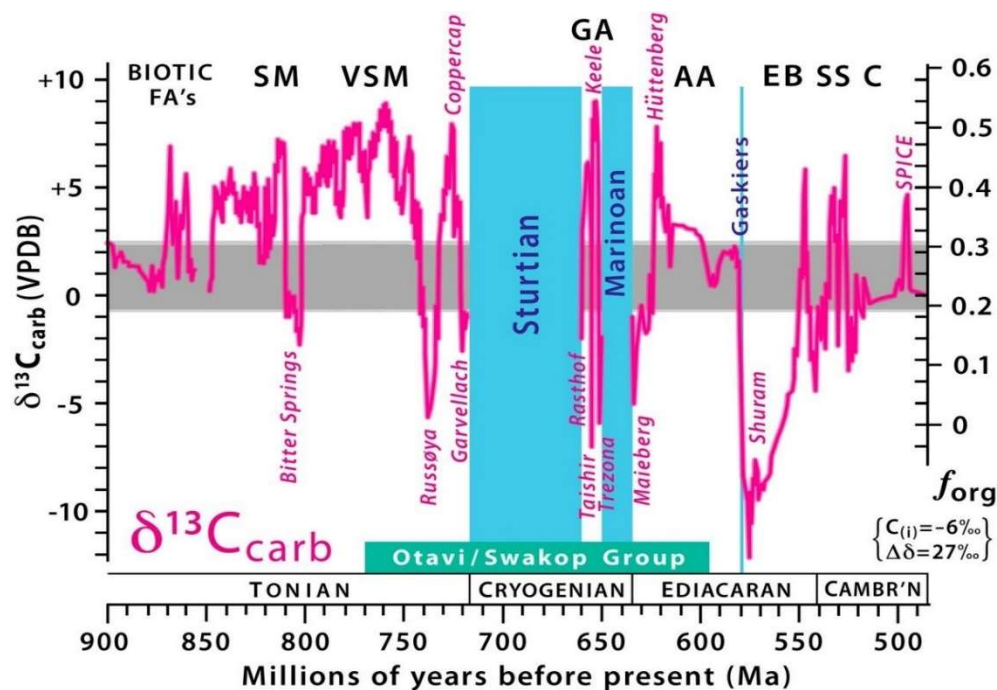
Figure 1.1: Composite δ^{13}C records of marine carbonates deposited between 900 and 490 Ma. Global glaciations are highlighted in blue and the names of major δ^{13}C excursions provided in magenta italics. (modified from Hoffman and Lamothe, 2019)

Though the purpose of this thesis is to explore the late Tonian carbon isotope record in northern Namibia, understanding the evolving ancient landscape and global climatic conditions in the Neoproterozoic is necessary to conceptualize the pre-Cryogenian δ^{13}C record. This chapter will

thus provide an overview of the Neoproterozoic carbon cycle and the interrelationship between the breakup of Rodinia and the Snowball Earth Hypothesis, followed by a review of sequence stratigraphy, its applicability as a correlative tool and the structural evolution of Neoproterozoic carbonate platforms.

1.2   The Interrelationship between carbonate geochemistry and the ocean

1.2.1   Carbon Cycle
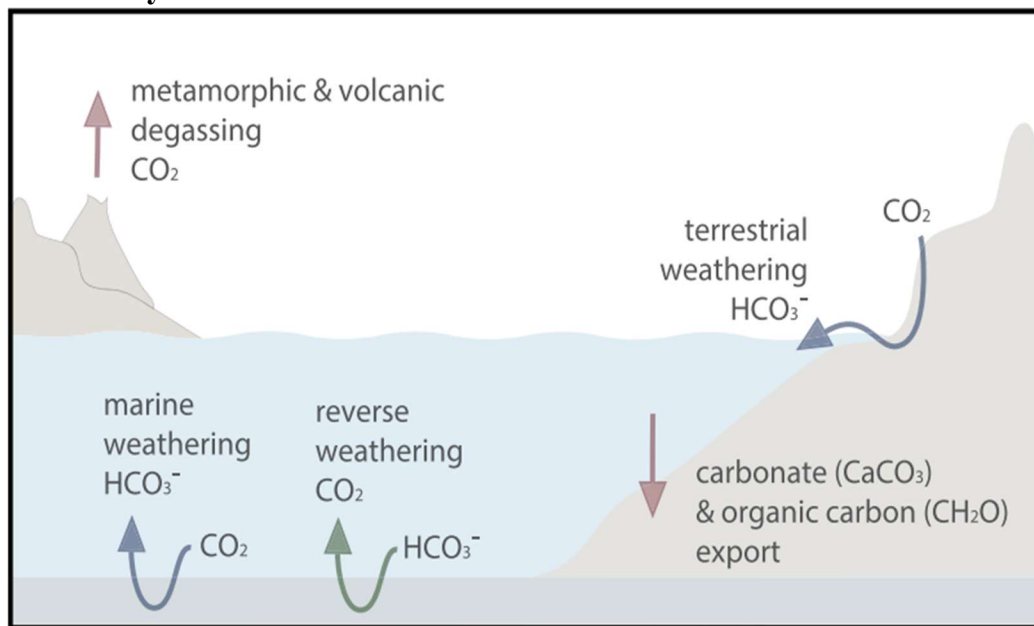
Figure 1.2: A simplified diagram showing the different sources and sinks in the geological carbon cycle (Isson et. al, 2020).

The concept of a closed carbon system was initially proposed by Ebelmen (1845), who hypothesized the balancing of the total global carbon between three distinct reservoirs: the atmosphere, the ocean, and the terrestrial biosphere (Figure 1.2). In its simplest form, the carbon cycle is governed by the interplay between volcanic outgassing, carbonation/decarbonation reactions, and silicate weathering. Ebelmen's theory suggests that in seawaters oversaturated with calcium ions derived from silicate weathering, any outgassed carbon dioxide will be integrated into the marine environment and subsequently deposited on the seafloor as carbonate sediments. These carbonate sediments are considered to be precipitated in chemical equilibrium

with seawater such that their chemical composition can be used as proxies for seawater chemistry (Urey, 1947). The chemical composition of marine carbonates, preserved in their carbon isotopic ($\delta^{13}C$) composition for example, should therefore be representative of the dissolved inorganic carbon pool of the seawater from which they were formed (Zeebe, 1999).

The carbon sequestered in sediments and rocks may also be reintroduced to the environment via metamorphic decarbonation during subduction or uplift and erosion. Consequently, the long-term marine carbon cycle can be portrayed as the interaction between organic carbon, be it particulate and dissolved carbon (POC and DOC), and dissolved inorganic carbon (DIC). There, these two carbon pools are mediated by separate sub-cycles or pumps: the biological carbon pump and solubility pump, respectively.

1.2.1.1   The Solubility Pump

The carbon solubility pump is one of the processes within the global carbon cycle that influences the exchange of carbon dioxide (CO_2) between the Earth's atmosphere and the oceans. It plays a crucial role in regulating the concentration of atmospheric CO_2, which is a key driver of climate change. When atmospheric carbon dioxide dissolves in the surface waters of the ocean, it is transformed to aqueous carbon dioxide $CO_{2\,(aq)}$. Once in solution, the $CO_{2\,(aq)}$ may react with water to form carbonic acid (H_2CO_3). The carbonic acid can further dissociate into bicarbonate (HCO_3^-) and carbonate (CO_3^{2-}) ions. These reactions are summarized in the following equation:

$$CO_{2(aq)} + H_2O_{(aq)} \leftrightarrow H_2CO_3{*}_{(aq)}$$
$$H_2CO_3{*}_{(aq)} \leftrightarrow HCO_3^-{}_{(aq)} + H^+$$
$$HCO_3^-{}_{(aq)} \leftrightarrow CO_3^{2-}{}_{(aq)} + H^+$$

(Eq. 1)
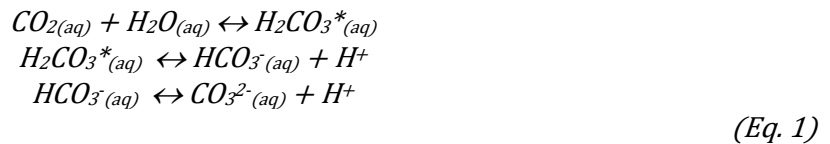
The combined presence of these four carbonate species— aqueous carbon dioxide, carbonic acid, bicarbonate, and carbonate—is referred to as dissolved inorganic carbon (DIC), and the species

may rapidly interchange with each other to maintain chemical equilibrium (Johnson, 1982).

Using the presence of these same carbonate species, Zeebe (1999) proposed the concept of a seawater pH continuum whereby at the mid- and most basic point of this pH continuum, the total dissolved inorganic carbon in seawater is expressed mainly in the form of HCO_3^- and CO_3^{2-}, respectively.

As the surface waters of the ocean are in constant motion due to currents, wind and temperature differences, the downward movement of water drives the dissolved inorganic carbon (DIC) from the surface into deeper ocean waters. Overtime, this transported DIC begins to accumulate and may remain undisturbed in the deep ocean for a very long time. The complementary loop of the solubility pump occurs via upwelling. As waters from the deep ocean return to the surface, the stored DIC may also be transported back into these surface waters, where it can interact with the atmosphere once again.

1.2.1.2   The Biological Carbon Pump

Oxygenic photoautotrophs likely originated early in Earth's history (Hodgskiss et. al, 2019). Much like cyanobacteria today, early cyanobacteria often existed in colonies, forming extensive layered mats or stromatolites where they trapped sediment particles in shallow marine environments. These microbes also had the ability to harness sunlight to combine the carbon dioxide (CO_2) with the surrounding water to produce organic matter (CH_2O), as seen in Equation 2:

$$CO_2 + H_2O + sunlight \rightarrow CH_2O + O_2$$

(Eq. 2)
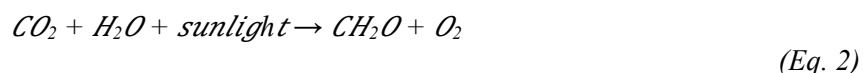
In this process, the natural predilection for $CO_{2\ (aq)}$ containing the lighter carbon isotope (^{12}C) as opposed to the heavier ^{13}C isotope leads to of the fractionation of $^{13}C/^{12}C$ ratios, such that

organic matter is ^{12}C-enriched. After cell death, this organic matter, classified as either dissolved organic carbon (DOC) or particulate organic carbon (POC) depending on its size, then has one of two fates: it will either sink and become incorporated in the sediments, or it will be remineralized back to its original inorganic carbon form as a result of heterotrophic consumption.

1.2.2 The application of carbon isotopes to the Interpretation of Global Carbon Cycle

In an undisturbed state, the biological and solubility carbon pumps regulate carbon concentrations across different reservoirs, maintaining relative stability. Three naturally existing carbon isotopes are present in the global carbon system, existing in specific proportions within each reservoir. The most prevalent of these isotopes are the stable ^{12}C and ^{13}C isotopes. Radiocarbon, or ^{14}C, has a short half-life and is not relevant to carbon isotope studies in deep time applications. Carbonate isotope ratios are expressed in per mil units in standard delta (δ) notation, which is defined according to Equation 3:

$$\delta^{13}C = \left(\frac{^{13}C/^{12}C(sample)}{^{13}C/^{12}C(standard)} - 1 \right) x\ 1000$$

(Eq. 3)

The Pee Dee Belemnite (PDB) or Vienna Pee Dee Belemnite (VPDB) is the international reference standard for stable carbon isotopes, with a ^{13}C/^{12}C ratio of 0.0112372 (Craig,1957; Coplen, 1988). Samples with δ^{13}C values > 0 are commonly referred to as 'enriched', whereas samples with δ^{13}C values < 0 are considered 'depleted' with respect to ^{13}C.

As highlighted in Section 1.2.1, atmospheric CO_2 once dissolved in the ocean, may take the form of either inorganic (C_{carb}) or organic (C_{org}) carbon. The isotopic composition of the former of which closely approximates the composition of the DIC reservoir in the ocean. The carbon isotope composition of organic carbon, $\delta^{13}C_{org}$, is typically significantly ^{13}C-depleted relative to the DIC pool ($\delta^{13}C_{carb} - \delta^{13}C_{org} \approx$ 20–30‰; Hayes *et al.*, 1999). As such, the fraction of carbon

removed from the DIC pool as organic carbon (f_{org}) has a strong control on the $\delta^{13}C$ composition of residual seawater DIC. Consequently, steady state, secular variations in $\delta^{13}C_{carb}$, a proxy for $\delta^{13}C_{DIC}$, are commonly interpreted in terms of the f_{org} term, which represents the fraction of carbon buried in the marine system as organic carbon (Kump and Arthur, 1999). The $\delta^{13}C_{org}$ record can also capture variations in $\delta^{13}C_{DIC}$, but because the fractionation between DIC and C_{org} is large and variable, it is a less precise proxy (Hayes *et al.*, 1999).

The preservation of the distinct inorganic signature in carbonate sediments requires carbonate precipitation, which is partly dependent on the supply of cations via silicate weathering. Silicate weathering refers to the process by which continental (silicate) rocks are broken down as a consequence of chemical dissolution. The reaction pathway for the weathering of calcium silicate minerals is commonly approximated generically as:

$$CO_{2(g)} + H_2O + CaSiO_3 \rightarrow 2HCO_{3\ (aq)}^{-} + Ca^{2+} + SiO_2$$

(Eq. 4)
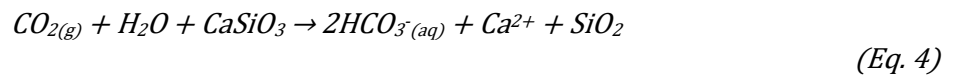
Importantly, other silicate minerals, including Mg-rich minerals, are also subjected to silicate weathering. The process of silicate weathering is strongly implicated in the regulation of global climate since it is temperature dependent, itself linked to CO_2 abundance in the atmosphere, generating a negative feedback. Once dissolved and transported into the ocean via riverine runoff, the bicarbonate and calcium ions (on the right-hand side of equation) must accumulate until supersaturation is reached and calcium carbonates can actively precipitate from the water column. The precipitation as well as the dissolution of calcium carbonate is determined by the following chemical exchange equilibria:

$$CO_{2(aq)} + H_2O \leftrightarrow HCO_{3\ (aq)}^{-} + H^+$$
$$Ca^{2+}_{(s)} + 2HCO_{3\ (aq)}^{-} \leftrightarrow CaCO_{3(s)} + H_2O$$
$$CO_{2(aq)} + H_2O + CaCO_{3(s)}^{+} \leftrightarrow Ca^{2+}_{(s)} + 2HCO_3^{-}$$

(Eq. 5)
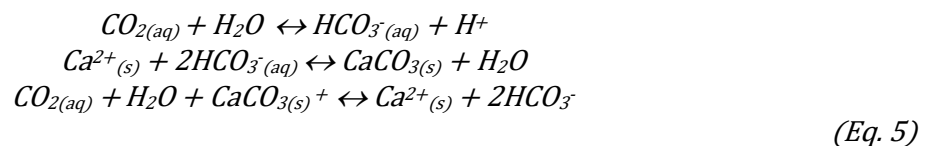
As the carbon cycle functions as a closed system, significant perturbations to one reservoir impact the others. Consequently, fluctuations in carbon content or isotopic composition within the global ocean, can be used to track changes in the global carbon cycle. Variations in $\delta^{13}C$ are particularly useful for Precambrian successions, where large isotopic fluctuations provide a means for correlating otherwise commonly poorly dated stratigraphic successions.

1.2.3   The breakup of Rodinia and the Snowball Earth Hypothesis

Palaeogeographic reconstructions of the Early Neoproterozoic suggest that the continents were arranged in a pre-Pangean supercontinent known as Rodinia (Li *et al.*, 2008). Whilst the precise arrangement of these continents within Rodinia remains a topic of debate, paleomagnetic data and geological evidence indicate that the bulk of Rodinia resided near the equator by the latter Tonian (Meredith et. al, 2017), when the Ombombo Subgroup was deposited. This equatorial positioning, as proposed by Kirschvink (1992), might have contributed to global cooling, potentially resulting in what he termed as "Snowball Earth." The "Snowball Earth" hypothesis suggests that the Earth was completely or nearly entirely covered in ice during multiple glacial episodes for which there exists evidence for low-latitude ice sheets (Kirschvink, 1992; Hoffman *et al.*, 1998b). This hypothesis arose from the appearance of distinct sedimentary glacial deposits and post-glacial cap carbonates on almost every major craton and has been bolstered by paleomagnetic data from multiple cratons (Harland, 1964; Fairchild et. al, 1989; Eyles and Eyles, 1989; Hoffman et. al, 1998a).

Though the mechanisms driving these glaciations have been a subject of ongoing research, many researchers believe that Rodinia's progressive breakup contributed to the profound environmental changes that characterize the Neoproterozoic Era. One of the first major consequences of this rifting, marked by the characteristic 'unzipping' of the Australian and

Laurentian cratons in the formation of the extensive Proto-Pacific ridge system, is pervasive volcanism (Meredith *et. al*, 2017; Meredith *et. al*, 2021). Early Rodinia break-up also appears closely related to extensive plume volcanism, much like the break-up of Pangaea (Lyu et. al, 2017). The abundance of fresh continental basalt over extensive areas of low-latitude, rifting continents, would have led to sharp increases in silicate weathering sufficient to overwhelm the negative silicate weathering feedback and trigger an albedo runaway into a snowball glacial state (Hoffman and Schrag, 2002; Goddéris *et al.*, 2003; Cox *et al.*, 2016; Dufour *et al.*, 2023).

Plate tectonics and volcanic degassing would have persisted throughout the Earth's frozen state, however, the cold climates reduced the hydrological cycle of the snowball events and inhibited weathering, thus permitting a buildup of CO_2 (Berner *et al.*, 1983; Walker *et al.*, 1981; Caldeira and Kasting, 1992). The gradual accumulation of atmospheric CO_2 over millions of years to critical levels sufficient to overcome the radiative effects of the ice albedo likely facilitated atmospheric warming and the onset of melting in low latitudes (Hoffman and Schrag, 2002). At this point, the ice-albedo feedback would have operated in reverse, leading to rapid deglaciation (Caldeira and Kasting, 1992; Hyde *et al.*, 2000; Crowley *et al.*, 2001).

1.2.4 Intrinsic Controls on the $\delta^{13}C$ signatures of shallow water carbonates

Changes in atmospheric carbon levels across geological epochs have been linked to variable climate and ocean conditions, expressed globally in the carbonate $\delta^{13}C$ values of glacial-non-glacial cycles, including the Neoproterozoic "snowball" Earth glaciations. The use of these carbon isotopes as paleoclimatic indicators or correlation tools assumes that the signals preserved in these carbonates faithfully represent primary global ocean conditions. Recent studies, however, challenge this assumption, highlighting how distinct environmental characteristics and processes can generate similar variations in the recorded $\delta^{13}C$ values. Research on the Great

Bahamas Bank Platform and Enewetak Atoll, in particular, have highlighted how local facies control and diagenesis can significantly influence recorded $\delta^{13}C_{carb}$ trends in shallow water environments, potentially disconnecting them from the global carbon record (Geyman and Maloof, 2021; Smith and Swart, 2022). Each carbonate lithofacies, whether ooids, microbialites, skeletal sands, or carbonate muds, reflects a unique depositional environment and biological community. Each of these diverse environments may then impart varying $\delta^{13}C$ signatures owing to differences in carbon sources, biological fractionation, mixing, and diagenetic alteration. The possibility of such large-scale and variable overprinting in recorded $\delta^{13}C_{carb}$ values emphasizes the challenges of understanding these isotopic signals and their relationship to global marine conditions. Additionally, in enclosed basins or lagoons where interaction with the open sea is limited, the influence of localized environmental changes such as increased burial of organic matter or shifts in productivity may be amplified. This local decoupling could lead to the resulting carbonates becoming more enriched with heavier carbon and oxygen isotopes due to evaporation-related Rayleigh fractionation (Gat and Bowser, 1991; Horton *et al.*, 2016). In certain instances, the impact of evaporation might be so significant that covariations between $\delta^{13}C$ and $\delta^{18}O$ in the isotopic records are absent, making it challenging to distinguish global oceanic $\delta^{13}C$ variations from those caused by evaporation (Horton *et al.,* 2016), especially if distinctively evaporitic sediments are not preserved. These challenges underscore the necessity of establishing a thorough, time-calibrated sequence stratigraphic framework within which to evaluate variations in $\delta^{13}C$. This framework, which captures time equivalent facies variations, provides more accurate constraints on local versus global causes of $\delta^{13}C$ variability in the carbonate record, thereby enhancing their value as reliable paleoclimatic indicators and tools for correlation.

1.3 Sequence Stratigraphy

1.3.1 Overview
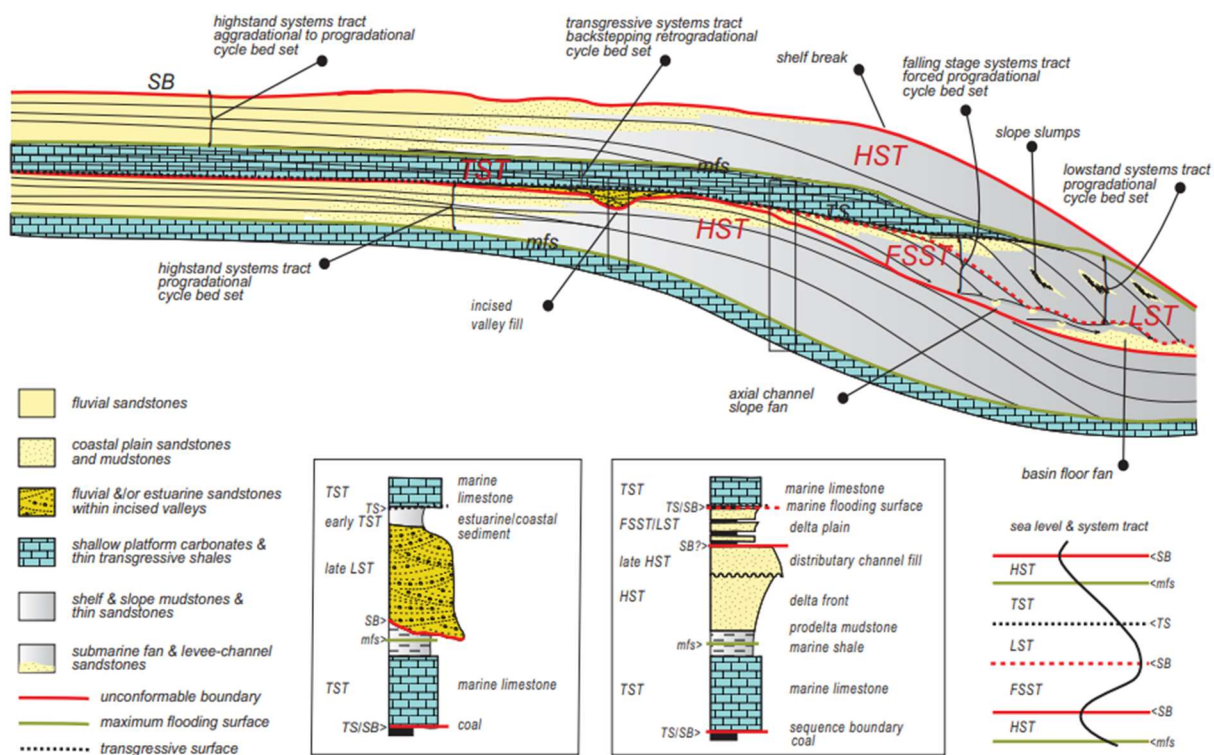
Figure 1.3: Standard sequence stratigraphic model and system tracts for a mixed carbonate-clastic succession (taken from Catuneanu *et. al, 2011).*

Sequence stratigraphy is an approach for interpreting the stratigraphic record that accounts for the stratigraphic geometries resulting from the generation of accommodation space and sediment delivery. These complex sedimentary geometries capture the response of the basin to changing sedimentation rates, tectonically or geodynamically controlled subsidence or uplift, and eustatic sea level fluctuations. Therefore, sequence stratigraphy provides a window into the processes which create the stratigraphy across both temporal and spatial dimensions. Sequence stratigraphic workflows often divides basin sediments into discrete depositional sequences,

whose development are linked to fluctuations in sediment supply and the available accommodation space (Figure 1.3).

Sloss (1963) first coined the term "depositional sequences" to describe traceable, unconformity-bound stratigraphic units that span large continental areas. These unconformities, he suggested, stemmed from prolonged exposure and erosion along basin margins. The relative inland occurrence of these subaerial unconformities, however, precluded the Sloss model's application to contemporaneous marine successions, unless there was an intercalation of shallow marine and non-marine strata. Subsequently, and based on access to extensive offshore seismic stratigraphic data, Vail *et al.* (1977) amended this model to address this constraint. Their revised sequence stratigraphic model redefined depositional sequences as a succession of relatively conformable, distinct, yet genetically related strata bounded by an unconformity and/ its correlative conformity.

A sequence can be subdivided into four phases: the lowstand, transgressive, highstand and falling stage systems tracts which together represent a full relative sea level cycle (Schlager, 2005). These system tracts occur in a specific order, but (i.e., lowstand systems tract, transgressive systems tract, highstand systems tract, and finally falling stage systems tract) no systems tract can appear twice in a single sequence, however not all system tracts must be present in a single sequence. Furthermore, each systems tract is deposited during an interval of consistent shoreline trajectory that reflects the interplay between the supply of sediment and the generation (or loss) of accommodation space (Van Wagoner *et al.,* 1988). Each of these systems tracts is bounded by sequence stratigraphic surfaces that develop as a result of a change in the shoreline trajectory. Each systems tract, therefore, contains a variety of sedimentary facies representing the full range of depositional environments present during a phase of shoreline trajectory. Examples of these

major stratigraphic surfaces include subaerial unconformities and their correlative conformities (i.e., their projection into the marine realm), maximum regressive surfaces, and maximum flooding surfaces. Table 1 provides more thorough definitions of the sequence stratigraphic nomenclature used herein.

Term	Definitions
Accommodation space	The space available for potential sediment accumulation (Jervey, 1998).
Depositional sequence	A relatively conformable succession of genetically related strata bounded at their upper surface and base by unconformities and their correlative conformities (Vail, *et al.,* 1977).
Sediment Supply	The amount of sediment delivered to a particular area or basin during a specific period.
Parasequence	A relatively conformable succession of genetically related beds or bedsets bounded by marine flooding surfaces or their correlative surfaces (Van Wagoner, *et al.,* 1988).
Parasequence set	A succession of genetically related parasequences that form a distinctive stacking pattern that in many cases is bounded by major marine-flooding surfaces and their correlative surfaces
Regression	A seaward movement of the shoreline indicated by a seaward migration of the littoral facies in a given stratigraphic unit (Mitchum, 1977)
Transgression	A landward movement of the shoreline indicated by a landward migration of the littoral facies in a given stratigraphic unit (Mitchum, 1977)
Correlative conformity	A stratigraphic surface that may not represent any hiatus or significant physical interruption in sedimentation. Instead, it corresponds to a time-equivalent surface or layer with consistent and continuous deposition and may serve as a marker for correlating across various stratigraphic sections.
Marine flooding surface	A surface separating younger from older strata, across which there is evidence of an abrupt increase in water depth.
Maximum flooding surface	A depositional sequence indicative of a time of maximum flooding or transgression. This surface also marks the boundary between the transgressive and highstand systems tracts (Posamentier and Allen, 1999; Mitchum, 1977).
Maximum regressive surface	A depositional surface marking the end of regression prior to the first significant flooding event in a sequence. This surface marks the top of the lowstand system tract and the base of the overlying transgressive system tract if present.
Ravinement surfaces	A diachronous erosional surface created by rising sea levels and nearshore marine erosion.

Term	Definitions
Sequence boundary (SB)	A stratigraphic surface that marks the end of one sequence and the beginning of another. In the context of depositional sequences, a sequence boundary corresponds to a subaerial unconformity and its correlative conformity.
Unconformity	A surface of subaerial erosional truncation (and, in some areas, correlative submarine erosion) or subaerial exposure indicating a significant hiatus in deposition.
System tract	Genetically associated stratigraphic units that were deposited during specific phases of the relative sea-level cycle (Posamentier and Vail, 1988)
Falling Stage Systems Tract	Deposits formed during a phase of sea level fall (forced regression) during which the shoreline progrades and downsteps. In nearshore settings, this systems tract commonly consists of reworked shoreline sediments. It is bound below by the basal surface of forced regression and above by a subaerial unconformity or correlative conformity.
Lowstand Systems Tract (LST)	Deposits formed in the initial phases of rising sea levels as the rate of sedimentation exceeds the rate of sea level rise. These normal regressive deposits are bounded by a subaerial unconformity or its corresponding conformity at the base and a maximum regressive surface at the top.
Highstand Systems Tract (HST)	Deposits that form during the later phase of rising base levels, when the rate of sea level rise falls below the rate of sedimentation. These normal regressive deposits are delimited by a maximum flooding surface at the lower end and either a sequence boundary or a composite surface at the upper end.
Transgressive Systems Tract (TST)	These deposits are generated when the rate of sea level rise surpasses the rate of sedimentation, causing the shoreline to backstep. They are delineated by a maximum regressive surface below and a maximum flooding surface above.
Regressive Systems Tract (RST)	A general term for deposits formed during a phase of shoreline progradation. The RST includes the falling stage, lowstand, and highstand systems tracts.
Lithofacies	Sediments with a discrete set of observable physical, chemical, and biological qualities.
Lithofacies associations	A group of coexisting sedimentary facies that characterize a certain depositional environment.

Table 1: Sequence stratigraphic terminologies and concepts

1.3.2   Hierarchy of Sequences

Given that the primary controls on sequence formation — tectonics, eustasy, and sediment accumulation have inherent periodicities — sequence stratigraphy is predicated on the arrangement of sedimentary successions in an ordered hierarchy of cycles defined by discrete stratigraphic surfaces (Vail *et al.,* 1977; Vail *et al.,* 1991). This hierarchical arrangement of sedimentary sequences implies that a lower order sequence may be composed of numerous higher order sequences, each representing a different period or event of sediment deposition.

Parasequences are the smallest recognized sedimentary units within the sequence hierarchy. Though not limited to sequence stratigraphy, the term "parasequence" is commonly considered to approximate shorter 4th to 5th order sequence cycles (0.01-0.5 million years). Parasequences are characterized by a single cycle of sediments bounded by a sharp marine flooding surface. These accumulated sediments exhibit a similar stacking pattern (i.e., either fining or coarsening upwards) and are often associated with short term changes in sea level (Van Wagoner *et al.,* 1988). However, parasequences are defined as being bound by marine flooding surfaces, which may not correspond consistently to a single sequence stratigraphic surfaces. Consequently, their use within a sequence stratigraphic framework can cause confusion.

Third-order sequences commonly consist of multiple parasequences or higher order sequences. These sequences are linked to medium-term eustatic cycles and are frequently distinguished by a unique stacking of depositional systems and facies. A sequence set (2nd order) is a collection of genetically linked sequences that have been deposited over the course of 5-50 million years and often show long-term eustatic cycles. These second and third order cycles showcase typical sequence architecture with the presence of system tracts and sequence boundaries marked by exposure surfaces (Duval *et al.,* 1998). The term supersequence or Sloss sequence is used for the

lowest order sequences. These characterize sedimentary successions that can span millions of years (50-100 million years) and correspond to a single tectonic phase in the evolution of a basin (Vail *et al.,* 1991).

1.3.3   The Evolution of Sequence Stratigraphic Models

Sequence stratigraphy has evolved significantly since it was first introduced by the petroleum industry in the 1970s (Vail, 1977). Many of the refinements within sequence stratigraphy can be credited to the relative timing and placement of the subaerial unconformity and its correlative conformities (Catuneanu, 2002). Despite these advances in the realm of sequence stratigraphy, it is important to note that there is no single model that can be applied to all sedimentary scenarios because the applicability of each existing model varies depending on the tectonic settings, types of data are available, and the spatial scale over which these data are acquired. Here I present an overview of the six sequence stratigraphic models (Figure 1.4), including the three depositional sequence models, the genetic sequence model, and the transgressive-regressive sequence model currently in use.

Key references / Major events	Depositional model II	Depositional model III	Depositional model IV	Depositional model II	Genetic sequence	T-R sequence
Key references	Haq et al. (1987) Posamentier et al. (1988)	Van Wagoner et al. (1988; 1990) Christie-Blick (1991)	Hunt and Tucker (1992;1995) Helland-Hansen & Gjelberg (1994)	Posamentier and Allen (1999)	Frazier (1974) Galloway (1989)	Johnson and Murphy (1984) Embry and Johannessen (1992)
End of transgression	HST	Early HST	HST	HST	HST	RST
	TST	TST	TST	TST	TST	TST
End of regression						
Onset of base level rise	Late LST (wedge)	LST	LST	Late LST (wedge)	Late LST (wedge)	
Onset of base level fall	Early LST (fan)	Late HST (fan)	FSST	Early LST (fan)	Early LST (fan)	RST
	HST	Early HST (wedge)	HST	HST	HST	

Legend: Subaerial unconformity, Correlative conformity, Sequence boundary, Maximum regressive surface, Maximum flooding surface, Basal surface of forced regression, Transgressive ravinement surface. TST - Transgressive systems tract; HST - Highstand systems tract; RST - Regressive systems tract; LST - Lowstand systems tract; FSST - Falling stage systems tract

Figure 1.4: The established sequence boundaries, systems tracts and other associated stratigraphic surfaces for each sequence stratigraphic model taken from Makhubele and Bordy (2021).

Depositional Sequence I

The Depositional Sequence I model centres itself on the establishment of a sequence boundary as defined by a subaerial unconformity and its correlative conformity. According to this model, the sequence boundary develops at the initiation of base level fall.

Depositional Sequence II (Haq et. al, 1987; Posamentier et. al, 1988)

The Depositional Sequence II model maintains the sequence boundary established in Depositional Sequence I and is divided into four distinct systems tracts: highstand (HST), lowstand (LST), transgressive (TST), and shelf margin systems tracts (SMST). To address concerns regarding the correlative conformity at the base of the lowstand fan in Depositional Sequence I, this model identifies two sequence types based on the level of erosion below a subaerial unconformity and its downward reach. The initial sequence type, referred to as Type 1, is marked by a subaerial unconformity extending to the edge of the shelf. In contrast, Type 2 sequences are characterized by subaerial unconformities confined to the basin margins. These sequences also feature the shelf margin systems tract (SMST), situated above the sequence boundary, and subsequently covered by a transgressive surface.

Depositional Sequence III (Van Wagoner et. al, 1988; 1990)

The Depositional Sequence III model addresses some of the drawbacks found in Depositional Sequence II by combining sequence types 1 and 2 and shifting the sequence boundary to the end of base level fall. Moreover, this revised model removes the shelf margin systems tract, and integrates the earlier lowstand fan deposits into the late highstand systems tract.

Depositional Sequence IV (Hunt and Tucker, 1992; 1995; Helland-Hansen and Gjelberg, 1994)

The Depositional Sequence IV model originated from the understanding that forced regression occurs when base level drops. Plint (1988) and Hunt and Tucker (1992) introduced the term

falling stage systems tract (FSST) as a means to integrate this dynamic within the sequence stratigraphic framework. This proposed systems tract is demarcated by the basal surface of marine erosion at its lower boundary. Its upper limit is defined by a subaerial unconformity while its corresponding conformity sits at the base of the redefined lowstand systems tract. This redefined lowstand systems tract begins during the latter phases of base level decline and extends into normal regression during the early stages of base level rise.

The Genetic Stratigraphic Sequence (Frazier, 1974; Galloway, 1989)

In contrast to the depositional sequence models, the genetic stratigraphic sequence model places an emphasis on maintaining the stratigraphic integrity of three-dimensional depositional systems rather than relying on the development of subaerial erosion surfaces brought on by eustatic sea level changes. Instead, the sequence boundaries of Galloway's (1989) genetic sequences are defined by the maximum flooding surface, which separates the transgressive systems tract below from the highstand systems tract above. This approach is particularly useful in studying drill hole data where gamma ray logs are available, because these readily pick out both the maximum flooding and the maximum regressive surfaces. Much like the structure of Depositional Sequence II, though, the flooding surface-bounded sequences within the genetic model are subdivided into four systems tracts: the early lowstand, late lowstand, transgressive and highstand systems tracts.

The Transgressive-regressive (T-R) sequence (Johnson and Murphy, 1984; Embry and Johannessen, 1992)

The Embry and Johannessen's (1992) T-R sequence model presents an alternative approach to defining depositional sequences and addresses some of the limitations in existing depositional and genetic sequence models. Their T-R sequences are defined by composite surfaces consisting

of subaerial unconformities or ravinement surfaces and their corresponding maximum regressive surfaces. In marine basinal settings, maximum regressive surfaces are used to delineate the sequence boundary as opposed to correlative conformities because it is easier to detect in shallow marine settings using variable outcrop and subsurface data. In nonmarine settings, the subaerial unconformity serves as the sequence boundary because it represents a critical pause in sedimentation. The T-R sequence model identifies only transgressive and regressive systems, separated by a maximum flooding surfaces. This model is most widely used in outcrop studies and is particularly useful where identification of falling stage systems tracts associated with a drop in base level is not necessary.

1.3.4 Sequence Stratigraphy as a Correlative Tool

The use of sequence stratigraphy at the local or regional scale serves as a powerful tool for both facies analysis and regional correlation. The recognition of major stratigraphic surfaces, such as sequence boundaries and system tracts, assists in the identification and correlation of stratigraphic units with comparable facies across regions, even in areas separated by considerable distances. Furthermore, this graphical representation of the spatial distribution of discrete facies and their lateral transitions allows for more accurate interpretations of paleogeographic settings and reconstructions of ancient landscapes, contributing to a better understanding of regional geological history. Should these sequences transcend regional domains, their corresponding sequence boundaries, serving as temporal indicators, facilitate the correlation of stratigraphic units across continents or basins. These interconnected sequences, often characterized by unique stacking patterns and facies distributions linked to various phases of basin subsidence, uplift, and sediment infill across the different basins, shed light on Earth's geological history. They unveil major shifts in basin architectures prompted by global environmental events, like fluctuations in

sea levels. Consequently, this approach aids in interpreting the evolutionary history of individual basins and significantly enriches our understanding of Earth's historical trajectory. Furthermore, the application of sequence stratigraphy as a method for correlation goes beyond its geological significance. In fact, it acts as a foundational framework for multiple fields, including paleoclimatology, paleoceanography, and hydrocarbon exploration (Feng et. al, 2015). The capacity to connect stratigraphic sequences across extensive geographical areas allows geologists to deduce past climatic variations, oceanic conditions, and the distribution of resources, making it a valuable tool in studying the ancient stratigraphic record.

1.4 Precambrian Carbonate Systems

1.4.1 The evolution of Carbonate Precipitation Styles

Based on the assumption that the chemical composition of carbonate sediments serves as a reliable proxy of ancient open-ocean seawater, the identification and preservation of the different sedimentation patterns and styles provide a record of Earth's evolving surface conditions. It follows then that these rocks can be used to reconstruct and track variations in not only the global carbon cycle, but also sea level and the biosphere over more than 3 billion years (Schidlowski, 1987).

Early in Earth's history, marine carbonate precipitation was largely restricted to the neritic zone and occurred abiotically via direct precipitation onto the seafloor (Grotzinger and Kasting, 1993). Throughout the Archaean, a combination of high atmospheric CO_2 concentrations and seawaters enriched with Mg^{2+}, Fe^{2+} and Ca^{2+}, facilitated the widescale formation of massive abiogenic carbonate precipitates across the seafloor. As a result, localized carbonate sediments in shallow

marine settings were characterized by upward-divergent crystal fans, cement beds, isopachous encrustations, and occasional marine tufas (Grotzinger and James, 2000).

The emergence of photosynthetic cyanobacteria in the late Archaean to Paleoproterozoic, combined with increasing atmospheric and marine oxygen levels, resulted in a gradual decline in this style of direct seafloor precipitation (Higgins *et al.,* 2009; Cantine *et al.,* 2020). In Precambrian shallow marine carbonate platforms, microbial mats—likely supported by cyanobacteria but comprising diverse groups of interconnected microorganisms—captured carbonate sediments and triggered in situ carbonate precipitation. This process resulted in the development of distinct layered structures known as stromatolites, which are a common sedimentological feature of the Precambrian. With the proliferation of stromatolites into the middle Proterozoic, extensive carbonate platforms and ramps with similar architecture to those seen today in the Phanerozoic developed, despite the different processes driving carbonate precipitation (Grotzinger, 1989).

The Precambrian-Cambrian boundary (around 539 Ma; Linnemann *et al.,* 2019) marked a critical transition in Earth's history. The emergence of more complex multicellular life forms during this transitional period influenced environmental conditions and the resulting sedimentation style with a transition from abiotic and microbial carbonate production to extensive carbonate precipitation by animals and algae. This transition resulted in a first-order shift in the style of carbonate precipitation on carbonate platforms, with organisms like calcareous algae, archaeocyathids, and various other invertebrates contributing large amounts of carbonate sediments, while stromatolites receded as a major source of carbonates (Knoll, 2003; Wood, 2003).

1.4.2 Precambrian Carbonate Platforms

The formation of Precambrian platforms is commonly linked to the process of continental rifting and the breakup of supercontinents. Rift basins that formed in warm, shallow marine environments were conducive to carbonate deposition, allowing for the establishment of carbonate platforms in areas not swamped by siliciclastic sediment from proximal continental topography. Carbonate platforms are largely classified into two types: carbonate ramps and rimmed platforms. Carbonate ramps are defined as gently inclined platforms (typically less than 1°) that descend from a shallow-water shoreline or lagoon into a deeper-water basin environment without any significant break in the slope (Read, 1982; Burchette and Wright, 1992). Read (1982; 1985) redefined the idea of carbonate ramps by introducing two classes of ramps: homoclinal and distally steepened ramps, based on unique slope characteristics. While homoclinal ramps fit the broad description of carbonate ramps and geometrically resemble siliciclastic shelves, distally steepened ramps are defined by a large increase in slope near the seaward side of the deep ramp, as well as an abundance of debris flow deposits (Read, 1982). Rimmed carbonate shelves, on the other hand, are defined as shallow, nearly flat platforms with a semi-continuous to continuous rim or barrier along its outer margin and a steep slope (often up to 60 ° or more) into deep water (Ginsburg and James, 1974).

Precambrian carbonate platforms, regardless of their morphologies, were subject to the same short-term tectonic controls that govern the periodicity and growth of more modern platforms. Changes in accommodation space as a consequence of varying sea levels and the prevailing tectonic regime, resulted in the development of a variety of sedimentary basins, each characterized by differing styles of subsidence and distinct stacking patterns. It is this intricate interplay between tectonics and eustasy which facilitated progressive morphological transitions

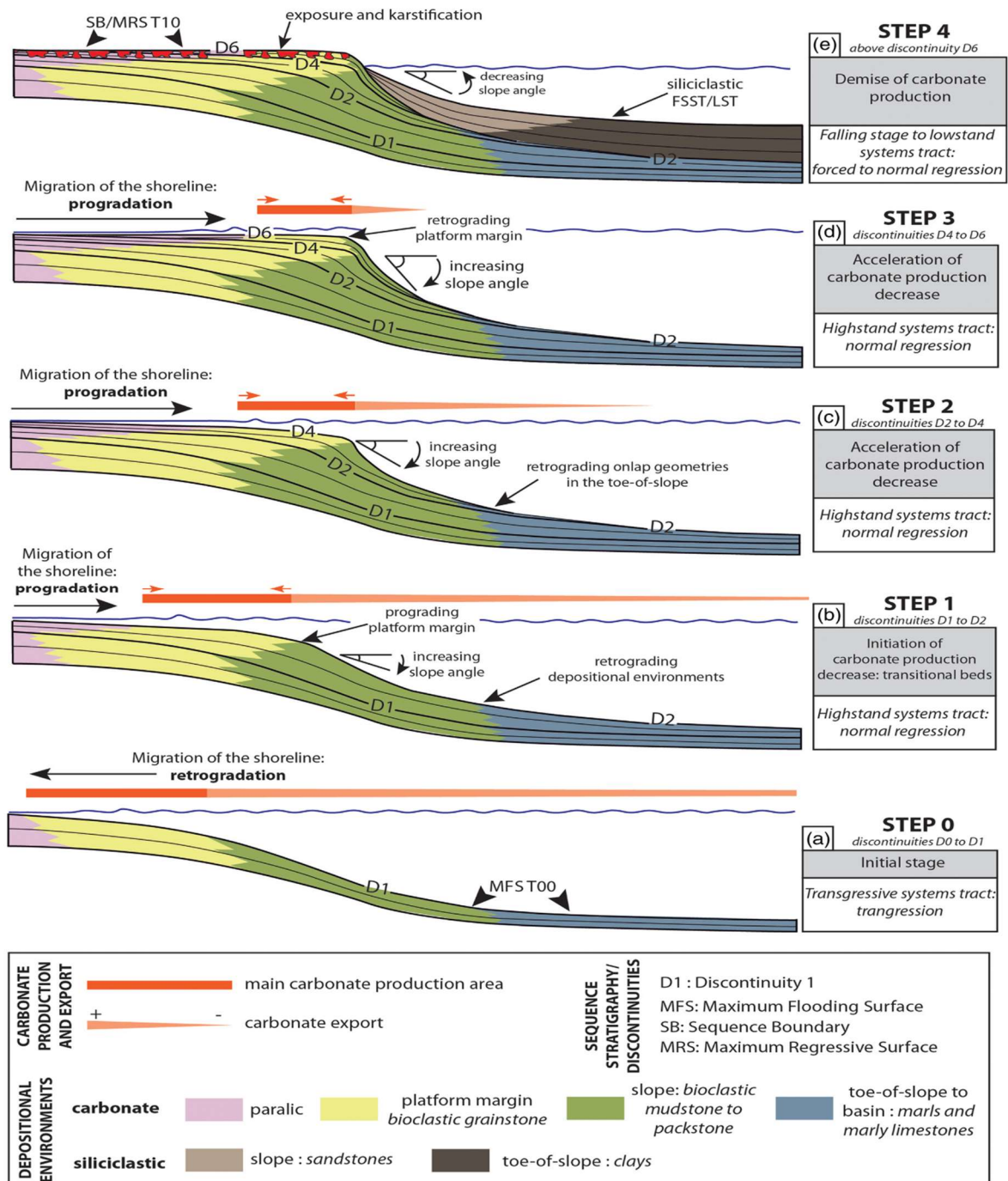from initial distally steepened ramps to rimmed platforms as seen in Figure 1.5 (Grotzinger, 1989).

Figure 1.5: Sequence stratigraphic model for the stepwise evolution of carbonate platforms (taken from Andrieu et. al, 2022)

Precambrian carbonate ramps (Figure 1.6), much like their Phanerozoic counterparts, were characterized by gentle slopes that displayed distinct facies zonations ranging from deep (below wave base) to shallow-water (intertidal) to supratidal settings. These deeper ramp settings were distinguished by the appearance of fairly fine-grained sediments like shale, banded iron formations, and micritic carbonate deposits, whilst the shallower ramp settings featured extensive stromatolite reefs. These stromatolites display a range of morphologies, spanning from thick, intricately branched columnar structures to thin sheets of small dome-shaped knolls and microdigitate low-relief columns, typically corresponding to decreasing depth profiles. Whilst much of the intertidal sequences were characterized by stromatolites, largely stromatolite-free tidal flats developed in the more proximal inner ramp settings and resulted in the development of a peritidal grainstone facies.
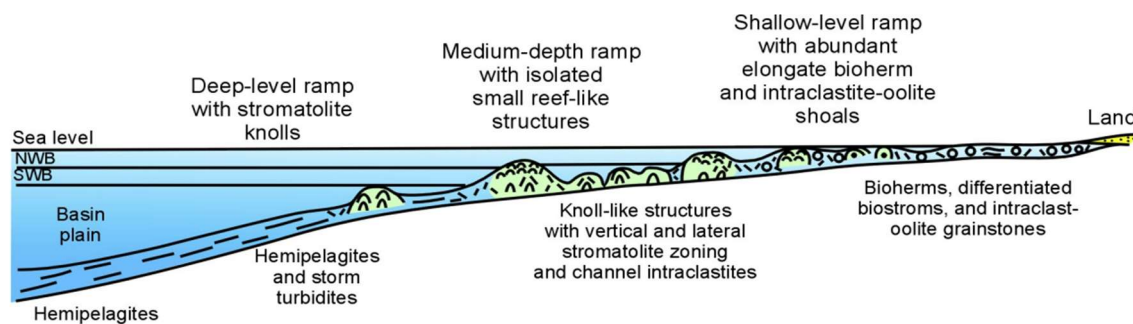
Figure 1.6: Proposed morphological structure of a distally steepened ramp in the Meso-Neoproterozoic basins. These carbonate ramps were characterized by a linear intrashelf and reef-like system of open carbonate shelf (taken from Khabarov, 2011).

Under highstand conditions, the aggradation of stromatolites in distal ramp settings can lead to the formation of a barrier reef. This barrier reef complex, composed of thick stromatolite accumulations with minor grainstones, separates a deepwater basin environment from its shallower inner platform counterpart. Consequently, Precambrian rimmed platforms, depicted in Figure 1.7a and b, were often characterized by four main depositional settings: a deepwater basin, foreslope, barrier reef, and inner platform.

The outer edges of these platforms featured a lateral transition from foreslope deposits, characterized by interbedded carbonate rhythmites, shales, and rare gravity flow megabreccias, to basinal deposits of primarily fine-grained siliciclastic and carbonate muds. Given the variability in basin dynamics, the facies observed in the inner platform settings were diverse. Barrier reef complexes could have transitioned laterally into back-reef biostromes, shoal-complexes featuring peritidal stromatolites and other microbial sediments, or shifted abruptly into a narrow lagoonal environment. Where shoal-complexes developed, there was a subsequent shift into a geographically extensive but environmentally restricted lagoonal facies.
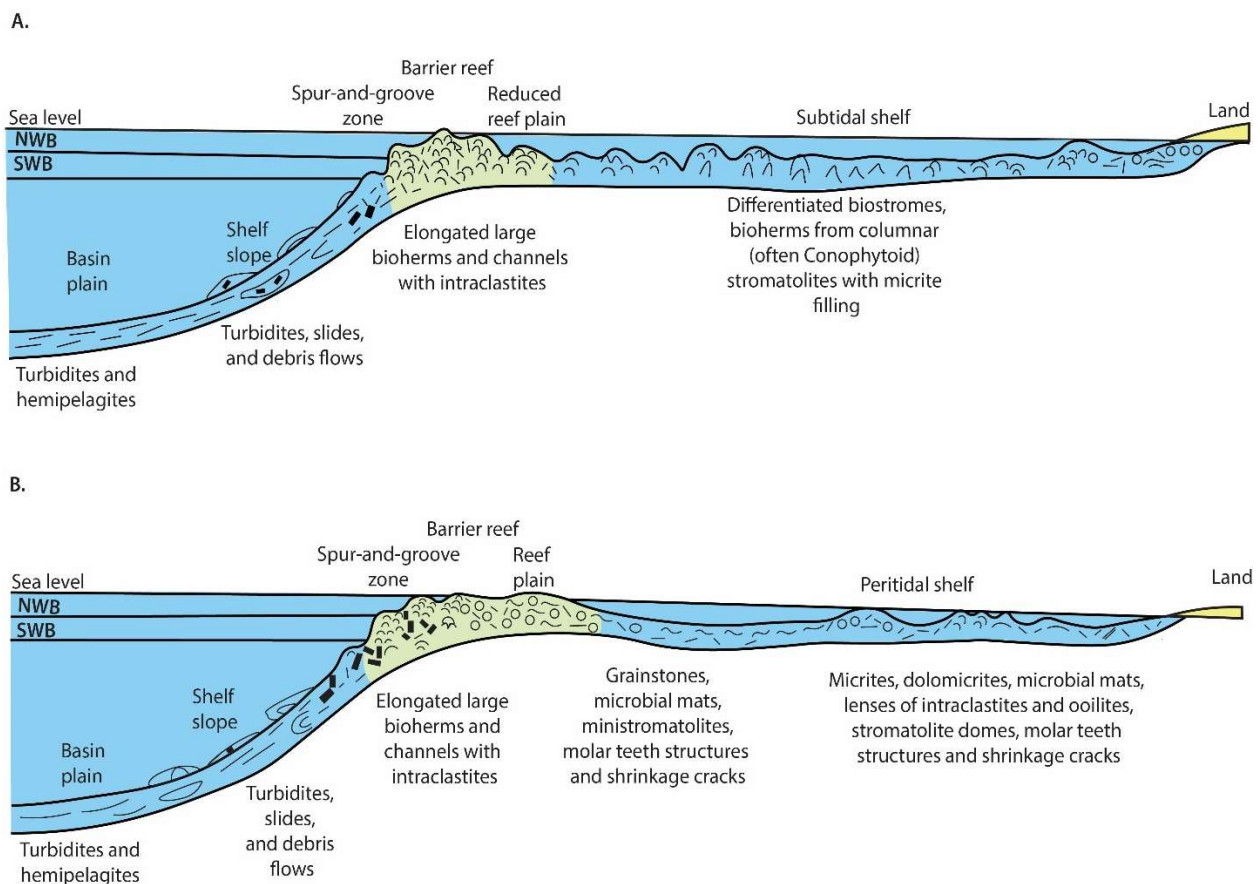
Figure 1.7: Proposed morphological structure of reef and reef-like systems in the Meso-Neoproterozoic basins. A) Rimmed carbonate platform with a wide peritidal inner shelf and a stromatolite barrier rim forming a shelf edge, and B) Rimmed carbonate platform with a wide subtidal inner shelf and a stromatolite barrier rim coinciding with the shelf edge (modified from Khabarov, 2011).

CHAPTER 2

2.1   Introduction

The Neoproterozoic Era (1000 to 541 million years ago) represents a time of major transitions in Earth and life history. During this era, several noteworthy events unfolded, including the global reconfiguration of continents (Hoffman, 1999), the persistence of harsh climatic conditions related to global glaciation or "Snowball" events, a widespread rise in environmental oxygen levels (Fike *et al.,* 2006; Campbell and Squire, 2010; Lyons *et al.,* 2014), and the emergence and diversification of complex organisms (Xiao and Laflamme, 2009). The Tonian, the first period of this era, was characterized by the widespread rifting of the Rodinia supercontinent, and subsequent creation of a series of rift basins. Gradual subsidence of these rift basins facilitated the establishment of extensive carbonate platforms. These platformal carbonates precipitated in or near isotopic equilibrium with the surrounding seawater (Urey, 1947). As a result, variations in atmospheric carbon dioxide levels linked to changes in climate and ocean conditions would have left distinct carbon isotopic (δ^{13}C) signatures in these carbonates. By examining interbedded volcanic ash beds and distinct biological assemblages of these carbonates, researchers can then establish a chronological record of Earth's climatic evolution.

A significant challenge, however, is the globally poor preservation of rock strata and the scarcity of associated biostratigraphical and/ radiometric data. The absence of these correlative tools has made it difficult to determine the ages of not only rock formations but also specific time intervals within the Precambrian (Halverson *et al.,* 2018; Lamothe *et al.,* 2019). Nevertheless, the exceptional preservation of the Otavi Group platform sediments in Namibia, facilitated by the

region's arid to semi-arid landscape, offers an excellent opportunity to gain insights into this dynamic period.

The Otavi Group is characterized by two distinct glaciogenic deposits (Hoffmann and Prave, 1996) and a carbon isotope record with several carbon isotopic excursions. Interestingly, its middle to late Tonian (ca. 800–750 Ma) carbon isotopic record shows very muted $\delta^{13}C$ variations, despite the prominence of high $\delta^{13}C$ values. Partly resulting from the limited structure to the $\delta^{13}C$ record, the middle–late Tonian geological record remains relatively poorly time-calibrated (Halverson *et al.*, 2022).

The ca. 760 Ma Devede Formation, the oldest carbonates of the Otavi Group, predates the first Neoproterozoic Snowball Earth event and serves as an important archive of not only the fragmentation of Rodinia but also the changing climatic conditions as Earth transitioned into these glaciations. Although fluctuations in the carbon isotopic record – seemingly unrelated to glaciations – have been observed in this formation, the mechanism controlling the expression of these geochemical signatures is still unknown. Consequently, in an effort to clarify the early depositional history of the Tonian aged platform strata found throughout the Kaoko Belt, high resolution stratigraphic logs were made across northern and southern exposures of the Devede Formation.

This chapter presents the published and unpublished carbon isotope data from measured sections of the Devede Formation. Lithological variations across these measured sections are analyzed and used to establish a facies model for the Devede Formation, which in turn facilitates development of a sequence stratigraphic interpretation of this unit. Observed facies changes are then combined with chemostratigraphic data and used to investigate the stepwise evolution of the rift basin.

2.2 Geological Setting

The Neoproterozoic rocks of northwestern Namibia occur in two orthogonal orogenic belts: the Kaoko and Damara belts. Within this domain, eleven major tectonostratigraphic zones have been defined (Miller, 2008). The study area lies within the Otavi Fold Belt (Figure 2.1), which comprises Miller's Northern Platform and Northern Margin zones. This ~750 km arculate fold belt extends as far northwest as the Angola border and east to the Otavi Mountainland (Miller, 2008). The Otavi Group was deposited in sedimentary basins that formed as a result of the rifting associated with the break-up of Rodinia.
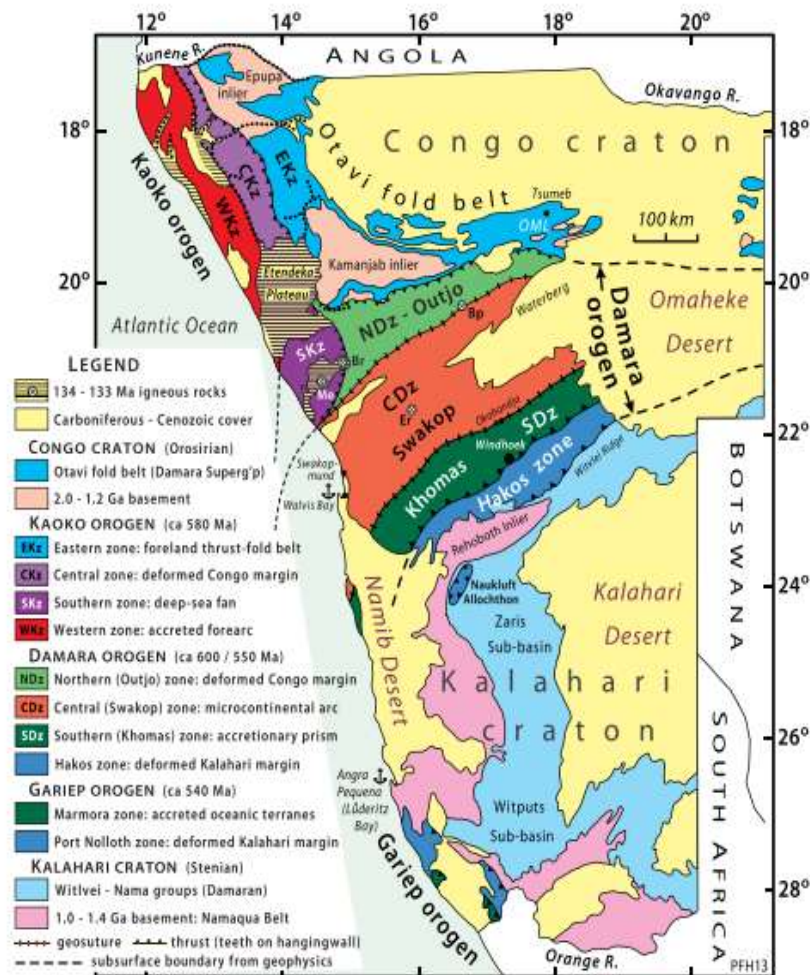

Figure 2.1: The tectonostratigraphic zones, belts, and inliers of Namibia (taken from Hoffman et. al, 2021)

North-south crustal stretching linked with the early breakup of the supercontinent Rodinia resulted in the formation of a rift basin along the southern margin of the Congo craton. The earliest rift-related deposits in this developing rift basin were the siliciclastics of the early Neoproterozoic Nosib Group (Miller, 2008). Likewise, the east-west Makalani Ridge, a basement high arising from south-dipping normal faulting, developed as episodic rifting persisted through to the late Tonian (ca. 900–720 Ma). This ridge marks the southern limit of the ca. 780–755 Ma Ombombo Subgroup. To the north of the Makalani Ridge, a large carbonate platform comprising mainly the Devede Formation of the middle Ombombo Subgroup, developed Makalani sub-basin. As a result of continued, episodic uplift of the ridge, carbonate deposition was punctuated by northward shedding of siliciclastic sediments from the Makalani high. Extension continued into the Cryogenian Period but migrated south, localizing the basin margin on the Huab Ridge during deposition of the Abenab Subgroup, which unconformably overlies the Ombombo Subgroup and extends further south (Figure 2.2). The latest Tonian Ugab Subgroup, which is found only south of the Huab Ridge, post-dates the Ombombo Subgroup and manifests the southward migration of the zone of extension.
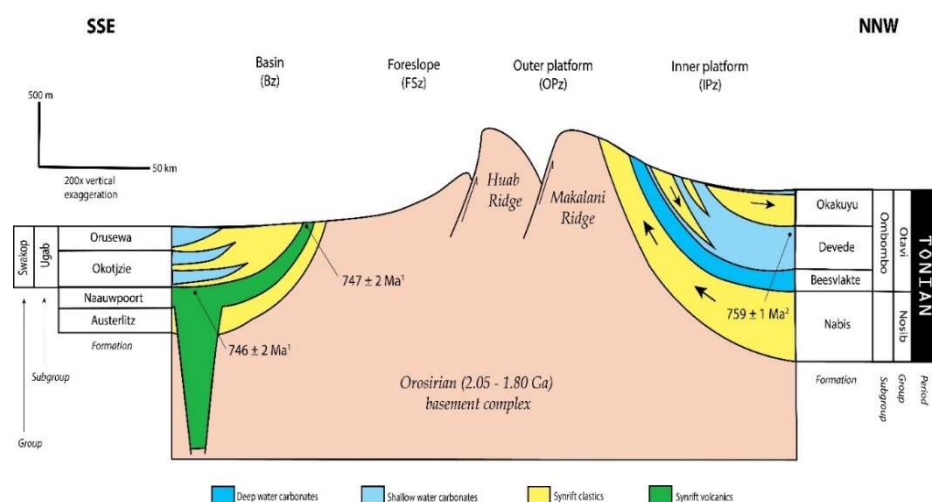

Figure 2.2: A generalized cross-section of the Otavi Platform at the end of the Tonian Period (modified from Hoffman et. al, 2021). Arrows indicate paleoflow direction. Radiometric dates are from the following references: 1: Hoffman et al. , 1996; 2: Halverson et al. , 2005.

The basal Abenab Subgroup comprises the Sturtian-aged, glaciogenic Chuos Formation. Rifting largely ceased by ca 650 Ma, with the Gruis-Ombaatjie contact in the Abenab Formation broadly marking the rift-drift transition (Halverson *et al.,* 2002). The upper Abenab Formation is bound by a disconformity which corresponds to the onset of Marinoan glaciation. Marinoan glacial deposits are assigned to the Ghaub Formation, which is only patchily preserved on the platform but can be very thick in foreslope deposits south of the Huab Ridge (Domack and Hoffman, 2011; Hoffman *et al.,* 2021). The Ghaub Formation is the basal unit of the Tsumeb Subgroup, the remainder of which comprises a thick succession (<2 km) of platform carbonates. Progradation of the carbonate platform to the south resulted in shedding of carbonate debris into the deep Otavi sub-basin (Hoffman and Halverson, 2008).

2.2.1   The Ombombo Subgroup

The dominantly carbonate Ombombo Subgroup records the development of a carbonate platform situated north of the prominent Makalani Ridge rift shoulder (Figure 2.2). Classification of the carbonate facies in the Ombombo Subgroup follows a modified version of the Halverson et. al (2002) and Hoffman and Halverson (2008) scheme (see Table 2 for the corresponding definitions). The Ombombo Subgroup is patchily underlain by a series of fluvial sandstones and occasional alluvial fan conglomerates belonging to the Nabis Formation. The Nabis Formation, which rests nonconformably on ca. 1.9 Ga Congo craton basement, is inferred to be approximately 900-760 Ma, but it has never been directly dated (Miller, 2008). It is inferred that the Nosib Group formed as a result of the southward shedding of terrigenous sediments during the early rifting and extensional phases of basin development, which is also manifested in the Zambia-Congo Copperbelt to the northeast (Miller, 2008). The contact between the Nabis Formation and the Ombombo Subgroup is a sharp flooding surface.

The Ombombo Subgroup consists of three formations (from bottom to top): the Beesvlakte, Devede, and Okakuyu (Hoffmann and Prave, 1996; Hoffman and Halverson, 2008). Paleocurrent measurements from clastic sediments in the lower Devede Formation indicate a northward flow direction, consistent with these sediments originating from the uplifting of the Makalani Ridge to the south. (Hoffman and Halverson, 2008).

The Beesvlakte Formation is approximately 200 meters thick and consists mainly of fine-grained siliciclastic and carbonate sediments. It can be divided into three distinct lithological members: a lower unit with pebble sandstones, siltstones, and phyllitic shale, a middle unit featuring laminated dolomites and cherty, sericitic dolomite units capped by microbialaminates, and an upper unit of recessive marble tectonite that gradually transition into the basal Devede Formation.

The overlying Devede Formation consists of ~400 m of predominantly dolomitic cyclical carbonates (Halverson *et al.,* 2005; Hoffman *et al.,* 2021). The lowermost carbonates are sometimes interrupted by the deposition of northward waning siliciclastic layers. The upper section of the formation, on the other hand, features abundant *Tungussia-type* stromatolites, marine cements, bladed gypsum pseudomorphs, nodular anhydrites, and magnesite (Hoffman and Halverson, 2008; Hood *et al.,* 2015; Stacey *et al.,* 2023). The Devede Formation is unconformably overlain by the Okakuyu Formation,

The Okakuyu Formation can be subdivided into two informal members: a clastic lower half and a dominantly carbonate upper half. In the lower clastic portion, cycles displaying a vertical transition from siltstones to sandstones and conglomerates are thought to reflect deltaic deposition. Conversely, the upper carbonate portion is defined by a thick cliff-forming

stromatolitic dolostone indicating brief restablization of the carbonate platform (Hoffman and

Halverson, 2008).

	Facies	Description	Depositional Environment
Shallowest ↑ *Shoaling*	Microbialaminate	Thin, crinkly laminated carbonate sediments, typically planar but may form low relief mounds. May have sedimentary structures that suggest a shallow depositional environment such as tepee structures and breccias	Intertidal to supratidal zone
	Grainstone	Carbonate sands. Fine to medium-bedded, tabular to irregular. Often display dark-colored silicification, likely due to the high primary permeability, which occasionally preserves giant ooids and crossbedding.	Sub- to lower intertidal zone, under influence of waves and/or tidal currents
	Stromatolite	Mounded microbial growth structures, often Tungussia-type columnar stromatolites with divergent branching patterns, and pinkish color. Conophyton-type stromatolites may also be present.	Sub-tidal to intertidal zone.
	Cement-breccia	Disrupted or brecciated, laminated dolomite beds that have been extensively cemented. May contain a variety of sedimentary structures including oncoids, sheet cavities, carbonate shrubs, shrinkage cracks, tepee structures and breccia horizons. Closely associated with stromatolites.	Sub-tidal zone
Deepest	Ribbonite	Finely laminated silt to fine-sand-sized carbonate laminae to thin beds showing low angle cross-stratification, minor scour surfaces, and occasional ripple cross lamination, with interbedded carbonate mud (marly ribbonite)	Sub-tidal, mid-shelf, influenced by storm waves.
	Rhythmite	Parallel-laminated carbonate muds; may also contain thin turbidites	Below storm wave base

Table 2: Carbonate lithofacies classification scheme of Hoffman and Halverson (2008) updated with the cement-breccia facies described by Hood et al. (2015).

2.2.2 Devede Formation Stratigraphy

The Devede Formation is predominantly found in the Otavi Fold Belt within the Kaokoveld region of Namibia. The Otavi Fold Belt stretches laterally from the eastern Owambo Basin in the east to the Sesfontein Thrust in the west. Its northern and southern bounds are delineated by the Epupa and Etendeka Inliers, respectively. Recent studies of the Devede Formation by Hood *et. al* (2015) have highlighted lithological variations in the Devede Formation observed across the northern and southern Kaokoveld region. This section provides a general overview of the stratigraphy of the Devede, and the spatial variability encountered in the Kaokoveld region.

2.2.2.1 Southern Kaokoveld

In the southern Kaokoveld (*Figure 2.3*), the Devede Formation can be divided into two informal members based on lithology: a lower member, comprising mixed clastics and carbonates, and an upper member, which consists of almost pure carbonate. Shallow-water shales, sands, conglomerates, and microbially laminated carbonates in the lower Devede Formation are arranged in meter–decameter scale parasequences. The clastic parasequences, which consists of dark brown to grey siltstones, fine to coarse grained feldspathic sandstones, and conglomerates with well-rounded clasts of basement rocks, are confined to the first 125 to 150 m of the Devede Formation. These siliciclastic sediments form a northward-thinning tongue and are characterized by mud-cracks, inverse and normal grading, well-developed trough crossbedding, symmetrical and starved ripples, occasional load structures and sedimentary dikes. Consequently, these siliciclastic lithofacies, are interpreted to record the downslope transportation of terrigenous sediments during the episodic uplift of the southern Makalani Ridge.
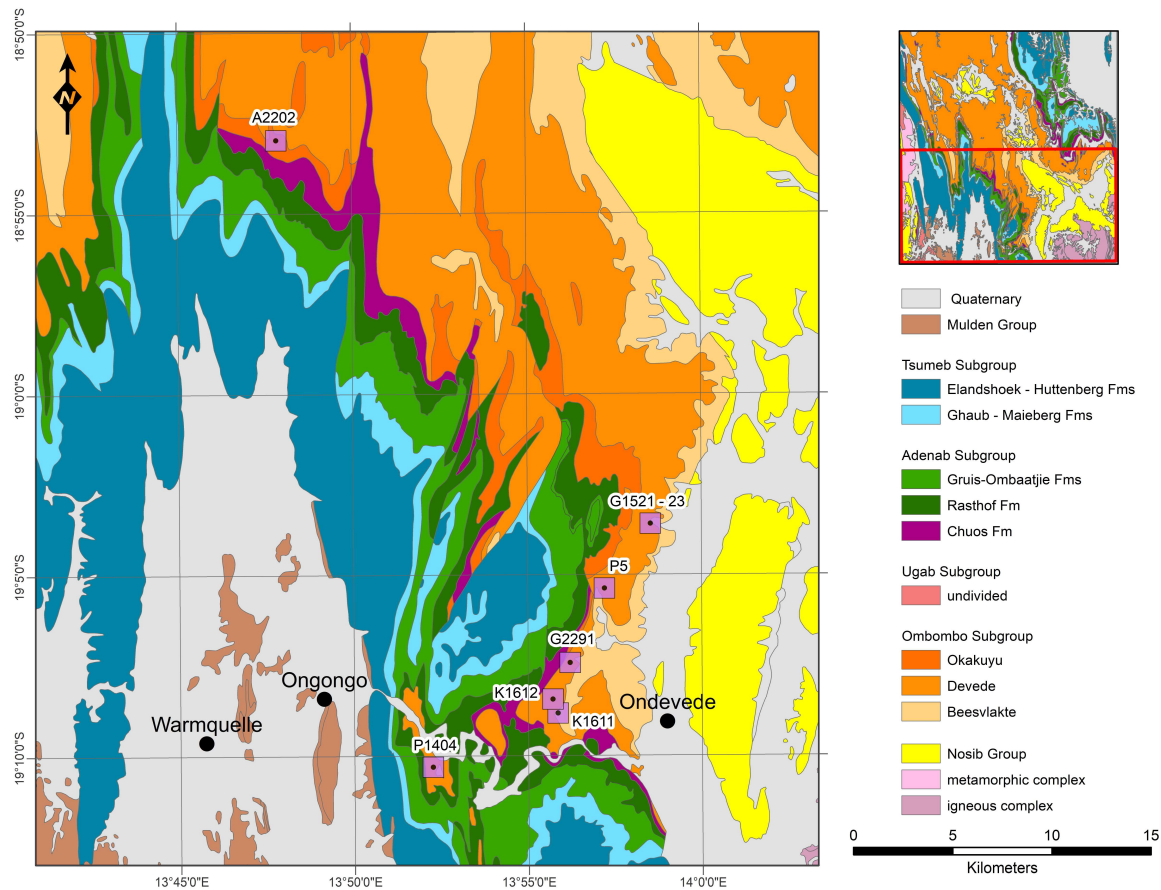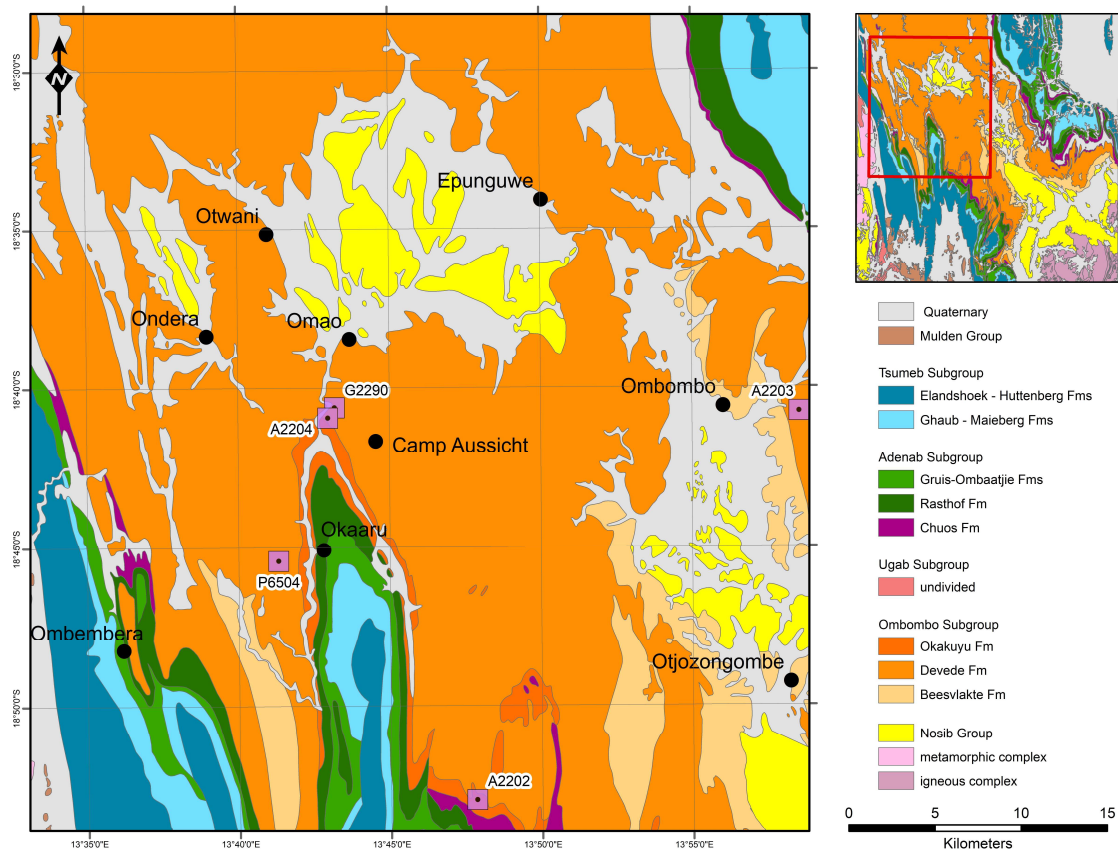
Figure 2.3: Geologic map of the Southern Kaokoveld modified from Hoffman and Halverson (2008). Measured sections are denoted as purple boxes. Inset map in top right corner the grey area shows the location of the Southern Kaokoveld study area in relation to the larger Kunene Region.

The upper Devede member is distinguished by the presence of a thick *Tungussia-type stromatolite* biostrome. The upper member is arranged in deca- to hectometer coarsening upward carbonate cycles. At the most southern extent of the Kaokoveld, these cycles appear initially with decameter-thick interbeds of ribbonites and grainstones, before ultimately transitioning into a 75-m thick grainstone unit. Further north, this upper member is predominantly arranged in shale-ribbonite-stromatolites cycles with occasional microbialaminite carbonate caps. The uppermost strata of this member are expressed as a northward transition from interbeds of Tungussia and ribbonites to pure ribbonites, rhythmites and shales. These final deposits are thought to document the drowning of the carbonate platform.

2.2.2.2 Northern Kaokoveld

In the northern Kaokoveld (*Figure 2.4*), the Devede Formation is almost pure carbonate, devoid of coarse-grained siliciclastic sediments such as conglomerates and sandstones. Instead, the unit in this region is characterized by metre to decameter scale cycles of rhythmically alternating shale and limestone beds, along with the appearance of a distinct, heavily cemented limestone facies that has not been observed in southern sections. This unique limestone facies can be sub-divided into three subfacies: a laminated cementstone, an intermediate laminated cement breccia and a brecciated cement microbialaminate.

Figure 2.4: Geologic map of the Northern Kaokoveld modified from Hoffman and Halverson (2008). Measured sections are denoted as purple boxes. The small map in top right corner the grey area shows the location of the Northern Kaokoveld study area in relation to the larger Kunene Region.

Typically found associated with stromatolites, the thinly laminated carbonate sediments appear with crinkly laminations cemented by a thin layer of carbonate cement and are thought to

represent a sub-tidal environment (Hood *et. al*, 2015). Where stromatolites are absent, the brecciated cement unit caps the cement facies. Much like the southern Kaokoveld, the upper half of the system appears deeper, and heavily cemented laminated carbonates combine with shales and ribbonites to form microbially laminated beds.

2.3 Methods

2.3.1 Fieldwork

Fieldwork was carried out primarily on previously unlogged exposures of the Ombombo Subgroup in the Kaokoveld region. Stratigraphic sections were measured perpendicular to bedding using a 2-m collapsible measuring stick ('Jacob staff'). In a small mountain range to the north of the Otjize Syncline, one full section and one partial section were measured along the major road C43 (Figure 2.4). At this locality, carbonate samples were collected at ~3 m intervals where possible. Similarly, just east of Otjomatemba, a second partial section of the Upper Devede Formation was measured, and samples taken at every ~1m where possible for carbon and oxygen isotope analysis.

Siliciclastic sediments were described based on grain size as argillite, siltstone, sandstone, or conglomerate. Lithological composition of grains or clasts, as well as sedimentary structures such as crossbedding and grading, were noted. Carbonate units were classified following carbonate lithofacies scheme modified from Halverson *et al*. (2002) (Table 2). Where observed, non-gradational transitions between facies were noted and described as flooding (i.e., transgressive) surfaces, erosional scour surfaces, or subaerial exposure surfaces. These new stratigraphic logs and isotopic data were synthesized with previously published (Hoffman *et al*., 2021) and unpublished results and used to generate a sequence stratigraphic framework of all the measured sections (see Table 3) and $\delta^{13}C_{carb}$ profiles.

	Section	Latitude	Longitude	Location
1	P1404*	S 19°10'18.5"	E 013°52'15.6"	Ongongo
2	P5*	S 19º05'22.9"	E 013º57'11.9"	Otjisakumuka
3	G1521*	S 19°03'36.0"	E 013°58'32.3"	Beesvlakte
4	G1523*	S 19°03'48.7"	E 013°58'05.3"	Beesvlakte
5	K1611	S 19°08'49.8"	E 013°55'51.4"	Omutirapo
6	K1612	S 19°08'26.8"	E 013°55'42.7"	Omutirapo
7	G2291	S 19°07'26.2"	E 013°56'12.6"	Okambonde
1	G2290*	S 18°40'36.9"	E 013°43'11.6"	Otjize North
2	A2202*	S 18°52'58.3"	E 013°47'50.7"	Otjomatemba
3	A2203	S 18°40'45.4"	E 013°58'32.4"	Otjize
4	A2204*	S 18°40'34.5"	E 013°43'02.0"	Otjize North
5	A2205*	S 18°40'55.9"	E 013°42'58.3"	Otjize North
6	P6504	S 18°45'27.0"	E 013°41'12.1"	Okaaru

Table 3: Measured sections used in the formation of the sequence stratigraphic framework the Devede Formation. The coordinates are for the bases of each measured section, and asterisks denote sections with carbon isotope data.

2.3.2   Facies Analysis

The extensive and well-preserved exposures of the Devede Formation in the Kaokoveld region provided an excellent opportunity for facies analysis. A total of six complete stratigraphic sections and two half sections, with a maximum stratigraphic height of roughly 470 meters, were carefully examined, and documented through detailed, bed-by-bed sedimentological logging. The different facies belts, facies associations and lithofacies were identified based on lithological composition, texture, observed contact relationships, the occurrence of characteristic sedimentary structures, and relationships to other facies. Additionally, the petrographic analysis of polished thin sections of the cement breccia facies, as described in Hood *et al.* (2015), was also considered in the analysis of the sedimentary facies.

2.3.3 Sequence Stratigraphy

Though it is common to use transgressive-regressive sequences in Proterozoic sequence stratigraphy, the temporal correlations of the mixed carbonate-siliciclastic strata within our sequence stratigraphic framework is adapted from the Depositional Sequence IV model put forward by Hunt and Tucker (1992; 1995) and later modified by Catuneanu (2006). Here, individual sequences are distinguished by abrupt shifts in facies and depositional stacking patterns. The boundaries of these sequences are often indicated throughout the region by discrete reddened exposure surfaces at the top of coarsening-upward (regressive) cycles, which also constitute maximum regressive surfaces since they are followed by the beginning of the next lowstand systems tract (LST). The constituting parasequences are found to be generally separated by flooding surfaces and less frequently, accompanied by subaerial exposure surfaces. Five major sequence stratigraphic surfaces are identified within this sequence stratigraphic framework: sequence boundaries (SB), flooding surfaces (FS), maximum flooding surfaces (MFS), regressive surfaces of marine erosion (RSME), and maximum regressive surfaces (MRS).

2.3.4 Carbon and oxygen isotope geochemistry

During the course of our fieldwork, a total of 98 carbonate samples was collected from the Ombombo Subgroup: 83 from the Otjize North region and 15 from Otjomatemba. Samples were analyzed in the Stable Isotope Geochemistry lab at McGill University.

Fist-sized carbonate samples were cut into slabs using a diamond lapidary blade to expose unweathered surfaces, then rinsed and dried. A drill press equipped with dental drill bits was used to produce relatively small quantities of fine powder from the fresh surfaces of the samples

for $\delta^{13}C_{carb}$ and $\delta^{18}O_{carb}$ analyses, avoiding veins and fractures. Approximately 120 μg of powder from each sample was weighed out for analysis on a Nu Instruments Perspective mass spectrometer coupled to a NuCarb automated carbonate preparation device. Carbon and oxygen isotope ratios were measured simultaneously in dual inlet mode. Analytical runs contained 40 samples with 10 in-house reference materials (NCM and UQ6) regularly interspersed. The samples were heated to 70°C and sequentially reacted with orthophosphoric acid (H_3PO_4) to produce CO_2, which was then cryogenically isolated. The isotopic ratios of the extracted CO_2 were measured against a reference gas, and $\delta^{13}C_{carb}$ and $\delta^{18}O_{carb}$ were calculated and calibrated to VPDB, with a 1σ precision <0.05 ‰.

Cross plots of carbon and oxygen isotope data from each section were used to assess for alteration, with R^2 values calculated to quantify the degree of covariation. Usually, the process of meteoric diagenesis leads to lower $\delta^{18}O$ values due to the fact that meteoric water has a lower $\delta^{18}O$ value compared to seawater. This diagenetic impact competes with early dolomitization, which tends to increase $\delta^{18}O$ values by 2–4‰ (Halverson *et al.,* 2007).

2.4 Results

2.4.1 Facies Analysis

This study defines twenty-one (21) distinct lithofacies (LF) grouped into seven (7) facies associations and three (3) facies belts. Each facies association is interpreted to represent a specific environment within the Makalani sub-basin. Consequently, the sedimentary characteristics and lateral grading of these recognizably different facies associations into other adjacent units are interpreted as the carbonate system's response to relative sea level fluctuations throughout the deposition of the Devede Formation. These facies associations include: 1) beach,

2) fan-delta complex, 3) evaporative lagoon, 4) shoal reef, 5) restricted lagoon, 6) sand shoals and 7) protected lagoon. Although the Devede Formation has undergone significant dolomitization, sedimentary structure remain well preserved and as such crystal sizes are considered to be representative of the original grain sizes.

2.4.1.1 Supratidal to Intertidal
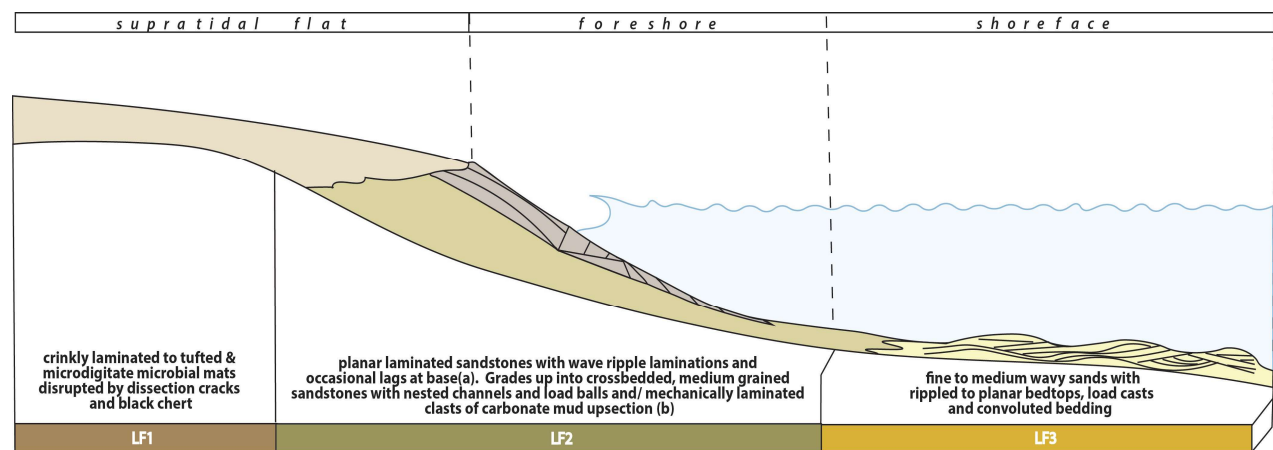
2.4.1.1.1 Facies Association 1: Beach (FA1)

Figure 2.5: Facies model for the different zones along the storm dominated beach of the Devede Formation. Note that this figure has a strong vertical exaggeration.

Lithofacies 1: Microbialaminates

Medium grey, cryptocrystalline, microbially laminated carbonate mudstones with occasional tepee structures. These meter-scale beds are typically found associated with crinkly laminated to linked domal stromatolites and black cherts. Microbialaminates are typical of the intertidal to lower supratidal environment (Kunzmann et.al, 2019). The stratified growth form of these sediments and transitional nature of the contact with the stromatolites is consistent with deposition in a low-energy, upper inter- to supratidal environment (James, 1978). Using the presence of tepee structures, a more supratidal flat environment, characterised by subaerial exposure, is proposed for this lithofacies (see *Figure 2.5*).

Lithofacies 2: Planar sandstones

Fine to medium grained sandstones with low angle planar lamination, alongside wave-ripple lamination and load structures (LF2a). These sandstones grade up into either a unit of mechanically laminated clasts of carbonate mud (edgewise-conglomerates) or medium grained, crossbedded sandstones characterized by large, nested channels and metre-scale load balls (LF2b). The associated load structures are formed as a result of wave-induced liquefaction during storm activity (Pemberton *et al.*, 2012), whilst the edgewise conglomerates themselves are formed from the erosion of a tidal flat and/ or shoreface sediments by intense storm waves or currents (Sepkoski, 1982). The close association of these planar sandstones with microbialaminates, occasional stromatolites and the sediments of LF2b is consistent with an intertidal to shallow subtidal environment. Consequently, a foreshore setting is proposed for this lithofacies (*Figure 2.5*).

Lithofacies 3: Wave laminated sandstones

Fine-to-medium grained sandstone with well-developed wavy and crinkly laminations. Occasionally, these sandstones may also have rippled or planar laminated bedtops and mudcracks. Likewise, their associated basal contacts are sharp and are often characterized by load casts and rare convoluted bedding structures. They typically occur in metre-scale intervals found with tufted and laterally linked domal microbialaminates. A lower subtidal environment is suggested for this lithofacies. The occurrence of basal ripple laminated sands with an abundance of soft sediment deformation features, the vertical increase in grainstones and appearance of trough crossbedding is consistent with this proximal lower shoreface environment (*Figure 2.5*).

2.4.1.1.2 Facies Association 2: Fan -delta complex (FA2)

Lithofacies 4: Conglomerates

Conglomerates are rare but occur in the lower 80 m of exposures in the southern Kaokoveld. They usually occur in decameter-thick intervals and are interbedded with thin, fine- to medium-grained sandstone beds. These conglomerates carry sub-rounded to well rounded clasts from a wide variety of lithologies including quartz, quartzite, granodiorite, and amphibolite. An upward decrease in the presence of sandy interbeds and matrix suggest that these conglomerate units become more clast-supported upsection. Likewise, a vertical variation in grading can be observed with the dominance of thick, reversely graded beds (LF4a) in the lower parts of the sequence and normally graded conglomerates with erosional basal surfaces in the upper parts (LF4b). The presence of normal and reverse grading in sandstones and conglomerates suggests that these clastic sediments were deposited sub-aqueously as a result of flood-induced and gravity-driven granular avalanches. Likewise, the presence of large grain sizes, sandstone-mudstone interbeds, and well-rounded clasts in these conglomerate beds is consistent with a southern, upslope fluvial or shallow marine source. Consequently, these sediments are interpreted as delta front deposits (Figure 2.6). The initial predominance of conglomerates, followed by a vertical transition into normal graded, pebbly sandstones of the more southern clastic parasequences is interpreted to record deposition in the axis of a mouth bar.

Lithofacies 5: Pebble sandstones

These pebblestones (along with minor cobblestones) include metasedimentary, granitoid, quartz and quartzite clasts. These pebblestones are often interbedded with crossbedded sandstones with megaripples and desiccation cracks. Likewise, the presence of wave ripples, crossbedding and

dispersed granules in the sands and muds is consistent with an intertidal off-axis mouth bar setting (van Yperen et. al, 2020).
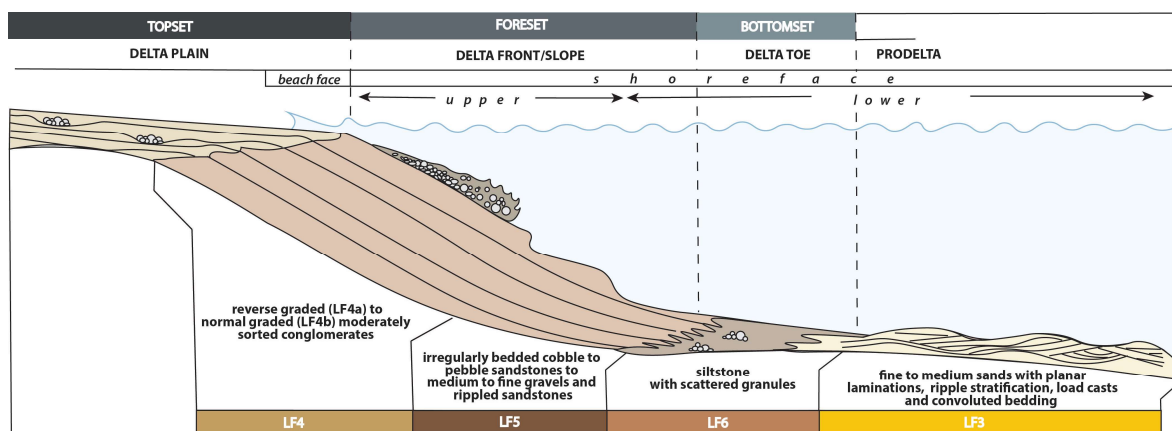
Figure 2.6: Facies Model for the deposition of a fan-delta (McConnico and Bassett, 2007)

Lithofacies 6: Siltstone with scattered granules

Very dark grey siltstones with dolomite interclast lag at the base. These siltstones are also marked by the presence of sandy starved ripples, cm-scale lenticular grit/granule layers, wave ripples, load clasts, and spectacular sedimentary dykes. This unit grades up into the pebble sandstone facies. Here, the ultimate disappearance of conglomerates and the development of muds and ripple cross-laminated sandstones is interpreted to represent deposition in a more distal environment such as the delta toe or mouth bar fringe.

2.4.1.1.3 Facies Association 3: Evaporative Mudflat (FA3)

Lithofacies 7: Laminated dolomicrite with nodular anhydrite and gypsum pseudomorphs

Nodules of cream-coloured pseudomorphs after anhydrites and/or gypsum crystals cemented in a tan to grey laminated dolomicrite. Remnant vugs of these isolated crystals have been filled with quartz or chalcedony. Marlier units of this lithofacies are characterized by centimeter spaced, north-northeast trending extensional shear bands. Likewise, this lithofacies often overlies crinkly laminated stromatolites. The marly microbialaminate host sediment of these evaporite deposits is

suggestive of a low energy supra- to upper intertidal environment (Desjardins et. al, 2012). The evidence for enterolithic anhydrite precipitation in particular indicates that the environment was characterized by seasonally high atmospheric temperatures (>35°C) and high evaporation rates (Kendall, 1992). Though some of the anhydrites pseudomorphs may have been primary, most of the nodular anhydrites may form from the replacement of gypsum deposits (Kendall, 1992).

Lithofacies 8: Argillaceous limestones/shales (Shallow water rhythmites)

Decimeter scale beds of green to grey argillaceous carbonates and shales. Typically found underlying LF7 sediments, these marly thin beds may appear with boudins of dolomites and centimeter scale pyrite clasts. The predominantly fine-grained nature of this lithofacies and its stratigraphic position in shoaling upwards parasequences is indicative of deposition in a low-energy intertidal environment. The corresponding absence of erosional structures is consistent with deposition in this quiet environment. Consequently, this lithofacies is representative of the lower intertidal zone of a lagoon. The green color of the shale and presence of small authigenic pyrite grains imply that euxinic conditions existed at depth in these lagoons.
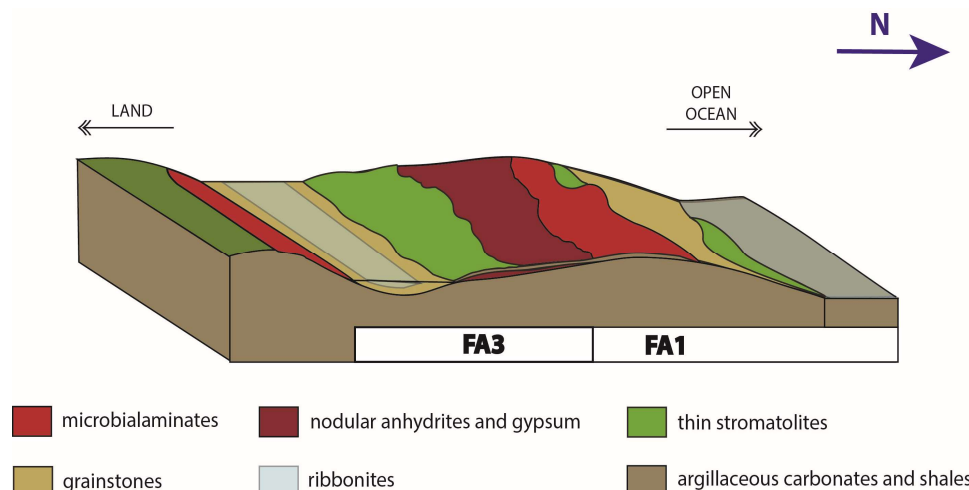
Figure 2.7: Schematic model for the distribution of the cyclic peritidal and laminated dolomicrite facies in the intertidal to supratidal evaporative lagoon depositional environment (revised from Gensac et. al, 2015)

2.4.1.2 Intertidal to Subtidal

2.4.1.2.1 Facies Association 4: Shoal Reef (FA4)

Lithofacies 9: Ooid grainstones

The ooid grainstone lithofacies is typically medium grey to cream in color and consists of ooids up to 2 mm in diameter with sparry cement. Though uncommon, this lithofacies may also contain coarse grained intraclasts. With a maximum thickness of 2.5 m, the oolite beds are associated with the other lithofacies in FA4 as well as FA1. Ooids commonly form in high-energy shallow subtidal environments such as shoals and beaches (Jones and Desrochers, 1992). The occasional occurrence of this lithofacies with ribbonites and columnar stromatolites is consistent with deposition in moderate to high-energy settings (James and Bourque, 1992; Inden and Moore, 1983). Consequently, these grainstones are interpreted to represent high energy storm and shoal deposits.

Figure 2.8: Schematic model of reef structure and facies distribution in the sub- to intertidal zone (modified from Corkeron and Slezak, 2020)

Lithofacies 10: Cross-bedded and intraclastic grainstones

Marked by its characteristic trough crossbedding, the cross-bedded grainstones exist as relatively thick beds (4-10m) of light grey dolomite. These crossbedded grainstones are often found in association with fine-grained sediments such as argillites, siltstones or micritic dolomite. The intraclastic grainstones, on the other hand, are composed of relatively thin cream to pink beds (<5 m) of intraclastic dolograinstones. Whilst the intraclastic grainstones may be found intercalated with micritic dolomite, they are more commonly associated with FA1 deposits. The predominance of trough cross-stratification over swaley and planar stratification in these grainstones is suggestive of high wave energy setting, indicating an upper shoreface environment. Likewise, the intraclastic counterparts are indicative of a high energy regime, typical of the lowermost intertidal to shallow subtidal environment (James et. al, 1992). As such, the grainstones of this lithofacies are thought to be representative of storm deposits in shallow subtidal shoreface environments (Jones and Desrochers, 1992).

Lithofacies 11: Stromatolites

Though not abundant, cream to grey-colored *Conophyton* and *Kussiella-type* columnar stromatolites occur in the southern exposures of the Devede Formation. These unbranching stromatolites are largely inclined to the south and grade upwards into highly divergent, cream to pink *Tungussia-type* columnar stromatolites. *Tungussia-type* stromatolites dominate much of the unit and are occasionally associated with the branching conical stromatolites *Jacutopyton (see* Figure 2.9*).* Laminated sediments (rhythmites) occasionally occur between the *Tungussia* columns. Decimeter to metre-thick beds of pink to grey crinkly laminated and linked domal stromatolites are also common and may develop upwards into undulatory or draping laminaes. These stromatolite beds occur in shoaling upwards cycles with intraclastic grainstones, massive

grainstones, shales and nodular ex-anhydrites. The low relief, crinkly laminated nature of the stromatolites are suggestive of a low-energy environment with high shale or mud content (James, 1978; Johnson and Grotzinger, 2006). The upward change in stromatolite morphology from unbranched to largely digitate and dendroid stromatolites is indicative of the transition from a moderate to a high energy subtidal environment and consistent with the build up of a reef to sea level (Hofman, 1969; Hoffman, 1976; James, 1978). The upper assemblage of stratiform to low relief domal stromatolites is typical of moderate energy environments such as the upper subtidal to low intertidal zone (James. 1978; Kuang et. al. 2019). Using its stratigraphic relationships with the columnar stromatolites, an upper subtidal zone setting is proposed for these more stratiform sediments. This environment is further supported by the occurrence of type LF11 and LF15 grainstones, typical of the high energy, lower mid-littoral zone. Consequently, this lithofacies is interpreted as a high-energy reef shoal/ biostrome.

2.4.1.2.2 Facies Association 5: Restricted Lagoon (FA5)

Lithofacies 12: Planar laminated grainstone

Decimeter to meter scale intervals of planar laminated to massive tan dolograinstones. This lithofacies is commonly characterized by alternations with green argillites, laminated siltstones, fine grained sands, and stromatolites. Coarse grained oolites and trough cross bedded grainstones may also occur. Whilst the general fine-grained, laminated nature of the deposits in this lithofacies are suggestive of a somewhat low-energy tidal regime, the presence of ooilitic and cross-bedded grainstones is indicative of occasional exposure to wave energy, likely during storms, which transport the grains into a generally lower energy shallow subtidal environment.

Lithofacies 13: Dolostones with laminated and intraclastic magnesite.

Grey, fenestral or irregularly laminated mudstones and/ packstones with cream magnesite intraclasts and/or nodules and occasional white cherts. The laminated mudstone units exist as meter-scale beds with teepees and are characterized by isopachous, sparry cements. The fenestral fabric, the presence of isopachous cement and the laminated nature of the host sediments suggests deposition in shallow, quiescent waters (Duda et. al, 2016). Similar to the magnesites of the Skillogalee Dolomite (Frank and Fielding, 2003), these magnesite deposits are suggested to have been deposited in a fairly shallow-water lagoon. The occurrence intraclastic grainstone with white magnesite clasts episodic high-energy conditions, such as large storms, capable of reworking magnesite nodules or crusts (Jones and Desrochers, 1992),

2.4.1.2.3   Facies Association 6: Shoal (FA6)

Lithofacies 14: Massive grainstones

The grainstones of this lithofacies exist as 0.4-20 m-thick beds of tan to light grey coarse-grained dolomite with an abundance of chert. These largely recrystallized grainstone units are often found intercalated with muddy microbialaminates, ribbonites and occasional stromatolites. Moreover, these facies may also be overlain by facies from LF3. In the context of a carbonate platform, grainstone deposits are typical of sand shoals and beach deposits (James et.al, 1992). The occurrence of these grainstones in shoaling upwards cycles with ribbonite and stromatolites is consistent with deposition in a shallow subtidal setting (Hoffman and Halverson, 2008). Likewise, the association of these dolomitized units with sediments of LF9, L10 and LF11 further confines this lithofacies to a shallow subtidal to lowermost intertidal setting. Consequently, this lithofacies is considered to be representative of subtidal to lowermost

intertidal shoal deposits. Moreover, the more thickly bedded grainstone units represent the shoal core whilst the thinner, frequently intercalated beds or lenses are interpreted as shoal edge sediments. Its lateral transition into FA1 sediments and its appearance in shallowing upward sequences with FA4 sediments suggest that some of this lithofacies might have been deposited as back- tidal flat shoals or back-reef grainstones.

2.4.1.2.4   Facies Association 7: Protected Lagoon (FA7)

A: LF15

B: LF16

C: LF17
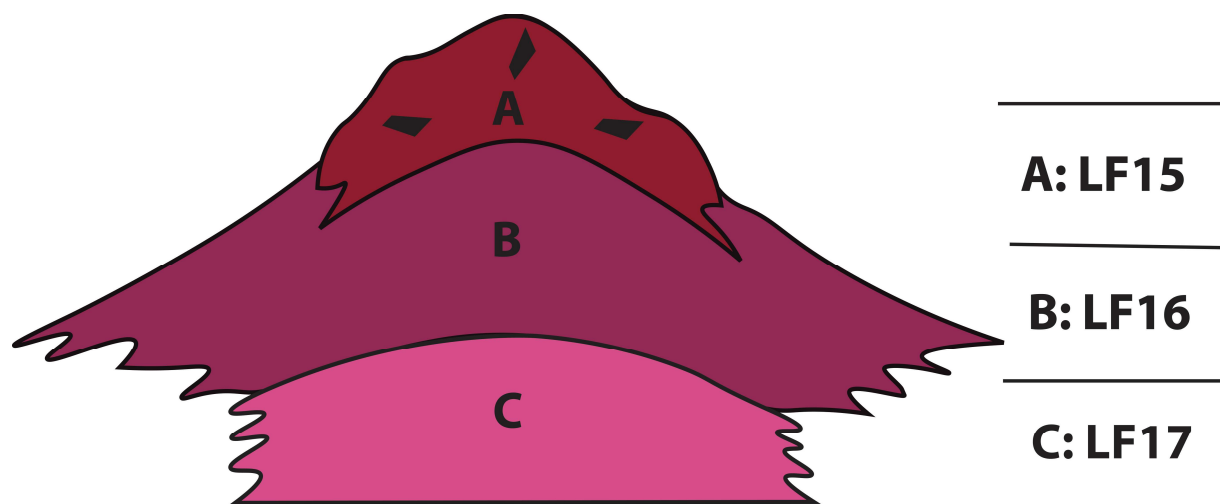
Figure 2.9: Schematic model of carbonate mound structure and facies distribution in the sub- to intertidal zone (modified from James and Bourque, 1992)

Lithofacies 15: Brecciated microbialaminate

Chert-rich, internally structureless pink beds comprised of angular dolomite clasts. These dolomite clasts are largely recrystallised to dolomite spar and are encrusted by a micritic microbial matrix forming irregular laminae (Figure 2.9). Often partial delamination and curling of fractured dolomite sediments can be seen at the lower interface of breccia beds. These brecciated and fractured beds then commonly grade into a more laminated grey dolomite with fenestrae and tepee structures. This facies is interpreted to have formed in a high-energy environment – possibly correlative to the middle to upper parts of the reef front. The close

association of this lithofacies with laterally linked, tufted and cabbage head stromatolites can be used to deduce a lower intertidal to upper subtidal setting (Kuang et. al., 2019) for these deposits. Similarly, the appearance of microbialaminates with laminoid-fenestral and tepee structures typical of supra- to upper intertidal settings (Kunzmann et.al, 2019), above the heavily fractured and brecciated microbialaminates is consistent with this environment.

Lithofacies 16: Cement breccia

Heavily cemented, pink, disrupted dolomite beds made up of curled, laminated 'rinds' of dolomite clasts surrounded by fibrous dolomite cements. Intraclasts of micritic dolomite may also occur within fractures (i.e., sheet cavities) or can make up entire breccia horizons. These intraclasts often display shrinkage crack and delamination fabrics (Hood *et. al*, 2015). Furthermore, petrographic analysis of these sheet cavities indicate that the cavity walls are often lined by fibrous dolomite cement crusts of up to 10 cm in thickness, and are occasionally overlain by multiple generations of fine-grained dolomite internal sediment (Hood *et al.*, 2015). Similarly, the roofs of these cavities are characterized by stalactitic shrub structures consisting of rounded clumps, or occasionally laminated, organic, dark grey dolomicrite. Relatively thin ooid grainstone and stromatolite beds with marine cements are often found associated with this unit. These stromatolitic units range in morphology from tufted or discrete cabbage-head like domes to columnar and are generally less than 20 cm in width.

General similarities in the nature and appearance of carbonate shrubs has led to their categorization as framestones in the modified Durham carbonate classification system (James, 1984). Framestones typically constitute the upper reef front environment of a marginal reef (James, 1984). It is proposed that this zonation can be equally applied to isolated carbonate mounds. Carbonate mounds are preferentially found in relatively low energy environments like the foreslope of gently

sloping platforms, deep basins, and quiet reef lagoons (James and Bourque, 1992). The close association of this lithofacies to FA.4 indicates that these carbonate mounds would have most likely been formed in a sheltered reef lagoon (Figure 2.9). Consequently, using the associated oolites and the range in stromatolite morphologies, this lithofacies can be more accurately assigned to a lower intertidal to subtidal setting. Likewise, with potentially build up of these sediments and resultant gradual entrance into "shallower" waters, the recorded increase in brecciation and sheet cavities in the stiffer, microbial mats can be attributed to increased wave energy where subaqueous cracking is induced by wave-induced stress (McMahon et. al, 2016).

Lithofacies 17: Laminated cementstone

Grey to pink, dolomitic shale with interlaminated bleached porcelaneous dolomite layers. This lower shale commonly displays convoluted bedding, with chaotic folding and brecciated dolomite laminae, and grades upward into a laminated pink-grey dolomite. Likewise, this lithofacies may be found closely associated with marly ribbonites and a distinct purple siltstone. The carbonates of this lithofacies are considered to be bindstones in the modified Dunham scheme. These bindstones may form in the reef crest and/or subtidal reef front environment. The coexistence of this laminated lithofacies with comparably thick, fine-grained micritic beds is consistent with deposition in a more distal, low energy subtidal setting (Figure 2.9). Likewise, following the suggestion of McMahon et. al (2016), the range from soft sediment deformation styles, as typified by convoluted bedding in the basal dolomitic shales of this lithofacies to the brecciation of the stiffer, porcelaneous dolomite laminae is consistent with sediment loading-induced subaqueous cracking at or near the sediment water interface.

Lithofacies 18: Ribbonites

Finely laminated silt-to-fine-sand-sized carbonate laminae with interbedded carbonate mud (marly ribbonite) that range in colour from light pinkish grey to grey. These decimeter to meter scale beds exhibit small scour surfaces, low angle cross-stratification, and sporadic ripple cross-lamination. The fine-grained nature of these sediments implies deposition in relatively quiet waters. The stratigraphic position and occurrence of this lithofacies in sequences with LF21, FA.4, and FA. 5 sediments confirms a subtidal setting influenced by episodic storm-generated waves and tractions currents.

Lithofacies 19: Rhythmite

Green to light grey parallel-laminated carbonate muds with occasional turbidites. Though rare, it usually occurs with argillite, siltstone or ribbonites. The fine-grained nature of these sediments implies deposition in relatively deep or protected such as a subtidal lagoon or offshore setting below storm wave base.

Facies 20: Siltstone

Thickly laminated purple siltstone intervals up to a meter thick are predominantly found in the Northern Kaokoveld region. Laminae vary laterally in thicknesses with noticeable swelling and pinching. They are typically associated with ribbonites (LF19) and the laminated cementstones (LF17) and are considered the siliciclastic equivalent of LF21.

Lithofacies 21: Shales

This lithofacies is characterized by finely laminated to massive dark grey shales and silty shales. The fine-grained nature of these sediments and its occasional association with tufted stromatolites are suggestive of deposition in a low-energy, shallow subtidal environment (Kunzmann *et. al*, 2019; Kuang et. al., 2019).

2.4.2 Sequence Stratigraphy

Since the deposition of the Ombombo Subgroup is linked to an extensional phase in the evolution of the Otavi basin, the subgroup as a whole can be treated as a single first-order sequence. The Devede Formation broadly corresponds to a second order sequence in the sequence hierarchy. All depositional sequences identified therein are 3rd order sequences, which themselves contain 4th order sequence cycles or parasequences.

2.4.2.1 Sequence Stratigraphic Architecture of the Southern Kaokoveld

Ten third-order depositional sequences have been identified and divided into systems tracts in the Southern Kaokoveld. Although eustasy may have contributed to base level fluctuations, it is inferred that episodic fault slip related to extension on the northern margin of the Outjo basin was the dominant mechanism behind these base level changes given that the presumed sediment source was the uplifted Makalani ridge (rift flank). In the two lowest sequences, increases in base level accompanying the beginning of the sequences are commonly closely associated with an influx of siliciclastic sediments (Figure 2.10). The start of the sequence stratigraphic record is perhaps most evident at Ongongo, the most southern measured section of the study area, though the presumed base of this first sequence is not observed here. The lowest visible systems tract is a highstand system tract (HST), represented by shallowing upwards cycles of predominantly grainstones and thin interbeds of calcareous shales, ribbonites and stromatolites. Though seemingly absent from the Otjisakumuka (P5) section, the HST is expressed as a series of

alternating microbialaminates, shales and occasional sandstones in sections near Beesvlakte (G1521).
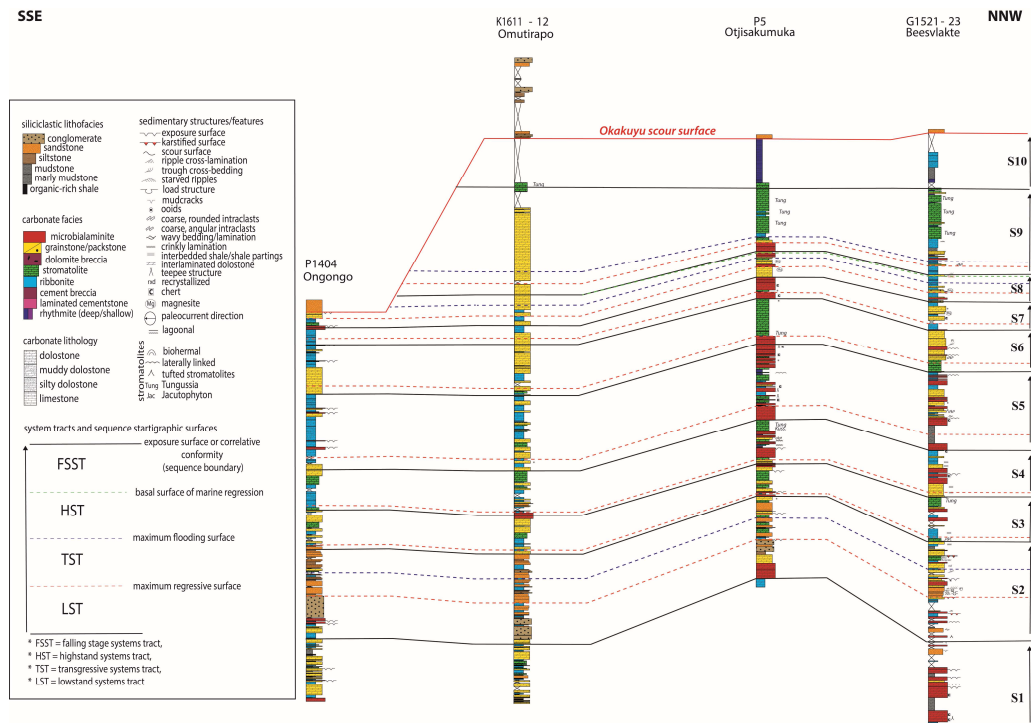
Figure 2.10: Sequence stratigraphic interpretation of the Devede Formation of the Southern Kaokoveld. Coordinates for the base of each section is provided in Table 3.

The base of Sequence 2 is recognized by an exposure surface and the deposition of a thin microbialaminate or grainstone unit that can be traced across all sections. In the Ongongo, Omutirapo and Otjisakumuka sections, the LST continues above the thin carbonate unit as a northward-waning interval of pebble conglomerates with occasional interbeds of sandstones and/or ribbonites. This conglomerate is absent in the Beesvlakte section where the LST is represented by medium-grained sandstones with intercalated microbialaminates. A TST overlies the sandstone-conglomerate unit, ending with a maximum flooding surface near the base of a sandstone and/or ribbonite unit. The subsequent HST is defined by the occurrence of coarsening upwards clastic cycles of predominantly sandstones, mostly capped by microbialaminates or grainstones.

The reappearance of small fining upwards siliciclastic cycles in the more southern Ongongo and Omutirapo sections, alongside a lateral transition to lagoonal shales and carbonates within the Otjisakumuka and Beesvlakte sections is used to infer the base of the LST in Sequence 3. As there is seemingly no TST preserved, the maximum flooding surface (MFS) is placed within a siltstone or ribbonite unit and is interpreted as the start of the HST. The deposits overlying the MFS boundary occur mainly as shallowing sequences of reefal carbonates. This shallowing-upward trend culminates in a grainstone-microbialaminate cap unit, interpreted as the top of the HST.

The base of Sequence 4 is marked by the deposition of a thin microbialaminate or stromatolite bed across most of the sections, followed by a LST predominantly consisting of grainstones and ribbonites. The overlying HST in the Ongongo and Otjisakumuka sections is represented by roughly 15 metres of ribbonites and stromatolites, whilst in the Omutirapo and Beesvlakte sections, it is represented by predominantly lagoonal grainstones, stromatolites and microbialaminates. The base of a thick interval of grainstone and microbialaminate within the Ongongo and Otjisakumuka sections respectively marks the maximum regressive surface (MRS) and the ultimate start of the LST within Sequence 5.

Likewise, the reintroduction of parasequences of lagoonal packstones and ribbonites make up the LST within the Omutirapo and Beesvlakte sections. Moreover, the end of the transgressive event and the MFS is marked by the occurrence of ribbonites or shales across almost all sections. The overlying HST deposits consists of mainly thick intervals of grainstones and stromatolites with occasional interbeds of microbialaminates and ribbonites.

Sequence 6 commences with a grainstone unit across all sections. Fining- upward and aggradational cycles of predominantly reefal to supratidal sediments are found to make up much

of the LST across the region. Much like sequences 4 and 5, no TST is preserved. Instead, the maximum flooding surface can be found atop a microbialaminate unit within the Otjisakumuka section, whilst its equivalent in the remaining sections is a finer grained grainstone and/ or stromatolite. The rest of the HST is dominated by a 20-m thick stromatolitic interval within the Otjisakumuka section and parasequences of predominantly ribbonites, microbialaminates and/ grainstones in the other sections.

A return of the supratidal black chert bearing microbialaminates in the Otjisakumuka section, and similar shallow water shoal facies in the other sections marks the start of sequence 7. This LST is expressed mainly as microbialaminates, grainstones and ribbonites. The end of the transgressive event and the MFS is marked by the occurrence of ribbonites or shales across almost all sections. The overlying HST deposits consists of mainly thick intervals of grainstones, microbialaminates and ribbonites.

The presence of chert at the base of microbialaminates and grainstone units in the outcrops near Beesvlakte and a more widescale shift into the restricted lagoon facies is used to infer the start of sequence 8. The first phase of the transgression (LST) is denoted by the deposition of a reasonably thin bed of grainstones and/ microbialaminates across all sections, with the only visible fining upwards parasequences expressed in the Beesvlakte section. A second TST follows in the overlying units with better developed fining upwards parasequences. This deepening-upward trend is interrupted by the deposition of finer grained grainstones and ribbonites, suggesting the presence of a maximum flooding surface. Alternating marly to pure ribbonite parasequences comprise the remaining HST in the Beesvlakte section, whilst the system tract is represented by thin, aggrading parasequences of grainstones and microbialaminates in the Omutirapo and Otjisakumuka sections respectively. A scour surface capping HST in the

Otjisakumuka section and the abrupt appearance of a coarse grained grainstone within the finer deepwater sediments downslope (Beesvlakte) are indicative of a FSST. The top of this thin grainstone bed marks the sequence boundary and the base of sequence 9.

Sequence 9 begins, once again, with a transgression recorded by aggradational parasequences across the Omutirapo, Otjisakumuka and Beesvlakte sections. The return of a scoured microbialaminate above this sequence is interpreted herein as a wave ravinement surface and marks the onset of the TST. With the exception of the Omutirapo section, the TST manifests as visible fining upwards shoal reef parasequences. A subsequent transition from reefal sediments to deeper water marly ribbonites is used to infer a significant flooding event and the start of the HST. Whilst this ribbonite unit is absent in the Omutirapo section, aggradational grainstones and coarsening upwards parasequences of predominantly Tungussia-type stromatolites, representing of the HST deposits, occur at this level and can be traced across all the sections.

The final system tract of the region begins at the base of a thin bed of stromatolites traceable across all sections. It is overlain by a deepening upwards trend represented by 30-35 metres of rhythmites, marly ribbonites, ribbonites and shales. Consequently, these lithologies are interpreted to record a transgression, although the LST is inferred to be absent and only the TST preserved, perhaps as a result of a marine erosive surface. The end of the TST is marked by its erosionally truncation beneath the Okakuya scour surface.

2.4.2.2 Sequence Stratigraphic Architecture of the Northern Kaokoveld

Contrary to the southern Kaokoveld, only eight third-order depositional sequences have been identified in the Devede Formation in the Northern Kaokoveld (Figure 2.11). The lowest visible systems tract is the LST of sequence 3. There, the LST is expressed as metre-scale stromatolite

parasequences. The MFS of this sequence is placed within the first ribbonite unit overlaying the

stromatolites. Moreover, the ensuing HST is marked by coarsening upwards parasequences of

grainstones, shales and ribbonites or marly ribbonites, alongside occasional stromatolites. The

reintroduction of decameter thick stromatolite beds and ribbonites in the Okaaru section (P6504)

is used to infer the end of the HST and the beginning of Sequence 4 within the Devede

Formation.
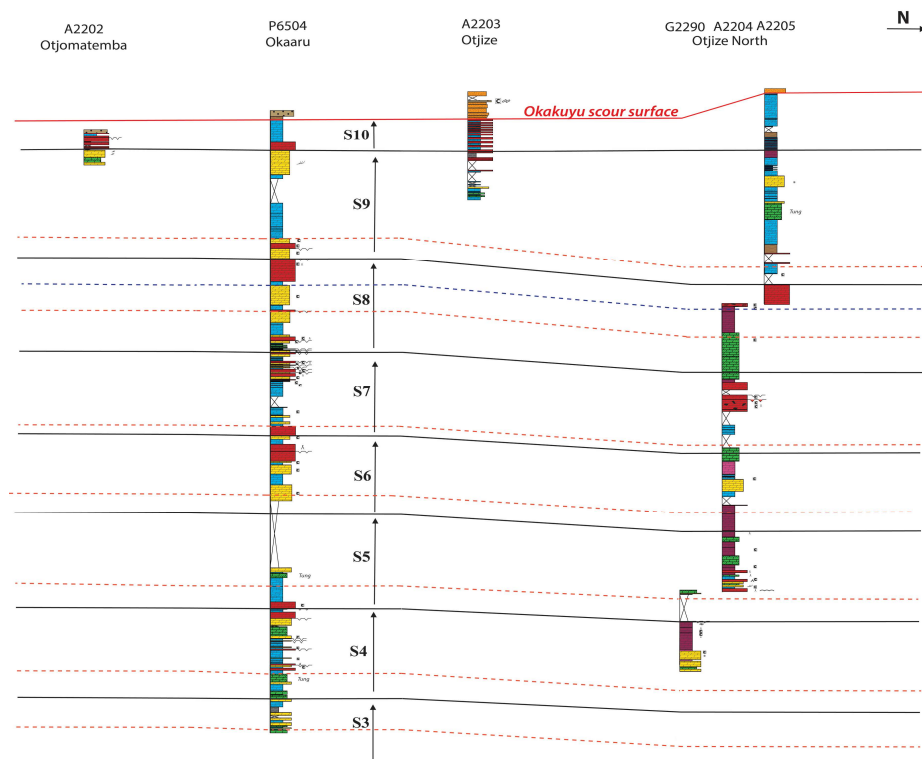
Figure 2.11: Sequence stratigraphic interpretation of the Devede Formation of the Northern Kaokoveld. Coordinates for the base of each section is provided in Table 3.

Similar to the first sequence, the LST of sequence 4 is only visible in the Okaaru section, where

it consists of fining upwards stromatolite to ribbonite parasequences. The maximum flooding

surface is generally found at the top of a distinct Tungussia stromatolite unit, and it is followed

by a significant lower ribbonite unit with several small-scale coarsening upwards parasequences.

The coarsening upwards trend extends northward towards Otjize, though the lower

parasequences consist mostly of grainstones. The lithology changes significantly upsection with the dominance of grainstones, stromatolites and microbialaminates in the upper HST at Okaaru and the appearance of heavily cemented microbially laminated sediments in Otjize North.

Exposure surfaces across both sections mark the base of Sequence 5. Though largely absent from the Otjize North section, an LST consisting of decametres of ribbonites and microbialaminates is observed at Okaaru. As no TST is preserved here, the MRS and MFS are considered the same and placed within a marly ribbonite unit. In Okaaru, thick grainstone-dominated parasequences constitute the overlaying HST, whilst coarsening upwards parasequences of reef and heavily cemented microbially laminated facies make up the HST north of Otjize.

Though absent in Okaaru, the occurrence of microteepees towards the top of a cement breccia unit in Otjize North is used to infer the presence of an exposure surface and the base of sequence 6. The LST is recorded by the deposition of massive grainstones and cement breccia across the Okaaru and Otjize North sections respectively. The MFS of this sequence is within each of these units. The deposition of coarsening upward parasequences of reef and shoal deposits across both the Okaaru and Otjize North sections capture the HST.

Sequence 7 begins with a thick microbialaminate unit in the Okaaru section and a corresponding stromatolite unit in the Otjize North section. In Okaaru, decameter fining upward parasequences of ribbonites and grainstones/microbialaminates make up the remaining LST. Though mostly covered in the Otjize North section, the LST is expressed by ribbonite-dominated fining upward parasequences. With no TST preserved, the maximum flooding surface is found within a traceable marly to pure ribbonite unit, followed by a well-developed HST. The HST begins with a meter thick ribbonite unit across both sections. The overlying parasequences coarsen upwards and become dominated by deposits of the reef crest to reef flat facies.

A traceable chert layer is used to infer the presence of an exposure surface and the start of sequence 8. Here, the base of the LST is denoted by the deposition of a reasonably thin bed of microbialaminate in Okaaru and heavily cemented stromatolites in Otjize North. The remaining LST in the Otjize section, like its base, is dominated by stromatolites, whilst the remaining LST in the Okaaru section is defined by a transition from a ribbonite-grainstone parasequence to a decameter thick grainstone unit. A second transgression ensues. The start of the TST in the Okaaru section records a fining upward trend with the deposition of microbialaminates and/ cherty grainstones to ribbonites. In the Otjize North section, the TST is expressed by a transition from stromatolites to predominantly fine-grained microbial cement lithologies. The subsequent maximum flooding surface is placed within a ribbonite unit in the Okaaru section and within a cement breccia unit in Otjize North. The ensuing HST is characterized by the deposition of a 10-15m thick microbialaminate interval across both sections. Within the Otjize North section, in particular, the HST is inferred from an upsection increase in brecciation and cement content in the microbial lithologies and the gradation to a thick interval of microbialaminate.

Similar to sequence 8, the base of sequence 9 is marked by an abundance of chert. The transgressive or deepening event begins with the deposition of massive grainstones and microbialaminates across the Okaaru and Otjize north sections, respectively. The overlying parasequences of the LST display general fining upward stacking patterns with a change in lithofacies from microbialaminates to grainstones in Okaaru and microbialaminates to ribbonites in Otjize North. A flooding surface. positioned within a traceable ribbonite unit, marks the base of the overlying HST. Whilst upward shale-ribbonite parasequences make up the majority of the HST in both Okaaru and Otjize North. the introduction of reef and shoal deposits characterizes the upper 75m of the HST across all sections.

The final sequences begins at the base of laterally continuous microbialaminate to cement breccia beds. A significant flooding surface demarcated by the abrupt transition from reef and shoal deposits to fine-grained deposits, marks the start of the HST. There microbialaminate lithologies are overlain by decameters of deep-water deposits, suggestive of continued deepening. Consequently, it is presumed that these lithologies collectively record the TST. Sequence 10 is erosionally truncated beneath the Okakuya scour surface such that the HST absent.

2.4.3 Carbon Isotope Results

2.4.3.1 Southern Kaokoveld
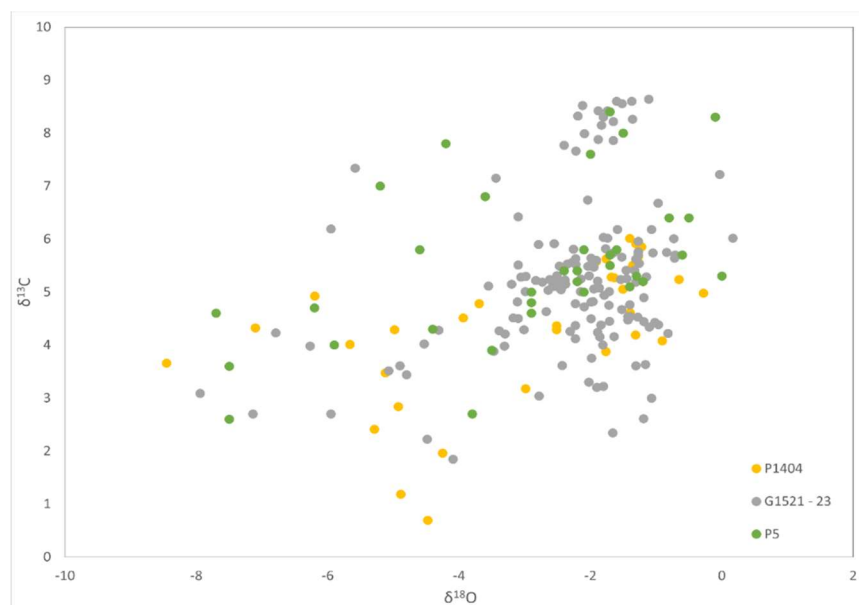
Figure 2.12: Crossplots of $\delta^{13}C$ and $\delta^{18}O$ data from Devede Formation sections P1404, P5 and G1521 – 23 in the Southern Kaokoveld region.

Carbon isotope results from the Southern Kaokoveld sections (Figure 2.12) show negligible correlation between $\delta^{13}C$ and $\delta^{18}O$. Though lower resolution, the designated type-section (P5) and Ongongo (P1404; Hoffman *et al*., 2021) closely matches the composite section (G1521-23) measured previously near Beesvlakte. Though absent in sections P5 and G1521, a steady rise in

carbon isotope values from 0 to 5‰ observed in P1404 represents the transition from the restricted Beesvlakte Formation to more platformal Devede Formation. Carbon isotope values in the next 200 m of the three sections show relatively stable δ^{13}C at around 5‰. Reoccurring declines in δ^{13}C are observed throughout the three sections where δ^{13}C values start at ~4‰ and drop by ~2 ‰ before gradually rising to a plateau of approximately 5‰. Though the δ^{13}C values of the uppermost 200 m of carbonates show more scatter, isotope values record two noticeable trends: i) fairly stable δ^{13}C values of ca. 6‰ to 7‰, and ii) an increase in δ^{13}C values from 7‰ to a plateau of ca. 8‰ before returning to around 6‰.
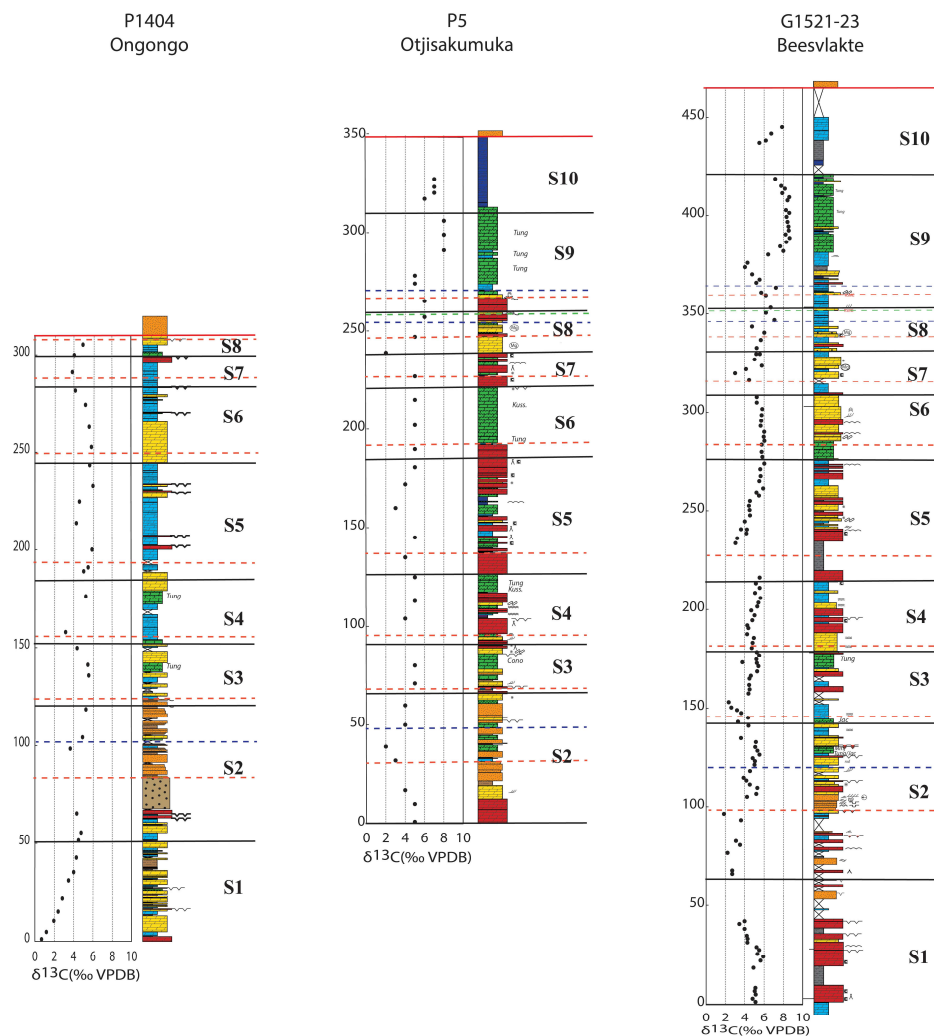
Figure 2.13: Sequence and carbon isotope stratigraphy of sections from the Southern Kaokoveld Region.

2.4.3.2 Northern Kaokoveld
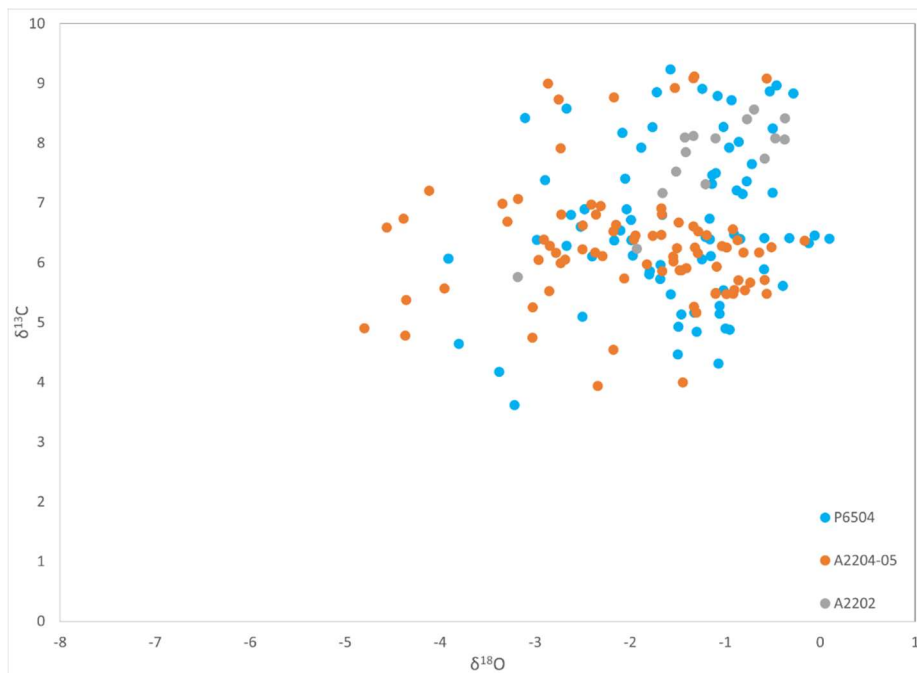
Figure 2.14: Crossplots of δ¹³C and δ¹⁸O data from Devede Formation sections A2202, P6504 and A2204-05 in the Northern Kaokoveld region.

Carbon and oxygen isotope results from the Northern Kaokoveld sections are plotted in Figure 2.14, where they demonstrate negligible correlation between $\delta^{13}C$ and $\delta^{18}O$. As seen in Figure 2.15, the Okaaru (P6504) and Otjize (*A2204-05)* sections record a gradual increase in $\delta^{13}C$ from ~5‰ at the base to around ~9‰ near the top of each section. Though no negative carbon isotope excursions ($\delta^{13}C < 0‰$) are observed, three distinct declines in the $\delta^{13}C$ values are seen in the lower 250 metres of both sections. In the first two instances, the $\delta^{13}C$ values show a steady rise to around ~7‰ before dropping back to ~5‰ near flooding surfaces, whilst in the final instance, carbon values fall to a low of ~4‰. The upper ribbonite unit of the sections shows an abrupt increase from ~5‰ to 9‰ before gradually falling to 7‰. A similar $\delta^{13}C$ trend is observed in A2202. Carbonates at the top of all three sections record a final decline towards the ~5‰ baseline below the Okakuya scour surface.
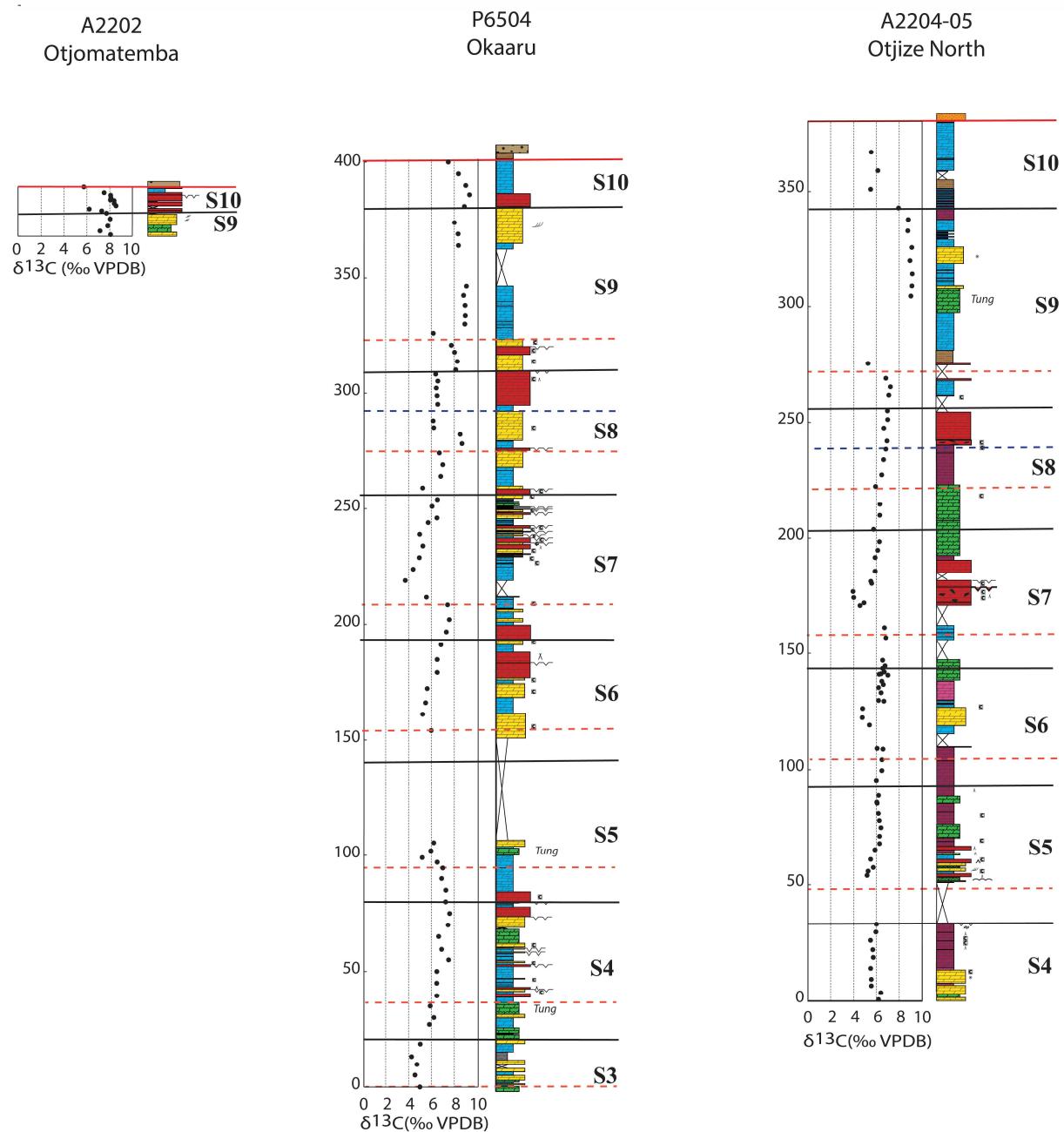
Figure 2.15: Sequence and carbon isotope stratigraphy of sections from the Northern Kaokoveld Region.

2.5 Discussion

2.5.1 Conceptual Depositional Model for the Devede Formation
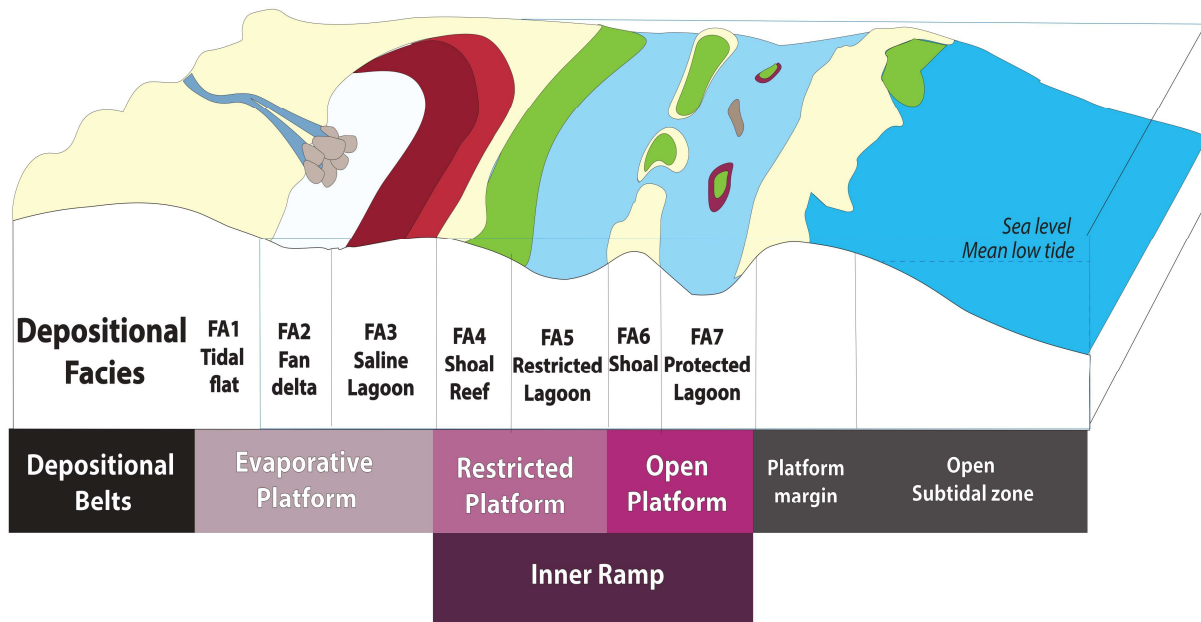
Figure 2.16: Mixed carbonate and siliciclastic platform environments of the Tonian Devede Formation of northwestern Namibia (modified from Xing et. al, 2022).

The Devede Formation records predominantly tectonically driven sea level fluctuations across a rimmed carbonate platform system on the episodically tectonically active southwestern margin of the Congo craton during the initial rifting of Rodinia. Facies analysis identified three depositional belts with a total of seven facies associations. A conceptual sedimentary model is depicted in Figure 2.16. Overtime, the persistence of lower sea-levels in a presumably more arid climate facilitated the development of a supratidal mudflat in vicinity of Otjisakumuka and an evaporative lagoon near Ongongo. Progressive aggradation of the shoreline in the southern part of the basin (Makalani ridge) and the platform margin north of Opuwa resulted in occasional isolation of the inner ramp from the open ocean and the establishment of a semi-restricted basin.

2.5.2 Tectonics and the stepwise evolution of the Makalani Sub-basin

1. Early Syn-rift Carbonate System

A Hypopycnal flows supply coarse-grained sediments to the basin

B As is typical of deltaic deposits, these siliciclastic sediments appear thickest and coarsest near the coastline and taper seaward.
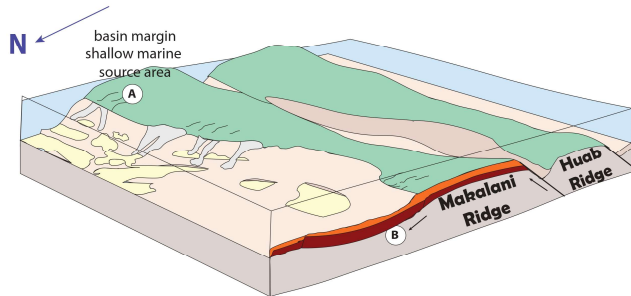
A deltaic orgin for these coarse grained sediment is consistent with the observed northward waning of the clastic sediments in S2.

2. Late Syn-rift Carbonate System
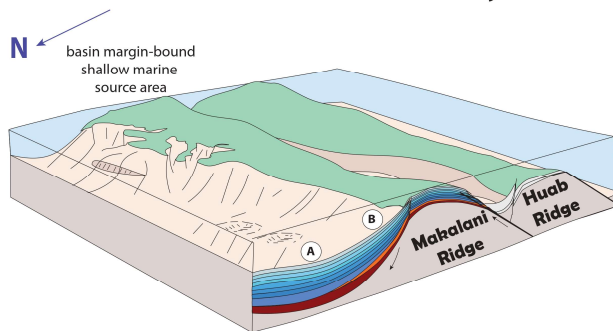
A A decrease in clastic sediments and steady subsidence allows for thick carbonate accumulation.

B Localized strain and associated tilting of sequences in response to block rotation.

| Beesvlakte Fm. | Pelagics | S1 | S2 | S3 | S4 | S5 | S6 | S7 | S8 | S9 | S10 |

☐ Sequence Boundary (SB)

Figure 2.17: Endmember type block models for the syn-rift deposition of the Devede Formation (modified from Tillmans et. al, 2021).

The depositional story of the Ombombo Subgroup began during the early phase of rift basin development (Figure 2.17a). The morphology of the rift basin was shaped by the activity of large-scale, east-west striking, south-dipping normal faults (Hoffman and Halverson, 2008; Miller, 2008). Initial marine transgression in this slowly subsiding basin, governed by crustal thinning, allowed for the deposition of the lower dolomite-shale unit of the Beesvlakte Formation in a fairly shallow perennial lagoon environment. Persistent marine influence and frequent flooding events associated with this rise in sea level resulted in the deepening of the lagoon

environment and the deposition of bioclastic sands, silt, and mud (i.e., the lower dolomite-shale interval). As sediment accumulation rates began to catch up with sea level rise, the basin shoaled until a broad lagoon developed. The increasing influence of evaporation in this shallower environment provided the conditions necessary for the largescale deposition of evaporites and the creation of a salina.

Subsequent sporadic flooding events facilitated the reestablishment of the shallower lagoon environment and the deposition of carbonate sands and muds. A transitional sequence of grainstones, shales and occasional ribbonites constitute the first deposits of the Devede Formation. There, the vertical transitions from finer grained sediments to massive, cross-bedded and/or ooid grainstones are used to infer small lateral shifts across the lower to upper slope of the lagoon as the platform tried to recover and finally caught-up with the rising relative sea levels (HST) associated with continued block rotation of the Makalani Ridge and subsequent thermal relaxation. Further north, a change in the dominant lithofacies from grainstones to shales, sands and muddy microbialaminates in section G1521 suggests a transition to a slightly different depositional environment. Much like its more southern counterparts, the prominence of these fine-grained lithologies in section G1521 indicates deposition in a low-energy environment.

Basement uplift along the southern limb of the Makalani Ridge resulted in the erosion and transportation of terrigenous materials by rivers as hyperpycnal flows onto the floor of the Makalani sub-basin. In this case, we hypothesize that the incoming flow experienced a rapid deceleration and loss of confinement at the river mouth, resulting in the accumulation of coarse-grained fractions in mouth bars and the transportation of fine-grained materials (silt/clay) as suspended load some distance from the coastline. This is expressed in the lowstand to transgressive systems tracts of sequence 2, which represents an apparent change in depositional

style from the prior microbialaminates and grainstones to relatively thick conglomerate-sandstone bed cycles. There, a fan-deltaic complex fed by mass flow and/or river-derived sand and gravel facilitated the downslope transportation of terrestrial sediments onto the slowly subsiding carbonate system. These sediments are characterized by spectacular sedimentary dykes, convoluted bedding, and load casts, consistent with contemporaneous faulting on the Makalani Ridge. The highstand systems tract of S2 is marked by a seaward shift in facies and a slow return to carbonate deposition.

This decrease in the terrigenous input facilitated the production and accumulation of carbonate sediments across the basin. Consequently, this sub-basin is draped by relatively pure shallow marine sediments. Steady subsidence and tilting of the Makalani block provided the accommodation space for the deposition of sequences 3–10 across the Makalani sub-basin (Figure 2.17b). The expansion of carbonate production across all sections marks the start of sequence 3. Here, the repeated ribbonite- packstone parasequences recorded at sections P1404 and K1611 are interpreted as cyclic peritidal lagoon or shoal edge sediments. Similarly, the packstone-stromatolite parasequences of P5 capture the tidal flat or shoal core, whilst the presence of *Jacutopyton* stromatolites in G1521 specifically indicates a shallow, subtidal reef front setting (Figure 2.18; Hoffman, 1969; Hoffman and Halverson, 2008). The lithological dominance of ribbonites implies a protected lagoon setting for much of section G1521 sediments. Moreover, an increase in fine-grained but similar lithology near P6504 indicates deposition in relatively deeper waters of the same lagoon. Consequently, sequence 3 captures sea level fluctuations across an intertidal reef to restricted lagoon environment.
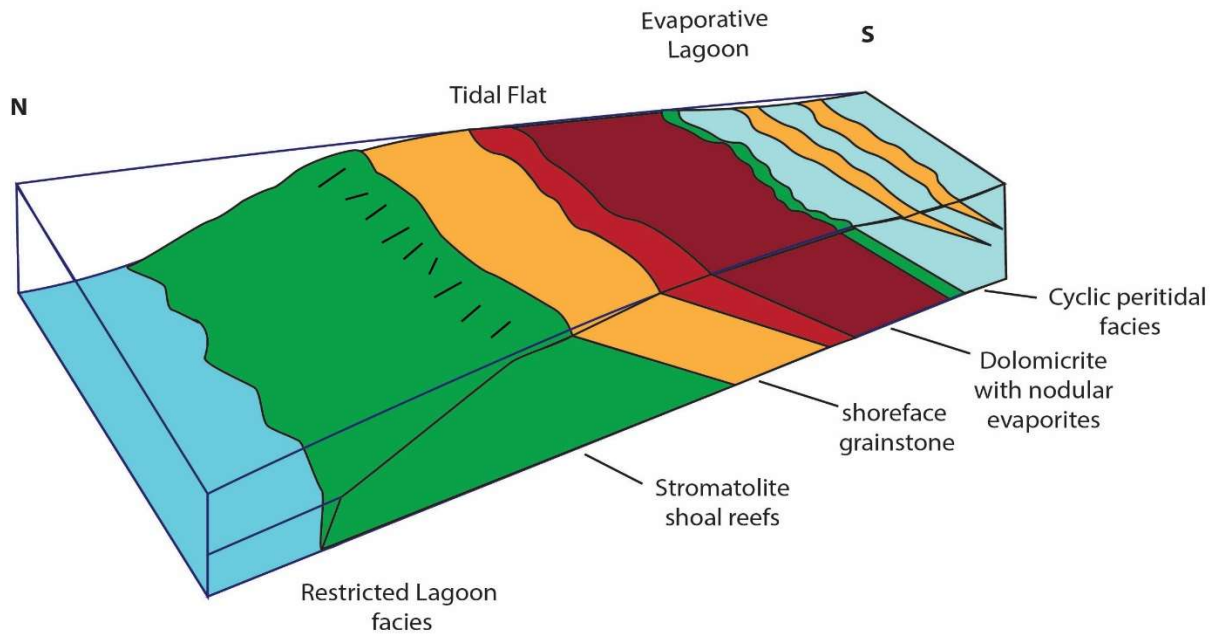
Figure 2.18: Facies model for the reef-shoal complex captured in the measured sections across the Kaokoveld (Modified from Lasemi et. al, 2012).

The lowstand systems tract of sequence 4 begins with the uniform deposition of a grainstone or microbialaminate bed. The first parasequences of the region (P1404) is characterized by typical cyclic peritidal cycles, whilst K1611 records a transition from microbialaminates to alternating sands and grainstones. Such a transition indicates an upward shift along the lower evaporative lagoon slope. In a similar manner, the occurrence of a thin parasequence of siltstones and microbialaminates in P5 is inferred to represent the mudflat. The predominance of reefal sediments and planar grainstones in section G1521 suggests a subtidal, reef front lagoon setting. Similarly, repeated ribbonite-grainstone-stromatolite parasequences in P6504 are interpreted as patch reef sediments further downslope of the same lagoon. Overtime, these shoals and reefs begin to aggrade as the sedimentation rate catches up with the rate of sea level rise, thus explaining the HST parasequences (Figure 2.19).

A seemingly short transgression characterized by thin backstepping parasequences, punctuates the start of sequence 5. There, the occurrence of a predominantly grainstone parasequence in

P1404 is interpreted as the shoal base, the alternating ribbonite-grainstone and shale-microbialaminate sets recorded in K1611 and G1521 representative of the lower lagoon slopes respectively, and the microbialaminate bed of P5, the tidal flat. Subsequent pulses in sea level rise during the HST produce lateral shifts in facies expressed as cyclic peritidal parasequences as the platform tried to recover and catch-up with the rising sea level. Increased evaporation across the evaporative lagoon to tidal flat environments allowed for the growth of salts and anhydrites (section P5). Similarly, the laminoid-fenestral fabric and tepees in the microbialaminate units overlying the cement breccia facies of A2204-05 suggest that these reef front microbialites kept pace with these sea level fluctuations (Grover and Read, 1978).
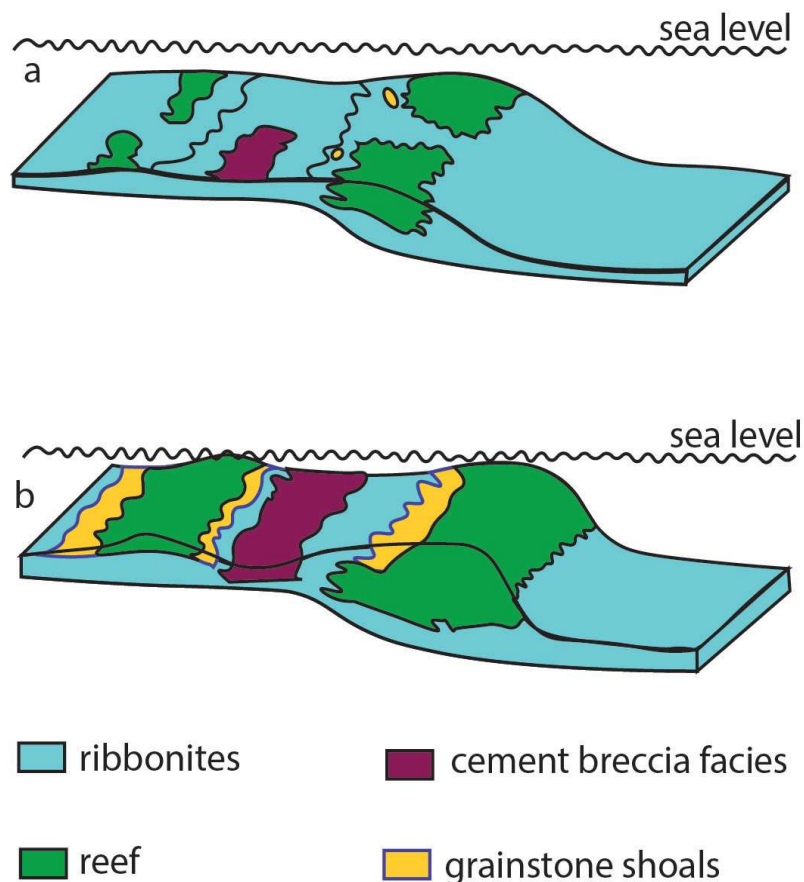
Figure 2.19: A model for the aggradational development of reef-shoals following a transgression (modified from Luo et, al, 2021). (a) Transgression and the initial establishment of reefs. (b) As the biological reefs begin to catch up with sea level, granular shoals develop behind the reefs (yellow) and a subtidal lagoon (purple) forms in the center.

The accumulation of fairly thick deposits of grainstones and stromatolites recorded during the highstand event (LST) of sequence 6 imply the aggradation and growth of the shoals towards sea level. Consequently, the cyclic peritidal parasequences and grainstones recorded in P1404 are regarded as shoal edge sediments. Additionally, the thick packstones to stromatolites of K1611 are interpreted as the back-reef grainstone shoal, whilst the *Tungussia* stromatolites of P5 imply the reef flat facies of a stromatolite shoal reef. A similar succession of packstones in G1521 is interpreted as the seaward edge of the shoal core. The ensuing HST chronicles the largescale drowning of the platform, except for the aggradation along patch reefs and reef crests as the carbonate system tries to catch up with the rate of sea level rise. Further to the north, the parasequences of P6504 and A2204-5 capture the drowning and reestablishment of sand shoals and patch reefs at different levels along the protected lagoon floor. It is also postulated that the shoal build up is replicated on the more northern platform margin shoal (Figure 2.19).

Continued platform development is marked by a pulsed transgression in sequence 8. As the rate of sedimentation failed to keep up with the rate of subsidence and/or rising sea levels, shallow water carbonate production began to wane across the platform. It was replaced by the steady but slow accumulation of deep-water carbonate sediments across the platform. Again, the activity of opportunistic microbial carbonate producers across the slopes of the relatively deeper protected lagoon allowed for the vertical accretion of reefs and shoals as seen in sections P6504 and A2204. The HST marks the catch-up phase of the rimmed platform development. Here, the rate of sedimentation along the platform shoals catches up with sea level rise and progradation begins over the platform (sections P5, G1523, P6504 and A2204). As sea level fell, the shallow-water sediments of the reef were eroded and transported basinward. Plint and Nummedal (2000) suggest that the presence of erosive-based shoreface sediments in the nearshore areas are

indicative features of the falling stage systems tract. Consequently, scour marks and the truncation of a previously shoaling upward parasequence in sequence 8 from the platform (P5) are utilized here to identify the initiation of forced regression, hence the base of the FSST.

A slow rise in sea level marks the beginning of S9. As new accommodation space is created, coastal onlap begins with the deposition of several backstepping parasequences (Figure 2.20a). As the rate of sediment supply begins to catch up with level rise, a highstand systems tract (Figure 2.20b.) develops across the seemingly stationary rimmed platform. This is marked by the appearance of aggradational parasequences within the fringing reef (P5 and G1523) environment and a transition from organic to intertidal carbonate parasequences (P6504 & A2205). A subsequent transgressive event ensued, producing more visible fining upward carbonate cycles within the more landward/coastal exposures. As sedimentation catches up with rising sea level, carbonate sediments prograde across the rim (HST). Here, section A2202 represents the supratidal platform crest, whilst sections P5 and G1523 represent the reef flat. Likewise, P6504 and A2205 represent the reef front of the protected lagoon with scattered microbial reefs nucleated on previous bathymetric highs.
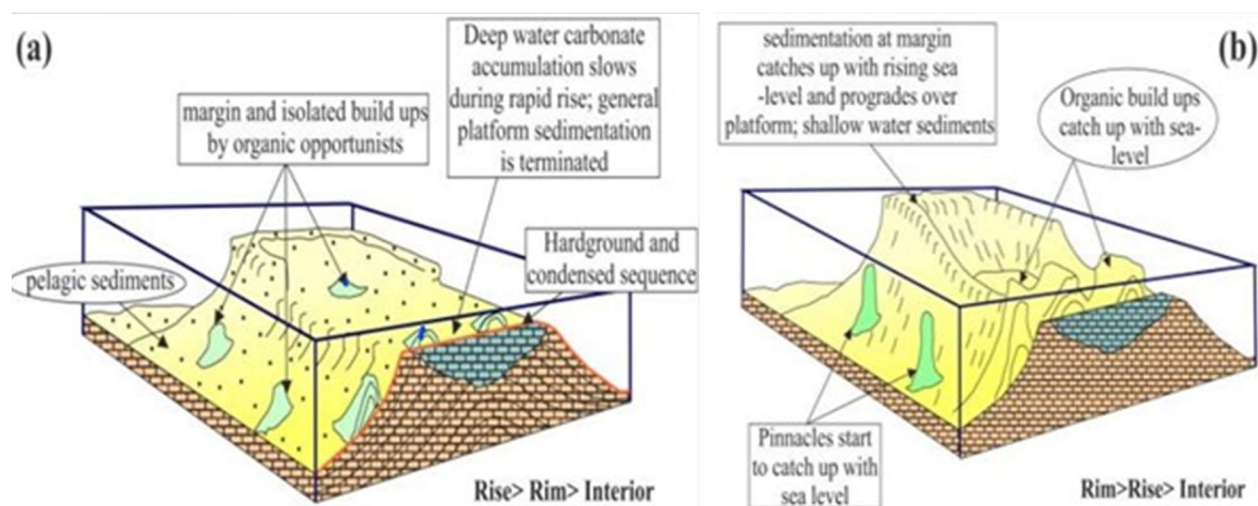
Figure 2.20: (a) Platform drowning at start up phase as both the shoals and interior fail to match sea level rise. (b) Platform shoals catch up with sea level rise (modified from Kendall and Schlager, 1981).

The final sequence (S10) of the basin marks another transgression, but here parasequences are preserved. the prevalence of marls and shales in this systems tract implies deposition in relatively deep, quiet waters. A plausible explanation for the occurrence of stromatolites and the heavily cemented limestone facies at the base of this sequence is that these sediments represent remnants of drowned reefs and/or other microbial buildups along the basin floor. Consequently, sections P5, G1523, A2202 and P6504 are thought to first represent typical drowned platform reefs, whilst A2204 captures the microbial reefs along the lagoon slope similar to that seen in Figure 2.21.
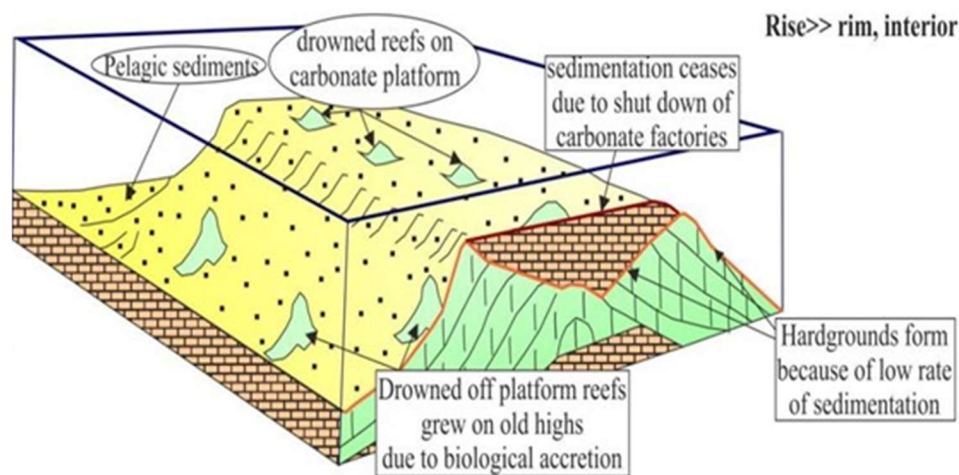
Figure 2.21: Drowning of the carbonate platform due to rapid sea level rise (modified from Kendall and Schlager, 1981)

2.5.3 Regional Correlations and Composite Section

Though $\delta^{13}C$ values in the upper Devede Formation are enriched by 1-2‰ in the northern Kaokoveld compared to sections in the southern part of the study area, the overall isotopic trends recorded across the Kaokoveld appear to be similar in nature, attesting to the reproducibility of the chemostratigraphic trends across the basin. However, the enriched $\delta^{13}C$ values in the Upper Devede Formation are interpreted to capture the additional influence of depositional setting on

the recorded $\delta^{13}C$ trends. Though this isotopic enrichment is tracked by a range of facies, our sequence stratigraphic interpretations highlight the development of progressively more restrictive conditions in the basin, as seen on the modern Bahamas platform (Geyman and Maloof, 2021). Consequently, stratigraphic correlation between the sections (Figure 2.22) was conducted on the basis of sequence stratigraphy, where the resultant spread in $\delta^{13}C$ values within each sequence is understood to reflect the intrinsic basin-wide variability in $\delta^{13}C$.

Composite carbon isotope curves, generated from multiple sections within a single basin, are useful tools for establishing global $\delta^{13}C$ profiles, generating age models, and comparing coeval sedimentary successions from different basins (Halverson *et al.*, 2022). We constructed a composite carbon isotope curve through the Devede Formation by mapping the data from P1404, P5, A2202, P6504 and A2204-5 onto section G1521–3, which we treat as the reference section. Each of the correlated intervals was scaled to the thickness of the equivalent interval G1521-3 for the purpose of plotting the carbon isotope data from all sections onto the composite section in Figure 2.23. Importantly, the lower portion of the P6504 section presents a gradual increase in $\delta^{13}C$ from ~4 to 6‰ that can be connected with a similar magnitude or positive trend in the middle portion of G1521-3. Above the maximum flooding surface of S5, $\delta^{13}C$ values across P6504 and A2204-5 begin to stabilize at approximately 6 to 7‰ and can be correlated with similar signals in G1521-3. A large positive $\delta^{13}C$ excursion from ~5‰ to 9‰ near the top of S9 is traceable across the basin and appears to be facies independent. As such, this stratigraphic $\delta^{13}C_{carb}$ pattern is interpreted to record a primary seawater signature, at least at the scale of the basin. The $\delta^{13}C$ profile ends with a return to ~5‰ at the flooding unconformity followed by a final increase from baseline to stabilizing values at around 7-8‰ in the deep-water facies.
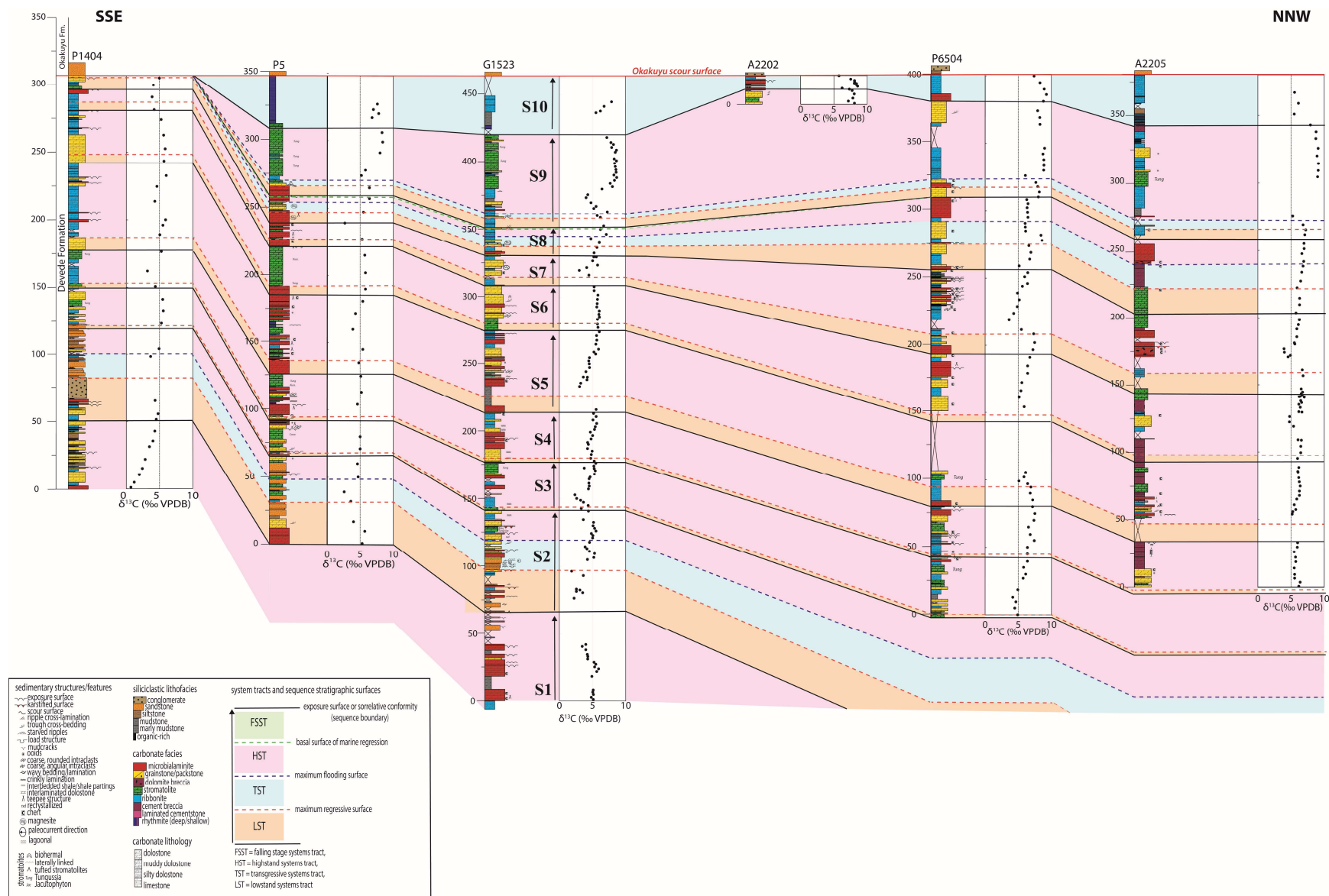
Figure 2.22: Sequence Stratigraphic correlation for the exposures of the Devede Formation throughout the northern and southern Kaokoveld.

2.5.4 Global correlation of the Late Tonian Isotope Record

This section details the provisional correlation of the Devede Formation with coeval units from Svalbard and Ethiopia (Park *et. al*, 2020; Halverson *et. al*, 2022). These locations were chosen primarily due to the stratigraphic completeness and well-studied nature of their later Tonian strata and the available age constraints. Based on the proposed sequence stratigraphic interpretations and correlations across the Kaokoveld region, the carbon isotope record of the Devede Formation is characterized by four noticeable trends. The first of these trends is the gradual increase in $\delta^{13}C_{carb}$ values from ~2 ‰ to 5 ‰ recorded within the first 75 metres near the proposed transitional contact with the underlying Beesvlakte Formation. The uppermost Devede Formation, on the other hand, is characterized by $\delta^{13}C$ values of around 6 - 8‰. Though the $\delta^{13}C$ values show some scatter, three distinct trends are present: i) an increase in $\delta^{13}C$ values from 7 ‰ to a plateau of ca. 8‰ associated with the appearance of the thick stromatolite biostrome, ii) a subsequent return to around 6 ‰ near the flooding unconformity, and iii) an abrupt increase from baseline values before gradually stabilizing at ~7‰ in the deeper-water facies.

Carbon isotope values from the upper 300 metres of the Backlundtroppen Formation in northeastern Svalbard are strikingly similar to those of the Devede Formation. Its first 50 metres record a steady increase from ~3‰ towards the 5 ‰ baseline, after which sustained high $\delta^{13}C$ values persist over hundreds of metres before declining again to the baseline (Halverson *et. al*, 2022). This first steady increase, like in the lower Devede, begins at the base of a ribbonite unit within a larger shallowing upward sequence of primarily grainstones. Likewise, a thick stromatolite biostrome in the Backlundtoppen Formation, similar to the "Tungussia member" in the Devede Formation, records sustained enriched $\delta^{13}C$ values, reaching as high as ~8‰, before
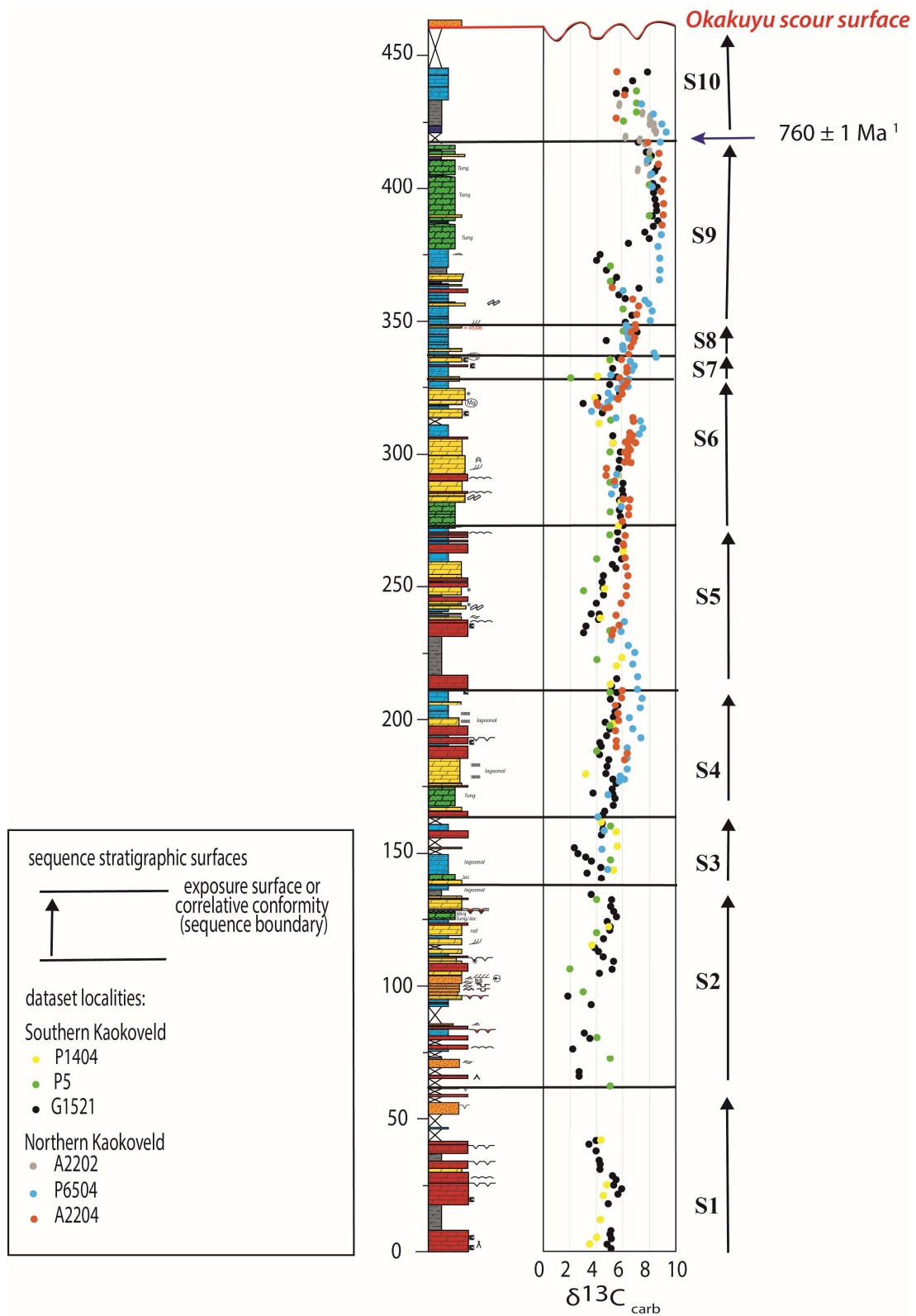
Figure 2.23: Composite carbon isotope profile of the Devede Formation. Age constraint from Halverson, 2005.

returning to ~5 ‰ at the base of the Kinnvika member at the top of the Akademikerbreen Group. As a result of the more precise integration of the 760 Ma Devede tuff in the Tonian isotopic record, it is recommended that the existing upper limit of the correlation be provisionally placed toward the base of the Kinnvika member within the Akademikerbreen Group's Backlundtroppen Formation. Furthermore, similar to the carbonates of the first twenty metres of S10, ^{13}C values of carbonates associated with a major flooding event in the first forty metres of the Kinnvika member show an abrupt increase to ~7‰ before falling back to the 5‰ baseline near the Kinnvika-Dartboard dolomite contact.

Building on this correlation, a comparable carbon isotope pattern emerges in the lower sections of the Calliston Lake Formation in Yukon, specifically within its Heterolithic Member. Here, a distinct 2‰ spike followed by a return to baseline is evident just beneath a black shale layer dated using Re-Os analysis (Strauss et al., 2015). It's postulated that the base of the upper stromatolitic bioherm, positioned around thirty-eight meters within the Heterolithic Member, acts as both the maximum flooding surface (MFS) and maximum regressive surface (MRS), coinciding with the initiation of a regional deepening event. Consequently, it's proposed to establish the lower correlation between the Calliston Lake and Devede formations at the base of this stromatolite unit. Moreover, while the Svalbard-Yukon correlation proposed by Halverson et al. (2022) is acknowledged, it's suggested that the corresponding Calliston Lake - Devede correlation be situated within Devede's S10 thick shale unit.

In the context of Ethiopia, though the values in the δ^{13}C record vary, an ascent from around 1 to 3‰ is preserved between 350 - 500 metres of the Didikama Formation that can be connected with a similar trend in the upper Devede Formation. Much like with the first 40m of the Kinnvika member and the first 20m of S10 in the Upper Devede, this increase coincides with a

major flooding surface (Park *et al.*, 2020; Halverson *et al.*, 2022). The coarsening upwards cycles above this flooding surface largely comprise of shales and siltstones capped by stromatolites and/ microbialaminates. As these more distinct shallowing upwards cycles begin to wane, the isotopes document a similar descent and return the base value of ~1‰, before increasing again and stabilizing in the deeper water facies. Based on the similarities between the sequence stratigraphic context and carbon-isotopic trends, it is proposed that the Tonian Devede Formation be correlated with the Backlundtroppen, Calliston Lake and Didikama formations as shown in Figure 2.24.

2.6 Conclusion

The late ca. 770–760 Ma Devede Formation in northwestern Namibia is an important benchmark for the Tonian period due to its exceptional preservation and detailed record of geochemical and sedimentary changes during the initial rifting of the Rodinia supercontinent. Facies analysis of this predominantly carbonate succession reveals a rimmed carbonate platform system, characterized by shallow marine to non-marine/evaporitic settings in the south and deeper but restricted subtidal environment to the north. A combined sequence and chemostratigraphic study of multiple sections across the Kaokoveld Region has been used to generate a composite section for the ca. 780 – 755 Ma Ombombo Subgroup. Additionally, global correlations aided by geochronology, sequence stratigraphy and carbon isotope chemostratigraphy suggest that the Devede Formation aligns closely with the Backlundtoppen Formation in Northeastern Svalbard and the Didikama Formation in Ethiopia. The flooding event of the final Devede sequence (S10), which marks the demise of the stable carbonate platform, appears to be traceable across the three basins, implying that these correlative sequences may have captured a possible global eustatic signal.
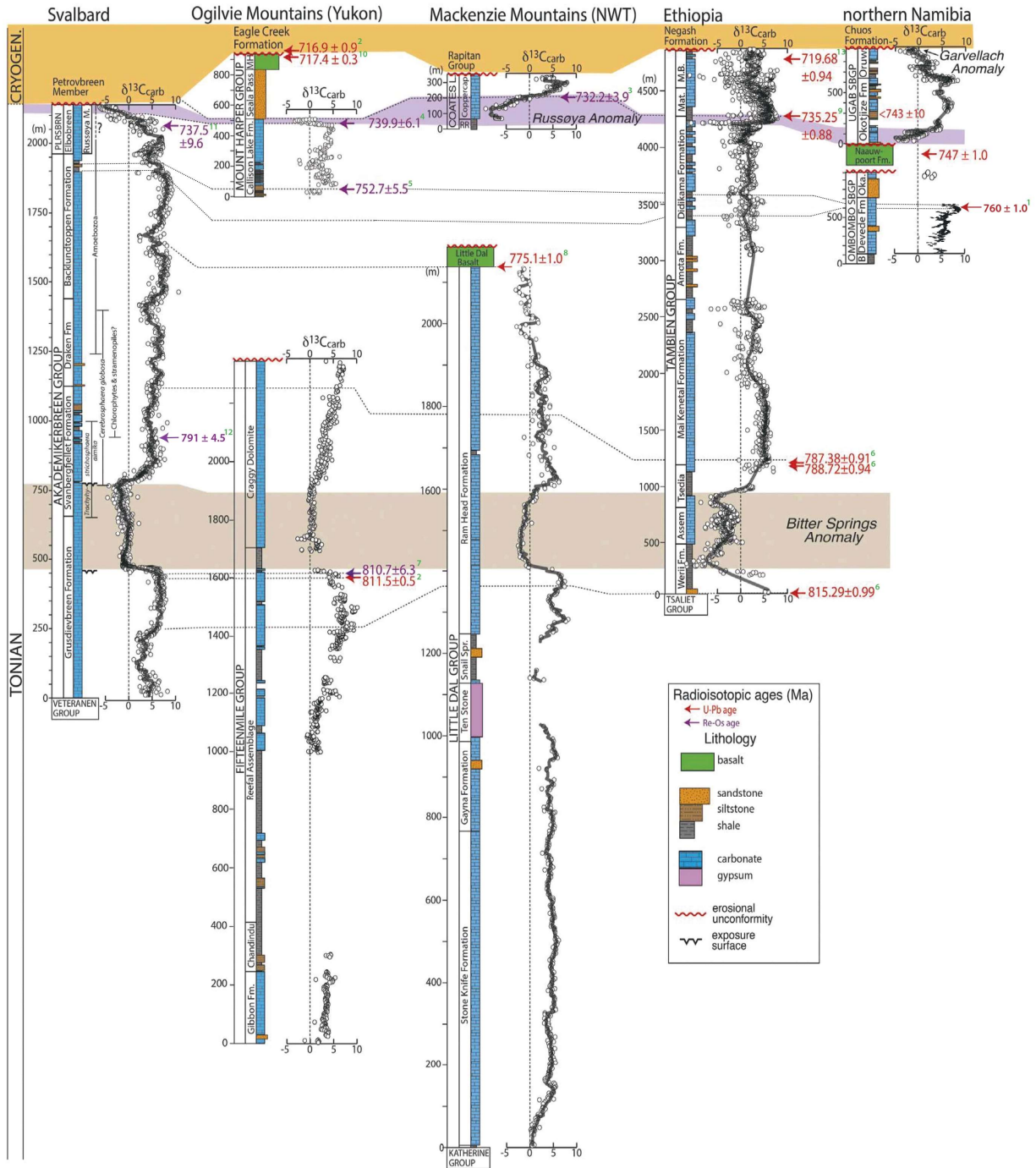
Figure 2.24: Proposed correlations between the Devede Formation and other Tonian successions via chemo- and sequence stratigraphy (modified from Halverson et.al, 2022). Age constraints used in this correlation were taken from Halverson et. al (2005)[1], Macdonald et. al. (2010)[2], Rooney et. al. (2014)[3], Strauss et. al (2014)[4], Rooney et. al. (2015)[5], Swanson-Hysell et. al (2015)[6], Cohen et. al (2017)[7], Milton et. al. (2017)[8], MacLennon et. al. (2018)[9], Macdonald et. al. (2010)[10], Millikin et. al (2022)[1,] Zhang et. al (2023)[12] and Cox et. al (2015)[13].

References

Andrieu, S., Krencker, F.N. and Bodin, S. 2022. Anatomy of a platform margin during a carbonate factory collapse: implications for the sedimentary record and sequence stratigraphic interpretation of poisoning events. *Journal of the Geological Society*:179 (6)

Burchette, T.P. and Wright, V.P. 1992. Carbonate Ramp Depositional Systems. *Sedimentary Geology*: 79, pp. 3-57.

Butterfield, N. J. 2015. Early evolution of the Eukaryota. *Palaeontology:* 58(1), pp. 5-17.

Caldeira, K. and Kasting, J. 1992. The life span of the biosphere revisited. *Nature*: 360, pp. 721–723

Campbell, I.H. and Squire, R.J.2010.The mountains that triggered the Late Neoproterozoic increase in oxygen: the second great oxidation event. *Geochimica et Cosmochimica Acta:* 74(15), pp. 4187–4206.

Canfield, D.E., Poulton, S.W. and Narbonne, G.M. 2007. Late-Neoproterozoic deep-ocean oxygenation and the rise of animal life. *Science:* 315, pp. 92–95.

Cantine, M. D., Knoll, A. H., and K. D. Bergmann. 2020. Carbonates before skeletons: A database approach*. Earth-Science Reviews:* 201.

Catuneanu, O. 2002. Sequence stratigraphy of clastic systems: concepts, merits, and pitfalls. *Journal of African Earth Sciences*: 35 (1), pp. 1-43

Cattaneo, A. and R. Steel. 2003. Transgressive deposits: A review of their variability. *Earth-science Reviews:* 62, pp. 187-228.

Catuneanu, O., Galloway, W.E., Kendall, C.G, Miall, A.D., Posamentier, H., Strasser, A. and Tucker, M. 2011. Sequence Stratigraphy: Methodology and Nomenclature. *Newsletters on Stratigraphy:* 44(3), pp. 173-245

Cohen, P.A., Strauss, J.V., Rooney, A.D., Sharma, M. and Tosca, N. 2017. Controlled hydroxyapatite biomineralization in an ~810-million-year-old unicellular eukaryote. *Sci. Adv:* 3.

Coplen, T.B. 1988. Normalization of oxygen and hydrogen isotope data. *Chemical Geology Isotope Geoscience section:* 72, pp. 293–297.

Corkeron, M. L. and Slezak, P. R. 2020. Stromatolite framework builders: ecosystems in a Cryogenian interglacial reef, *Australian Journal of Earth Sciences*: 67(6), pp. 833-856,

Cox, G. M., Halverson, G. P., Stevenson, R. K., Vokaty, M., Poirier, A., Kunzmann, M., Li, Z., Denyszyn, S.W., Strauss, J.V. and Macdonald, F.A. 2016. Continental Flood basalt Weathering as a Trigger for Neoproterozoic Snowball Earth. *Earth Planet. Sci. Lett.:* 446, pp. 89–99.

Cox, G.M., Strauss, J.V., Halverson, G.P., Schmitz, M.D., McClelland, W.C., Stevenson, R.S. and Macdonald, F.A. 2015. Kikiktat volcanics of Arctic Alaska-melting of harzburgitic mantle associated with the Franklin large igneous province. *Lithosphere:* 7, pp. 275–295

Craig, H. 1957. Isotopic standards for carbon and oxygen and correction factors for mass spectrometric analysis of carbon dioxide. *Geochimica et Cosmochimica Acta:* 12, pp. 133–149.

Crowley, T. J., Hyde, W. T. and Peltier, W. R. 2001. CO_2 levels required for deglaciation of a ''Near-Snowball'' Earth. *Geophysical Research Letters*: 28, pp. 283–286.

Domack, E.W. and Hoffman, P.F. 2011. An ice grounding-line wedge from the Ghaub glaciation (635 Ma) on the distal foreslope of the Otavi carbonate platform, Namibia, and its bearing on the Snowball Earth hypothesis. *Geological Society of America Bulletin:* 123, pp. 1448–1477.

Duda, J.P.,Van Kranendonk, M.J., Thiel,V., Ionescu, D., Strauss, H., Schäfer, N. and Reitner, J.2016. A Rare Glimpse of Paleoarchean Life: Geobiology of an Exceptionally Preserved Microbial Mat Facies from the 3.4 Ga Strelley Pool Formation, Western Australia. *PLoS ONE*: 11(1)

Dufour, F, Davies, J.H.F.L., Greenman, J.W., Skulski, T., Halverson, G.P. and Stevenson, R. 2023. New U-Pb CA-ID TIMS zircon ages implicate the Franklin LIP as the proximal trigger for the Sturtian Snowball Earth event. *Earth and Planetary Science Letters:* 618, 118259

Ebelmen, J.J. 1845. On the products of the decomposition of mineral species of the silicate family. *Ann. Mines*. pp. 3 - 66.

Embry, A.F. and Johannessen, E.P. 1992. T–R sequence stratigraphy, facies analysis and reservoir distribution in the uppermost Triassic-Lower Jurassic succession, western Sverdrup basin, Arctic Canada. *Norwegian Petroleum Society Special Publication*: 2, pp. 121-146.

Erwin, D. H. 2011. Early metazoan life: divergence, environment, and ecology. Philosophical Transactions of the Royal Society B. *Biological Sciences*: 366(1563), pp. 2838-2849.

Eyles, N. and Eyles, C.H., 1989. Glacially influenced deep-marine sedimentation of the Late Precambrian Gaskiers Formation, Newfoundland, Canada. *Sedimentology*: 36, pp. 601-620.

Duval, B., Cramez, C. and Vail, P. R. 1998. Stratigraphic cycles and major marine source rocks. In: De Graciansky, P. C., Hardenbol, J., Jacquin, T., Vail, P. R. (eds) Mesozoic and Cenozoic sequence stratigraphy of European Basins. *Society for Sedimentary Geology*, Special Publication: 60, pp 43–51

Fairchild, I., Hambrey, M., Spiro, B. and Jefferson, T. 1989. Late Proterozoic glacial carbonates in northeast Spitsbergen: New insights into the carbonate–tillite association. *Geological Magazine*: 126(5), pp. 469-490.

Fike, D.A., Grotzinger, J.P., Pratt, L.M. and Summons, R.E. 2006. Oxidation of the Ediacaran Ocean. *Nature:* 444, pp. 744–747

Frank, T.D. and Fielding, C.R., 2003. Marine origin for Precambrian carbonate-hosted magnesite? *Geology:* 31 (12), pp. 1101–1104.

Frazier, D.E. 1974. Depositional episodes: Their relationship to the Quaternary stratigraphic framework of the northwestern portion of the Gulf Basin. University of Texas at Austin. *Bureau of Economic Geology Geological Circular*: 71(1), pp. 27

Galloway, W. 1989. Genetic Stratigraphic Sequences in Basin Analysis I: Architecture and Genesis of Flooding-Surface Bounded Depositional Units. *The American Association of Petroleum Geologists Bulletin*: 73(2), pp. 125-142

Gat, J. R. and Bowser, C. 1991. The heavy isotope enrichment of water in coupled evaporative systems. In H. P. Taylor Jr., J. R. O'Neil, I. R. Kaplan (eds.), Stable Isotope Geo-chemistry: A Tribute to Samuel Epstein. *Geochemical Society Special Publication:* 3, pp.159–168.

Gaucher, C., Sprechmann, P., 2009. Neoproterozoic acritarch evolution. Neoproterozoic–Cambrian biota. In Gaucher, C., Sial, A.N., Halverson, G.P., Frimmel, H.E. (eds.), Neoproterozoic–Cambrian Tectonics. Global Change and Evolution: A Focus on Southwestern Gondwana. Developments in Precambrian Geology, vol. 16. Elsevier, pp. 319–326.Gehling, J.G., Runnegar, B.N. and Droser, M.L., 2014. Scratch Traces of Large Ediacara Bilaterian Animals. *Journal of Paleontology*: 88(2), pp.284-298.

Geyman, E.C. and Maloof, A.C. 2021. Facies control on carbonate δ^{13}C on the Great Bahama Bank. *Geology:* 49(9), pp. 1049–1054.

Ginsburg, R.N. and James, N.P. 1974. Holocene carbonate sediments of continental shelves. In: C.A. Burke and C.L. Drake (eds.). The Geology of Continental Margins. Springer-Veriag. New York, N.Y., pp. 137-155.

Goddéris, Y., Donnadieu, Y., Nédélec, A., Dupré, B., Dessert, C., Grard, A., Ramstein, G. and Francois, L.M. 2003. The Sturtian 'snowball'glaciation: fire and ice. *Earth Planet. Sci. Lett:* 211, pp. 1–12.

Grotzinger, J. P. 1989. Facies and Evolution of Precambrian Carbonate Depositional Systems: Emergence of the Modern Platform Archetype. In: Controls on Carbonate Platforms and Basin Development, *SEPM Spec. Publ:* 44.

Grotzinger, J.P. and J. F. Kasting. 1993. New constraints on Precambrian Ocean composition. *Journal of Geology*: 101, pp. 235–243

Grotzinger, J.P. and N.P. James. 2000. Precambrian carbonates: evolution of understanding. In: Carbonate Sedimentology and Diagenesis in the Evolving Precambrian World, *SEPM Spec. Publ.* 67, pp. 3-20.

Grotzinger, J. P., Adams, E. E., Schrag, D. P., Boyle, E. A., Hopmans, E. C., and Summons, R.E. 2005. Sulfur and carbon isotopic evidence for microbial sulfate reduction in the early Neoproterozoic era. *Science*: 308(5718), pp. 1014-1017.

Halverson, G.P., Hoffman, P.F., Schrag, D.P. and Kaufman, A.J., 2002. A major perturbation of the carbon cycle before the Ghaub glaciation (Neoproterozoic) in Namibia: Prelude to snowball Earth? *Geochem. Geophys. Geosystems:* 3, pp. 1–24.

Halverson, G. P., Hoffman, P. F., Schrag, D. P., Maloof, A. C., and Rice, A. H. N. 2005. Toward a Neoproterozoic Composite Carbon-Isotope Record. *Geol. Soc. America Bull*: 117, pp. 1181–1207.

Halverson, G.P., Hurtgen, M.T., Porter, S.M. and Collins, A.S. 2009. Neoproterozoic-Cambrian biogeochemical evolution. Dev. *Precambrian Geology:* 16, pp. 351–365.

Halverson, G.P., Kunzmann, M., Strauss, J. V. and Maloof, A.C. 2018. The Tonian-Cryogenian transition in Northeastern Svalbard. *Precambrian Research*: 319, pp.79 – 95

Halverson, G.P., Maloof, A.C., Schrag, D.P., Dudas, F.O. and Hurtgen, M.T. 2007. Stratigraphy and geochemistry of a ca 800 Ma negative carbon isotope interval in northeastern Svalbard. *Chemical Geology*: 237, pp. 5–27.

Halverson, G.P., Shen, C., Davies, J.H.F.L. and Wu, L. 2022. A Bayesian approach to inferring depositional ages applied to a late Tonian reference section in Svalbard. *Frontiers in Earth Science:* 10, 798739.

Haq, B.U., Hardenbol, J., and Vail, P.R., 1987. Chronology of fluctuating sea-levels since the Triassic. *Science:* 235 (4793), pp. 1156–1167.

Harland, W. B. 1964. Critical Evidence for a Great Infra-Cambrian Glaciation. *Geol. Rundsch*: 54, pp. 45–61.

Hayes, J.M., Strauss, H. and Kaufman, A. J. 1999. The abundance of ^{13}C in marine organic matter and isotopic fractionation in the global biogeochemical cycle of carbon during the past 800Ma. *Chemical Geology*: 161, pp. 103–125.

Helland-Hansen, W. and Gjelberg, J.G. 1994. Conceptual basis and variability in sequence stratigraphy: a different perspective. *Sedimentary Geology:* 92(1-2), pp. 31-52.

Herndl, G., and T, Reinthaler. 2013. Microbial control of the dark end of the biological pump. *Nature Geosci:* 6, pp. 718–724.

Higgins, J.A., Fischer, W.W., and D.P. Schrag. 2009. Oxygenation of the ocean and sediments: Consequences for the seafloor carbonate factory. *Earth and Planetary Science Letters*: 284, pp. 25–33

Hodgskiss, M. S., Dagnaud, O. M., Frost, J. L., Halverson, G. P., Schmitz, M. D., Swanson-Hysell, N. L. and Sperling, E. A. 2019. New insights on the Orosirian carbon cycle, early Cyanobacteria, and the assembly of Laurentia from the Paleoproterozoic Belcher Group. *Earth and Planetary Science Letters*: 520, pp. 141–152.

Hood, A.V.S., Wallace, M.W., Reed, C.P., Hoffmann, K.H. and Freyer, E.E. 2015. Enigmatic carbonates of the Ombombo Subgroup, Otavi Fold Belt, Namibia: A prelude to extreme Cryogenian anoxia? *Sediment. Geol:* 324, pp. 12–31.

Hofmann, H.J., 1969. Attributes of stromatolites. Geological Survey of Canada, Ottawa, Pap: pp. 69–139.

Hoffmann, K. and Prave, A. 1996. A preliminary note on a revised subdivision and regional correlation of the Otavi Group based on glaciogenic diamictites and associated cap dolostones. *Communications of the Geological Survey of Namibia*: 11, pp. 77–82.

Hoffman, P.F. 1976. Environmental diversity of Middle Precambrian stromatolites. In: Walter, M.R. (ed.), *Stromatolite*s. Elsevier, Amsterdam, pp. 599–611.

Hoffman, P.F. 1991. Did the breakout of Laurentia turn Gondwanaland inside-out. *Science:* 252, pp. 1409–1412.

Hoffman, P.F. and Halverson, G.P. 2008. Otavi Group of the Western Northern Platform, the Eastern Kaoko Zone and the Western Northern Margin Zone. In: Miller, R.M. (ed.), *The Geology of Namibia*. Ministry of Mines and Energy, Geological Survey, Windhoek, pp. 13-69.

Hoffman, P. F., Halverson, G. P., Schrag, D. P., Higgins, J. A., Domack, E. W., Macdonald, F. A., Pruss, S.B., Blattler, C.L., Crockford, P.W., Hodgin, E.B., Bellefroid, E.J., Johnson, B.W., Hodgskiss, M.S.W., Lamothe, K.G., LoBianco, S.J.C., Busch, J.F., Howes, B.J., Greenman, J.W. and Nelson, L.L. 2021. Snowballs in Africa: Sectioning a Long-Lived Neoproterozoic Carbonate Platform and its Bathyal Foreslope (NW Namibia). *Earth-Science Rev*iews: 219, 103616

Hoffman, P.F., Kaufman, J.A. and Halverson, G.P. 1998a. Comings and goings of global glaciations on a Neoproterozoic carbonate platform in Namibia. *GSA Today*: 8, pp. 1-9.

Hoffman, P.F., Kaufman, A.J., Halverson, G.P. and Schrag, D.P. 1998b. A Neoproterozoic snowball Earth. *Science:* 281, pp. 1342-46.

Hoffman, P.F. and Lamothe, K. G. 2019. Seawater-buffered diagenesis, destruction of carbon isotope excursions, and the composition of DIC in Neoproterozoic oceans. *Proceedings of the National Academy of Sciences:* 116 (38), pp. 18874–18879

Hoffman, P. F. and Schrag, D. P. 2002. The snowball Earth hypothesis: testing the limits of global change. *Terra Nova:* 14(3), pp. 129-155.

Horton, T.W., Defliese, W.F., Tripati, A.K. and Oze, C. 2016. Evaporation induced ^{18}O and ^{13}C enrichment in lake systems: A global perspective on hydrologic balance effects. *Quaternary Science Reviews:* 131, pp. 365-379

Hunt, D. and Tucker, M.E. 1992. Stranded parasequences and the forced regressive wedge systems tract: deposition during base-level' fall. *Sedimentary Geology*: 81(1-2), pp. 1-9.

Hunt, D. and Tucker, M.E. 1995.Stranded parasequences and the forced regressive wedge systems tract: deposition during base-level fall—reply. *Sedimentary Geology:* 95(1-2), pp. 147-160.

Hyde, W.T., Crowley, T.J., Baum, S.K. and Peltier, W.R. 2000. Neoproterozoic 'snowball Earth' simulations with a coupled climate/ice-sheet model. *Nature*: 405(6785), pp. 425-429

Inden, R. F. and Moore, C. H., 1983. Beach environment. In Scholle, P. A., Bebout, D. G., and Moore, C. H. (eds.), *Carbonate Depositional Environments*. American Association Petroleum Geologists Memoir: 33, pp. 211–265.

Isson, T. T., Planavsky, N. J., Coogan, L. A., Stewart, E. M., Ague, J. J., Bolton, E. W., Zhang, S., McKenzie, N.R, Kump, L.R. 2020. Evolution of the global carbon cycle and climate regulation on earth. *Global Biogeochemical Cycles*: 34(2).

James, N. P. 1978. Facies Models 10. Reefs. *Geoscience Canada:* 5(1), pp. 16–26.

James, N.P., 1984, Shallowing-upward sequences in carbonates, In Walker, R.G. (ed.), *Facies Models*. Geological Association of Canada, Geoscience Canada, Reprint Series 1(2), pp. 213–228.

James, N.P. and Bourque, P.A. 1992. Reefs and Mounds. In Walker, R.G. and James, N.P. (eds.), *Facies Models—Response to Sea-Level Change*. Geological Association of Canada, pp. 323–347.

Jervey, M.T.1988. Quantitative geological modeling of siliciclastic rock sequences and their seismic expression, in Wilgus, C.K., Hasting, B.S., Kendall, C.G. St.C, Posamentier, HW, Ross, CA, and Van Wagoner, JC, eds., Sea-level changes: an integrated approach: Tulsa, OK. *Society of Economic Paleontologists and Mineralogists*: Special Publication 42, pp. 47-69.

Johnson, J.G. and Murphy, M.A. 1984. Time-rock model for Siluro-Devonian continental shelf, western United States. *Geological Society of America Bulletin*: 95, pp. 1349-1359.

Johnson, K. S., 1982. Carbon dioxide hydration and dehydration kinetics in seawater. Limnol. *Oceanogr:* 27, pp. 849-855.

Jones, B., and Desrochers, A. 1992. Shallow platform carbonates. In Walker, R.G. and James, N.P. (eds.), *Facies Models—Response to Sea-Level Change*. Geological Association of Canada, pp. 227–301.

Kendall, A.C. 1992. Evaporites. In Walker, R.G. and James, N.P. (eds.), *Facies Models—Response to Sea-Level Change*. Geological Association of Canada, pp. 375-409.

Khabarov, E. M. 2011. Carbonate Sedimentation in the Meso-Neoproterozoic Basins in Southern East Siberia and Some Problems of Evolution of Reef Formation in the Precambrian. *Russian Geology and Geophysics*: 52(10), pp.1140–1153.

Kirschvink, J.L., 1992. Late Proterozoic low-latitude global glaciation: the snowball earth. In: Schopf, J.W., Klein, C. (Eds.), The Proterozoic Biosphere. Cambridge University Press, pp. 51–52.

Knoll, A.H. 2003.The geological consequences of evolution. Geobiology: 1(1), pp. 3–14.

Kuang, H.W., Fan, Z.X., Liu, Y.Q., Peng, N., Zhu, Z.C., Yang, Z.R., Wang, Z.X., Yu, H.L. and Zhong, Q. 2019. Stromatolite characteristics of Mesoproterozoic Shennongjia Group in the northern margin of Yangtze Block, China. *China Geology:* 2 (3), pp. 364–381.

Kump, L.R. and Arthur, M.A. 1999. Interpreting carbon-isotope excursions: carbonates and organic matter. Chemical Geology: 161(1), pp.181-198.

Lamothe, K. G., Hoffman, P. F., Greenman, J. W., and Halverson, G. P. 2019. Stratigraphy and Isotope Geochemistry of the Pre-sturtian Ugab Subgroup, Otavi/Swakop Group, Northwestern Namibia. *Precambrian Research:* 332, 105387.

Lasemi, Y., Jahani, D., Amin-Rasouli, H., and Z. Lasemi. 2012. Ancient Carbonate Tidalites. In: Davis Jr., R., Dalrymple, R. (eds). *Principles of Tidal Sedimentology*. Springer, Dordrecht: pp. 567–607.

Li, Z. X., Bogdanova, S. V., Collins, A. S., Davidson, A., De Waele, B., Ernst, R. E. and M. I. Wortel. 2008. Assembly, configuration, and break-up history of Rodinia: A synthesis. *Precambrian Research*: 160(1-2), pp. 179-210.

Linnemann, U., Ovtcharova, M., Schaltegger, U., Gärtner, A., Hautmann, M., Geyer, G., Vickers-Rich, P., Rich, T., Plessen, B., Hofmann, M., Zieger, J., Krause, R., Kriesfeld, L. and Smith, J. 2019. New high-resolution age data from the Ediacaran-Cambrian boundary indicate rapid, ecologically driven onset of the Cambrian explosion. *Terra Nova:* 31(1), pp. 49-58

Luo, W., Zejin, S., Yamin, T., and H. Xiuquan. 2021. Characteristics and Forming Processes of Reef-Shoal Reservoir in Changhsing Formation of the Eastern Sichuan Basin in Dianjiang, China. *Arabian Journal for Science and Engineering:* 47, pp 1-13.

Lyons, T., Reinhard, C. and Planavsky, N. 2014. The rise of oxygen in Earth's early ocean and atmosphere. *Nature:* 506(7488), pp. 307-315.

Macdonald, F.A., Schmitz, M.D., Crowley, J.L., Roots, C.F., Jones, D.S., Maloof, A.C., Strauss, J.V., Cohen, P.A., Johnston, D.T. and Schrag, D.P. 2010. Calibrating the Cryogenian. *Science*: 327, pp. 1241–1243.

MacLennan, S., Park, Y., Swanson-Hysell, N., Maloof, A., Schoene, B., Gebreslassie, M., Antilla, E., Tesema, T., Alene, M. and Haileab, B. 2018. The arc of the Snowball: U− Pb dates constrain the Islay anomaly and the initiation of the Sturtian glaciation. *Geology*: 46, pp. 539–542.

Mahon, R.C., Dehler, C.M., Link, P.K., Karlstrom, K.E., Gehrels, G.E., 2014. Geochronologic and stratigraphic constraints on the Mesoproterozoic and Neoproterozoic Pahrump Group, Death

Valley, California: A record of the assembly, stability, and breakup of Rodinia. *Geological Society of America Bulletin:* 126, pp. 652–664

Makhubele, M. and Bordy, E. 2021. Sequence stratigraphy in the Algoa and Gamtoos basins (South Africa): a shoreline's journey since the Middle Mesozoic. *Geo-Marine Letters*. 41

McConnico, T.S. and K. N Bassett. 2007. Gravelly Gilbert-type fan delta on the Conway Coast, New Zealand: Foreset depositional processes and clast imbrications. *Sedimentary Geology:* 186 (3-4), pp 147-166.

McMahon, S., Hood, A. and McIlroy, D. 2016. The origin and occurrence of subaqueous sedimentary cracks. *Geol. Soc. Lond. Spec. Publ*: 448, pp.285 - 309

Meredith, A.S., Collins, A.S., Williams, S.E., Pisarevsky, S., Foden, J.D., Archibald, D.B., Blades, M.L., Alessio, B.L., Armistead, S., Plavsa, D., Clark, C. and Müller, R.D. 2017. A full-plate global reconstruction of the Neoproterozoic. *Gondwana Research:* 50, pp. 84–134.

Meredith, A., Williams, S. E., Collins, A. S., Tetley, M. G., Mulder, J. A., Blades, M. L., Young, A., Armistead, S., Cannon, J., Zahirovic, S. and Müller, R. D. 2021. Extending Whole-Plate Tectonic Models into Deep Time: Linking the Neoproterozoic and the Phanerozoic. *Earth Science Reviews*: 103477.

Miller, R.M. 2008. The Geology of Namibia. In: Vol. 2, Neoproterozoic to Lower Palaeozoic. Ministry of Mines and Energy, Geological Survey of Namibia, Windhoek.

Millikin, A. E. G., Strauss, J. V., Halverson, G. P., Bergmann, K. D., Tosca, N. J., and Rooney, A. D. 2022. Calibrating the Russøya Excursion in Svalbard, Norway, and Implications for Neoproterozoic Chronology. *Geology*: 50(4), pp. 506-510

Milton, J. E., Hickey, K. A., Gleeson, S. A., and Friedman, R. M. 2017. New U-Pb Constraints on the Age of the Little Dal Basalts and Gunbarrel-Related Volcanism in Rodinia. *Precambrian Research:* 296, pp. 168–180.

Mitchum Jr., R. M..1977. Seismic Stratigraphy and Global Changes of Sea Level: Part 11. Glossary of Terms used in Seismic Stratigraphy In *Application of Seismic Reflection Configuration to Stratigraphic Interpretation*: Memoir 26, pp. 205 - 212.

Och, L.M. and Shields-Zhou, G. A. 2012.The Neoproterozoic oxygenation event: Environmental perturbations and biogeochemical cycling. *Earth-Science Reviews*: 110 (1–4), pp. 26-57.

Pisarevsky, S.A., Wingate, M.T., Powell, C.M., Johnson, S., Evans, D.A., 2003. Models of Rodinia assembly and fragmentation. *Geol. Soc. Lond. Spec. Publ*: 206, pp. 35–55.

Posamentier, H.W., Jervey, M.T., Vail, P.R., 1988. Eustatic controls on clastic deposition. I. Conceptual framework. In: Wilgus, C.K., Hastings, B.S., Kendall, C.G.St.C., Posamentier, H.W., Ross, C.A., Van Wagoner, J.C. (Eds.). Sea Level Changes– An Integrated Approach. *SEPM Special Publication*: 42, pp. 110– 124.

Posamentier, H. W. and Vail, P.R. 1988. Eustatic controls on clastic deposition II - sequence and systems tract models. In: Wilgus CK, Hastings BS, Kendall CGSC, Posamentier HW, Ross CA, Van Wagoner JC (eds) Sea-level changes: an integrated approach. *Society for Sedimentary Geology Special Publication*: 42, pp 25–154

Posamentier, H.W., and Allen, G.P. 1999. Siliciclastic Sequence Stratigraphy: concepts and applications. *SEPM Concepts in Sedimentology and Paleontology*: 7, p. 210.

Prave, A.R., Kirsimäe, K., Lepland, A., Fallick, A.E., Kreitsmann, T., Deines, Yu.E., Romashkin, A.E., Rychanchik, D.V., Medvedev, P.V., Moussavou, M., Bakakas, K. and Hodgskiss, M.S.W. 2022. The grandest of them all: the Lomagundi–Jatuli Event and Earth's oxygenation. *Journal of the Geological Society*: 179 (1), pp. 2021 – 2036.

Read, J. F. 1985. Carbonate platform facies models. The American Association of Petroleum Geologists Bulletin, 66: pp. 860–878

Read, J. F. 1982. Carbonate platforms of passive (extensional) continental margins: types, characteristics, and evolution. *Tectonophysics*: 81, pp. 195 - 212

Ridgwell, A, J, Kennedy, M.J., and K Caldeira. 2003. Carbonate deposition, climate stability, and Neoproterozoic ice ages. *Science*: 302, pp. 859–862.

Rooney, A.D., Macdonald, F.A., Strauss, J.V., Dud′as, F.O., Hallmann, C., Selby, D., 2014. ¨ Re− Os geochronology and coupled Os-Sr isotope constraints on the Sturtian snowball Earth. Proc. Natl. Acad. Sci. U. S. A: 111 (1), pp. 51–56.

Rooney, A.D., Strauss, J.V., Brandon, A.D., and Macdonald, F.A. 2015. A Cryogenian chronology: two long-lasting synchronous Neoproterozoic glaciations. *Geology:* 43, pp. 459–462.

Schidlowski, M. 1987. Application of Stable Carbon Isotopes to Early Biochemical Evolution on Earth. *Annual Review of Earth and Planetary Sciences:* 15, p.47-72

Schlager, W. 2005. Carbonate Sedimentology and Sequence Stratigraphy. SEPM (Society for Sedimentary Geology), Tulsa, OK. Concepts Sediment. *Paleontol:* 8, p. 200

Schrag, D.P., Berner, R.A., Hoffman, P.F., and G.P. Halverson. 2002. On the initiation of a snowball Earth. *Geochem. Geophys. Geosystems*: 3, pp. 1–21.

Shen, B., Dong, L., Xiao, S., and M. Kowalewski. 2008. The Avalon explosion: evolution of Ediacaran morphospace. *Science*: 319(5859), pp. 81-84.

Sloss, L.L. 1963. Sequence in Cratonic Interior of North America. *Geological Society of America Bulletin*: 74, pp. 93-114.

Smith, M.E. and Swart, P.K. 2022. The influence of diagenesis on carbon and oxygen isotope values in shallow water carbonates from the Atlantic and Pacific: Implications for the interpretation of the global carbon cycle. *Sedimentary Geology*: 434, 106147.

Stacey, J., Hood, A.S. and Wallace, M.W. 2023. Persistent late Tonian shallow marine anoxia and euxinia. *Precambrian Research:* 397, 107207

Strauss, J.V., Rooney, A.D., Macdonald, F.A., Brandon, A.D. and Knoll, A.H., 2014. 740 Ma vase-shaped microfossils from Yukon, Canada: Implications for Neoproterozoic chronology and biostratigraphy. *Geology:* 42, pp. 659–662.

Strauss, J. V., Macdonald, F. A., Halverson, G. P., Tosca, N. J., Schrag, D. P., and Knoll, A. H. 2015. Stratigraphic Evolution of the Neoproterozoic Callison Lake Formation: Linking the Break-Up of Rodinia to the Islay Carbon Isotope Excursion. *American Journal of Science*: 315, pp. 881–944.

Swanson-Hysell, N.L., Maloof, A.C., Condon, D.J., Jenkin, G.R.T., Alene, M., Tremblay, M.M., Tesema, T., Rooney, A.D. and Haileab, B. 2015. Stratigraphy and geochronology of the Tambien Group, Ethiopia: Evidence for globally synchronous carbon isotope change in the Neoproterozoic. *Geology*: 43, pp. 323–326.

Tillmans, F., Gawthorpe, R. L., Jackson, C. A. L., and A. Rotevatn. 2021. Syn-rift Sediment Gravity Flow Deposition on a Late Jurassic Fault-terraced Slope, Northern North Sea. *Basin Res.* 33, 1844–1879.

Urey, H. C. 1947. The thermodynamic properties of isotopic substances. *Journal of the Chemical Society of London*: pp. 562-581

van Yperen, A. E., Poyatos-Moré, M, Holbrook, JM, and I. Midtkandal. 2020. Internal mouth-bar variability and preservation of subordinate coastal processes in low-accommodation proximal deltaic settings (Cretaceous Dakota Group, New Mexico, USA). *Depositional Rec*: 6, pp. 431–458.

Vail P. R., Mitchum R. M., Todd R.G., Widmier J.M., Thompson S., Sangree J. B., Bubb J. N., and Hatlelid W. G. 1977. Seismic stratigraphy and global changes of sea level. In: Payton CE (ed) Seismic stratigraphy—applications to hydrocarbon exploration. *American Association of Petroleum Geologists Memoir:* 26, pp. 49–212

Vail, P.R., Audemard, F., Bowman, S.A., Eisner, P.N. and Perez-Cruz, C. 1991. The stratigraphic signatures of tectonics, eustasy and sedimentology - an overview. In: Einsele, G., Ricken, W., Seilacher, A. (eds.), *Cycles and Events in Stratigraphy*. Springer-Verlag, pp. 617–659.

Van Wagoner J. C., Posamentier H. W., Mitchum R. M., Vail P. R., Sarg J. F., Loutit T. S. and Hardenbol, J. 1988. An overview of the fundamentals of sequence stratigraphy and key definitions. In: Wilgus, C.K., Hastings, B.S., Kendall, C.G.S.C., Posamentier, H.W., Ross, C.A., Van Wagoner, J.C. (eds) Sea-level changes: an integrated approach. *Society for Sedimentology Geology*, Special Publication: 42, pp. 39–45

Van Wagoner, J.C., Mitchum Jr., R.M., Campion, K.M. and Rahmanian, V.D. 1990. Siliciclastic Sequence Stratigraphy in Well Logs, Core, and Outcrops: Concepts for High-Resolution

Correlation of Time and Facies. *American Association of Petroleum Geologists Methods in Exploration*: Series 7, p. 55

Xiao, S. and Laflamme, M. 2009. On the eve of animal radiation: phylogeny, ecology and evolution of the Ediacara biota. *Trends In Ecology & Evolution,* 24(1), pp. 31-40

Zeebe, R. E. 1999. An explanation of the effect of seawater carbonate concentration on foraminiferal oxygen isotopes. *Geochemica et Cosmochimica Acta*: 63, pp. 2001–2007

Zhang, T., Kellera, C.B., Hoggard, M.J., Rooney, A.D., Halverson, G.P., Bergmanne, K.D. Crowley, J.L. and Strauss, J.V. 2023. A Bayesian framework for subsidence modeling in sedimentary basins: A case study of the Tonian Akademikerbreen Group of Svalbard, Norway. *Earth and Planetary Science Letters*: 620, pp. 118317

Appendices

P1404	Devede Formation			33 samples
	Ongongo, Southern Kaokoveld, Namibia Devede Fm., Ombombo Subgroup, Otavi Group S19°10'18.5" E13°52'15.6" (base of section) late Tonian			
Unit	**Sample Height (m)**	$\delta^{13}C$	$\delta^{18}O$	
	334	4.98	-0.28	
	328.7	4.08	-0.91	
	319.8	3.88	-1.76	
	310.4	4.19	-1.31	
	303.1	5.24	-0.65	
	291.6	5.62	-1.76	
	281.5	5.85	-1.22	
	272.4	5.67	-1.27	
	261.5	6.01	-1.40	
	253.5	4.61	-1.40	
	242.5	4.29	-2.51	
	228.9	5.91	-1.31	
	219.9	5.51	-1.35	
	207.5	5.05	-1.51	
	194.8	5.27	-1.63	
	176.4	3.18	-2.99	
	168.2	4.37	-2.51	
	155.4	5.48	-2.45	
	150	5.57	-1.91	
	132.9	5.28	-1.68	
	118.5	4.93	-6.20	
	105.7	3.66	-8.45	
	66.2	4.33	-7.10	
	56.4	4.78	-3.69	
	52.3	4.51	-3.94	
	43.6	4.29	-4.98	
	36.3	4.01	-5.66	
	32.1	3.48	-5.12	

Appendix 1: Carbon and oxygen isotope data from section P1404.

P5	Devede Formation			70 samples
	Behind the Otjisakumuka Lodge; Okambonde, Southern Kaokoveld, Devede Fm., Ombombo Subgroup, Otavi Group S19º05'22.9" E13º57'11.9" (base of section) late Tonian			
Unit	Sample Height (m)	$\delta^{13}C$	$\delta^{18}O$	
	327	7.6	-2.0	
	323	7.0	-5.2	
	320	7.8	-4.2	
	317	6.8	-3.6	
	306.0	8.3	-0.1	
	299.0	8.4	-1.7	
	291.0	8.0	-1.5	
	278.0	5.8	-4.6	
	274.0	5.2	-1.2	
	265.0	6.4	-0.5	
	257.0	6.4	-0.8	
	247.0	5.5	-1.7	
	239.0	2.7	-3.8	
	227.0	5.3	0.0	
	215.0	5.7	-0.6	
	202.0	5.8	-1.6	
	190.0	5.8	-2.1	
	181.0	5.4	-2.4	
	172.0	4.3	-4.4	
	160.0	3.9	-3.5	
	145.0	5.4	-2.2	
	135.0	4.8	-2.9	
	125.0	5.1	-1.4	
	113.0	5.2	-2.2	
	104.0	4.6	-2.9	
	80.0	5.0	-2.1	
	71.0	5.0	-2.9	
	60.0	4.6	-7.7	
	50.0	4.7	-6.2	
	39.0	2.6	-7.5	
	32.0	3.6	-7.5	
	17.0	4.0	-5.9	
	10.0	5.7	-1.7	
	1.0	5.3	-1.3	

Appendix 2: Carbon and oxygen isotope data from section P5.

P6504	Devede Formation			70 samples
	Okaaru, Northern Kaokoveld, Namibia Devede Fm., Ombombo Subgroup, Otavi Group S18°45'27.0" E13°41'12.1" (base of section) late Tonian			
Unit	Sample Height (m)	δ¹³C	δ¹⁸O	
	392	7.92	-0.96	
	387	8.24	-0.50	
	382	8.27	-1.02	
	375	8.97	-0.46	
	370	8.72	-0.93	
	365	8.85	-1.72	
	360	8.87	-0.53	
	355	8.83	-0.28	
	350	6.07	-3.91	
	240	7.65	-0.72	
	335	7.93	-1.88	
	330	8.17	-2.08	
	325	8.03	-0.86	
	320	6.28	-2.67	
	315	6.47	-0.91	
	310	6.33	-0.12	
	305	6.40	0.10	
	300	6.46	-0.06	
	295	6.06	-1.24	
	290	6.11	-2.40	
	285	8.42	-3.10	
	280	8.58	-2.67	
	275	6.60	-2.52	
	270	6.90	-2.48	
	265	6.72	-1.99	
	260	5.14	-1.06	
	255	6.43	-1.21	
	250	5.96	-1.68	
	247	6.39	-1.16	
	242	5.62	-0.39	
	235	4.88	-0.95	
	230	5.16	-1.32	
	225	4.85	-1.30	
	221	4.31	-1.07	
	216	3.62	-3.22	
	201	5.47	-1.57	
	197	7.32	-1.14	
	193	7.47	-1.14	
	188	7.21	-0.88	
	182	6.74	-1.16	

P6504	Devede Formation			70 samples
	Okaaru, Northern Kaokoveld, Namibia Devede Fm., Ombombo Subgroup, Otavi Group S18°45'27.0" E13°41'12.1" (base of section) late Tonian			
Unit	Sample Height (m)	δ¹³C	δ¹⁸O	
	177	6.41	-0.32	
	172	6.40	-0.84	
	167	5.54	-1.02	
	162	5.28	-1.06	
	158	5.14	-1.46	
	152	5.89	-0.59	
	115	6.11	-1.15	
	110	5.86	-1.79	
	104.5	5.10	-2.50	
	100	6.41	-0.59	
	94.5	6.90	-2.04	
	90	6.80	-1.66	
	85	7.17	-0.50	
	80	7.15	-0.82	
	75	7.50	-1.10	
	70	7.36	-0.77	
	65	6.54	-2.10	
	59.5	6.80	-2.62	
	55	7.41	-2.05	
	50	6.38	-2.98	
	45	6.37	-2.17	
	39.5	6.38	-1.99	
	35	5.80	-1.80	
	30	6.12	-1.97	
	27	5.73	-1.68	
	18.5	4.93	-1.49	
	13	4.17	-3.38	
	9.6	4.64	-3.80	
	5	4.47	-1.50	
	0	4.90	-1.00	

Appendix 3: Carbon and oxygen isotope data from section P6504.

A2202	**Upper Devede Formation**			15 samples
	Knoll along a gravel road off the C43 with ash layers in place Otjomatemba, Northern Kaokoveld, Namibia Devede Fm., Ombombo Subgroup, Otavi Group S18º52'58.3" E13º47'50.7" (base of section) late Tonian			
Unit	**Sample Height (m)**	**δ¹³C**	**δ¹⁸O**	
	21.4	5.76	-3.18	
	18.9	7.53	-1.52	
	17.8	8.10	-1.42	
	16.8	8.12	-1.33	
	15.8	8.08	-1.10	
	15.5	8.40	-0.77	
	14.3	8.42	-0.37	
	13.3	8.57	-0.69	
	11.9	6.23	-1.93	
	11.1	7.32	-1.21	
	10.1	7.74	-0.58	
	7.6	8.06	-0.37	
	4.5	7.85	-1.42	
	2.3	7.17	-1.66	
	0.7	8.09	-0.47	

Appendix 4: Carbon and oxygen isotope data from section A2202.

G2290	**Lower Devede Formation**			10 samples
	near Camp Aussicht (along the C43), Okaaru Northern Kaokoveld, Namibia Devede Fm., Ombombo Subgroup, Otavi Group S18º40'36.9" E13º43'11.6" (base of section) late Tonian			
Unit	**Sample Height (m)**	**δ¹³C**	**δ¹⁸O**	
	33	5.99	-2.73	
	29.6	5.94	-1.09	
	26	5.47	-0.99	
	22	5.67	-0.74	
	18.7	5.71	-0.58	
	14	5.48	-0.92	
	9.3	5.54	-0.90	
	6.5	5.54	-0.79	
	3.5	6.37	-0.16	
	0.5	6.17	-0.64	

Appendix 5: Carbon and oxygen isotope data from section G2290.

A2204	**Devede Formation**			41 samples
	Within the bend of the C43 road, Okaaru Northern Kaokoveld, Namibia Devede Fm., Ombombo Subgroup, Otavi Group S19°03'36.0" E13°58'32.3" (base of section) late Tonian			
Unit	**Sample Height (m)**	**δ¹³C**	**δ¹⁸O**	
	189	6.91	-1.67	
	185.5	6.81	-1.66	
	181	6.61	-1.33	
	174.5	6.45	-1.76	
	169.5	5.91	-1.41	
	161.8	6.29	-2.84	
	157	6.28	-1.03	
	151	5.74	-2.06	
	145.7	6.25	-1.32	
	142	6.10	-1.55	
	138.9	5.87	-1.46	
	133	5.87	-1.48	
	128.5	5.50	-1.10	
	121.5	4.00	-1.45	
	107.4	6.69	-3.29	
	103	6.81	-2.36	
	93	6.74	-4.39	
	89	6.99	-3.34	
	85	6.59	-4.56	
	76.7	6.64	-2.15	
	73.5	4.78	-4.37	
	69.5	4.75	-3.03	
	66.3	5.38	-4.36	
	56.3	6.05	-2.68	
	56	6.56	-0.92	
	51.5	6.47	-1.67	
	46.8	6.46	-1.19	
	42.6	5.98	-1.82	
	35.9	6.17	-0.81	
	32.5	6.05	-2.96	
	33	6.02	-1.54	
	28.1	6.16	-1.29	
	25	6.24	-1.51	
	21.9	6.38	-0.87	
	18.2	6.26	-0.98	
	15	6.26	-0.51	
	12.3	5.86	-1.66	
	8.1	5.48	-1.10	
	4.6	5.71	-0.86	
	3	5.26	-1.33	

A2204	**Devede Formation**			41 samples
	Within the bend of the C43 road, Okaaru Northern Kaokoveld, Namibia Devede Fm., Ombombo Subgroup, Otavi Group S19°03'36.0" E13°58'32.3" (base of section) late Tonian			
Unit	**Sample Height (m)**	**δ¹³C**	**δ¹⁸O**	
	1.2	5.17	-1.30	

Appendix 6: Carbon and oxygen isotope data from section A2204.

A2205	**Upper Devede Formation**			19 samples
	near Camp Aussicht (along the C43), Northern Kaokoveld, Namibia Devede Fm., Ombombo Subgroup, Otavi Group S18°40'55.9" E13°42'58.3" (base of section) late Tonian			
Unit	**Sample Height (m)**	**δ¹³C**	**δ¹⁸O**	
	124	5.53	-2.85	
	116	6.11	-2.29	
	108	5.48	-0.56	
	100	7.92	-2.73	
	95	8.77	-2.17	
	90	8.73	-2.75	
	82.8	9.08	-0.56	
	77.1	8.92	-1.53	
	71.4	9.12	-1.32	
	66.2	9.09	-1.33	
	61.5	9.00	-2.86	
	32.6	5.25	-3.03	
	26.1	6.81	-2.72	
	22.4	7.21	-4.12	
	18.8	7.07	-3.18	
	12	6.95	-2.31	
	8.2	6.97	-2.41	
	4.5	6.63	-2.50	

Appendix 7: Carbon and oxygen isotope data from section A2205